Department of Mechanical Engineering

Dissertation presented in partial fulfilment of the requirements for the degree of

MSc (ENG)

The Development, Optimisation and Testing of an Unmanned Parafoil Launch System

Author:

William Alexander Norton

Supervisor:

Prof. Christiaan Redelinghuys

20 August 2010

DECLARATION

I know that plagiarism is wrong. Plagiarism is to use another's work and pretend that it is one's own.

Each significant contribution to, and quotation in, this report from the work of other people has been attributed, and has been cited and referenced. I have used the IEEE convention for citation and referencing.

This report is my own work.

I have not allowed, and will not allow, anyone to copy my work with the intention of passing it off as his or her own work.

……

William Alexander Norton

ACKNOWLEDGEMENTS

I would like to thank the following people for their advice, assistance and support during the completion of this project.

Professor Chris Redelinghuys, my supervisor who's guidance and advice has been invaluable to me throughout this project.

The National Aerospace Centre of Excellence for the funding, without which this project would not have been possible.

My parents Neville and Di Norton who have supported me in not only this dissertation but my time spent at university.

The Mechanical Engineering workshop staff, for their assistance and advice throughout the construction and testing phases of this project.

My colleague Jordan Adams and Iulia Sfarlea who's assistance and motivation have been invaluable to me over the course of my post graduate study.

The National Research Foundation for their assistance in my second year of post graduate study.

SUMMARY

Parafoils have been used in various aerospace, military and sport applications to return both personnel and payloads safely to the ground. Deflection of the trailing edge flaps by means of control lines allows for turn rates of up to 60° per second, which provides superior controllability when compared to conventional round parachutes. This steering ability has led to the development of autonomous control systems that are able to navigate a payload to land in close proximity to a designated landing site.

In order to develop an autonomous navigation system a suitable dynamic model of the parafoil with suspended payload is required to determine the parameters and characteristics of the system in free flight. Flexible ram-air inflated parafoils display high sensitivity to atmospheric disturbances which complicates the comparison of measured flight-dynamic data to theoretical models in an open air free flight test. In order to improve the quality of results in studying the flight dynamics of an unmanned parafoil system in free flight, controlled conditions and a repeatable flight path are required to perform data analysis for various trim configurations. This leads to the requirement of a launching system that ensures consistent inflation of the canopy and repeatable launch velocities for various canopy and payload configurations.

After assessing existing parafoil inflation and testing techniques, a new launching system enabling free flight testing of an unmanned parafoil and payload system was developed. The launch device was designed to perform as a testing apparatus to be used for future parafoil dynamic studies at the University of Cape Town.

A modular approach was taken in the design of the device where the parafoil inflation subsystem and payload acceleration subsystem were assembled and tested independently before integration to form the complete launch device. Springs energised both subsystems allowing for operation independent of an external power source and ensured the device was easily transportable to selected test sites.

The launch system successfully deployed the specified 6 m^2 parafoil with a 21kg payload suspended beneath the canopy. It was also found that the parafoil launch state was repeatable. The parafoil obtained a state of stable glide soon after release in favourable weather conditions. Atmospheric disturbances and time schedules limited the number of tests in which release velocity and parafoil trim angle were varied. Such a test series would allow more comprehensive identification of dynamic flight modes and glide slope angles.

Recommendations include locating a better suited test facility in which atmospheric disturbances and access can be more easily controlled to avoid dependence on weather forecasting. Shielding the springs and automating triggering devices would further increase safety for the operator by limiting potential mishaps.

CONTENTS

LIST OF FIGURES

LIST OF SYMBOLS

a	Distance from the piston to the fulcrum in the horizontal plane
A	Vertical distance from the spring attachment point on the frame to the fulcrum
A_p	Planform area of the parafoil
B	Horizontal distance from the spring attachment point on the frame to the fulcrum
c	Length of chain
C_D	Drag coefficient
g	Gravitational Acceleration
$F_{2\ series}$	Spring force exerted by two springs in series
F_a	Force of the actuator applied to the arm
F_D	Drag force exerted by the parafoil
F_i	Spring pretension force
F_{j_pdc}	Force applied perpendicular to the arm at point J
F_s	Force of the spring
h_{b_i}	Initial height of the centre of mass of the beam

h_{b_f}	Final height of the centre of mass of the beam
h_{cw_i}	Initial height of the counterweight
h_{p_f}	Final height of the payload
H_s	Height of the actuator above the fulcrum
I_0	Total inertia of the arm about the fulcrum. This consists of the beam's inertia, the payload's inertia and the counterweight's inertia (when applicable).
I_b	Inertia of the beam about the fulcrum, where the beam is approximated as a thin rod
I_p	Inertia of the payload
k_{2x4}	Spring constant for four parallel sets of two springs in series
l	Length of the link
L_0	Length of the spring in its relaxed state
L	Length of the beam
M_b	Mass of the beam
M_{cw}	Counterweight mass
M_{res}	The resultant moment about the fulcrum
M_t	Mass of trolley
M	Maximum bending moment
Q	Total length of spring unit
r	Distance between the fulcrum and pivot J
R_{cw}	Radius from the counterweight to the fulcrum

R_p	Radius from the payload to fulcrum
R_s	Radius from the spring attachment on the arm to the fulcrum
x_{eq}	Additional spring deflection added to the maximum deflection to simulate the inclusion of pretension forces in the springs.
α	Angle of attack
ε	Angle between the link and the perpendicular to the arm
θ	Inclination of the arm relative to the horizontal
φ	Angle between the link and the horizontal
ω	Angular Velocity

GLOSSARY OF TERMS

Parafoil	A non-rigid, ram air inflated wing system used to reduce descent rates of both humans and cargo.
Canopy	A generic term which in the case of this report refers to the ram air inflated wing that generates a lift force in flight.
ProE	Refers to the ProEngineer 3D CAD Package in which components were modelled.
NYLOC nut	A hexagonal nut with a small plastic insert into which the thread of the bolt taps on tightening. These nuts do not loosen easily and are well suited to installations where vibrations are common.
HDPE	High Density Polyethylene. A polyethylene thermoplastic with a high density and specific strength which can easily be machined.
Dynex Rope	A high strength rope made from Dyneema® fibre that is light and flexible yet stronger than steel cable of equal diameter.
Carabina	A stainless steel hook with a gate on one side used to clip items together. Used in the yachting and rock climbing industries.

CHAPTER 1

INTRODUCTION

1.1 OVERVIEW

The parafoil, which developed from conventional parachutes, takes the form of a non-rigid ram-air inflated wing with an aerofoil cross section. Parafoils improve on circular parachutes as they are steerable and generate lift which improves gliding performance.

This chapter aims to provide background information pertaining to the launch and flight characteristics of these ram-air inflated devices known as parafoils. Contemporary methods for launching various manned and unmanned vehicles are identified and their particular applications detailed. Thereafter the aim, scope and plan of development for the project are outlined.

1.2 BRIEF HISTORY OF PARACHUTES AND PARAFOILS

Circular parachutes have been used consistently since early in the 20th century to reduce descent rates of both personnel and payloads. Parachutes, with their high drag to weight ratio are well suited to the deceleration manoeuvres required for soft landing of payloads. Captain Albert Berry of the United States Army successfully jumped from an airplane at 1 500 ft in Missouri during 1912 [1] which marked the beginning of the US

military's use of parachutes to retrieve personnel from the skies. Since then parachute applications have included recovery of aircraft pilots, rocket components, re-entry vehicles, munitions, supplies, cargo and many more items. One of the disadvantages of conventional parachutes is their inability to be steered, thus leaving the parachute/payload system susceptible to wind dispersion, resulting in poor accuracy for airdrops from a high altitude as the system deviates from its ideal trajectory.

This lack of controllability was to be overcome with the invention of the parafoil. This invention has been credited to a kite maker, D. Jalbert in 1964, for his Ram Air canopy that consisted of an upper and lower surface with a sewn trailing edge and open leading edge. His design was further developed in the Aero-Space Department at the University of Notre Dame between 1965 and 1972 where several parafoils were tested at the Sandia Laboratories in New Mexico [2]. NASA subsequently showed an interest in the parafoil for its potential in controlling the final descent of emergency escape capsules for astronauts.

In the early 1970's the sport of paragliding was born which involved foot launching gliding parachutes off mountain slopes. These sport canopies largely influenced the development of the parafoil and ultimately led to the optimised canopies we see today.

1.3 Components of a Parafoil/Payload System

The major components of a parafoil and payload system are indicated in Figure 1.1.

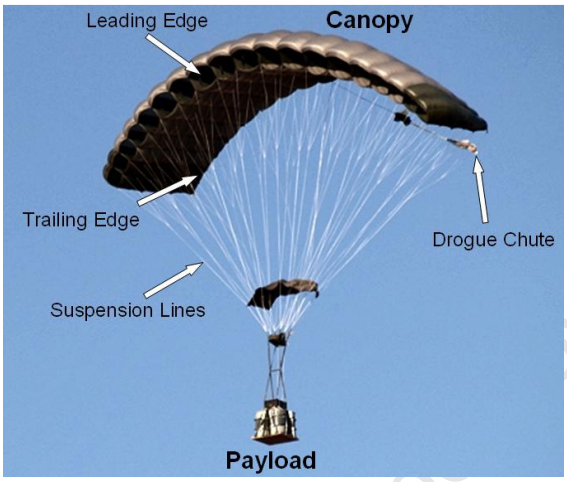

Figure 1.1: Components of a Parafoil/Payload System [3]

1.4 The Ram Air Parachute or Parafoil

These ram-air inflated devices consist of aerofoil shaped ribs separating the upper and lower surface of the parafoil forming an aerofoil cross section, inflated by means of ram pressure through the inlets on the leading edge. The planform is generally rectangular and forms a low aspect ratio wing with arc anhedral resulting from the suspension line convergence at the confluence point. The totally non rigid canopy is most commonly constructed from low or zero porosity material in order to maintain the pressure difference that keeps the wing inflated. The ribs are arranged in a chordwise fashion forming cells. The ribs generally have apertures cut in them to promote the equalisation of air pressure throughout the canopy to ensure a more uniform inflation.

Parafoils have good gliding performance with glide ratio's commonly exceeding 3:1 where this value is affected by the lift to drag ratio which changes with aspect ratio [4]. A parafoil will travel the same distance for a given decrease in height in still air

conditions regardless of the wing loading, although the velocity along the glide path will increase with wing loading. The rigging angle positions the canopy with respect to the payload at a particular angle of attack at which the parafoil will trim during flight. Flight tests have indicated that excessively high angles of attack lead to separation of the flow along the leading edge of the upper surface resulting in a stall. At excessively low angles of attack the leading edge on the upper surface can collapse, preventing ram air from maintaining the canopy's shape and resulting in a stall [5]. Typical angle of attack values range from 2 to 15 degrees where the angle is measured from the lower surface of the canopy to the free stream velocity vector.

The payload is supported by a number of suspension lines that branch out in a cascading fashion to distribute the load along alternate ribs in the canopy while reducing the total line drag. Early ram-air parachutes distributed the load from each suspension line by means of triangular fabric panels called "flares" extending from the ribs. This ensured less deformation of the lower surface of the canopy and helped channel the flow, reducing tip losses and aid directional stability. However the added mass, complexity of construction and drag of the flares outweigh the benefits [6]. As a result modern canopies do away with flares and instead distribute the load with tapes sewn to the ribs.

Suspension lines on modern parafoils are made of Kevlar which is a polyaramid material and is usually encased in Dacron (terylene), or polyethylene which is more commonly known as Dyneema or Spectramid [7]. Both materials offer high strength for a given diameter and thus minimise drag. The length of the suspension lines range between 0.6 and 1.0 times the span for modern parafoils where lines originating at similar chordwise positions are of equal length [6].

Steering and control is performed by asymmetrically deforming the trailing edge of the canopy by pulling down on the control lines or "brakes". This can result in turn rates of up to 60°/s or more [4]. Application of symmetrical deflection of the trailing edge is used

to perform the flare manoeuvre for landing [8]. While flying into the wind on final approach, the flare manoeuvre is performed, effectively reducing both the vertical and the horizontal speed components in order to minimise impact damage to the payload [9].

Conventional air drop deployment of a parafoil involves the release of a pilot or drogue chute which then extracts the main canopy. Similarly to conventional parachutes, parafoils experience a large opening shock as the canopy suddenly inflates. Development of a reefing technique has managed to reduce this opening shock by limiting the opening speed of the canopy. An example is the "slider" for which extensive modelling and simulation has been conducted for both conventional parachutes and parafoils [10] [11]. Sliders fitted to parafoils consist of a rectangular piece of nylon fabric and nylon webbing that is designed to descend the parafoils suspension lines during the inflation phase, thus inhibiting the spreading of the canopy and reducing the opening shock.

1.5 PARAFOIL APPLICATIONS

Great interest has been shown in parafoils for their ability to be controlled and steered through the air. This aspect lends itself to autonomously guided recovery systems that can ensure safe retrieval of equipment from high altitude with its wind penetrating and soft landing capabilities. Modern applications of parafoils are presented below.

1.5.1 SPACE

The use of parafoils by sport jumpers advanced the development of the canopies and reduced reliability concerns that were present in the mid 1960's. NASA took an interest in the use of parafoils and begun their Advanced Recovery Systems Program focussing on the development of large scale gliding parafoils to recover rocket boosters and space vehicles [12]. The aim of initial tests was to drop an unmanned parafoil suspended

payload at 10 000ft which was to autonomously guide itself using GPS to a pre-defined landing location, at which it should execute a flare manoeuvre and land into the wind.

Through many years of development and testing NASA successfully demonstrated an autonomous recovery of a prototype Crew Return Vehicle (CRV) designed to be a 'lifeboat' for astronauts on the International Space Station. This project, called the X-38 project, made use of a 7500 ft^2 parafoil recovery system supporting a 25 000 lbs payload, See Figure 1.2. Due to budget constraints NASA terminated its CRV programme in 2003 [13].

Figure 1.2: X-38 Prototype Crew Return Vehicle [14]

The above mentioned programme outlined the capabilities of an autonomous recovery system controlled by an advanced navigation system with reasonable spot landing accuracy. This is the largest parafoil to have been flown, at the time of writing.

1.5.2 MILITARY

Military applications of parafoils include the deployment of troops, equipment and terminal guidance of rockets or re-entry bodies. In order to accurately drop military payloads using conventional parachutes, the airplane must fly at low altitude, increasing the risk of attack from air defence and small arms [6]. The use of a parafoil with an autonomous control system allows for an airdrop at a greater offset distance and altitude which can then compensate for inaccuracies due to wind dispersion, resulting in a more accurate drop.

Parafoils are considered an option for retrieving tactical fixed wing Unmanned Aerial Vehicles (UAV's) where a high degree of mobility is required [4]. This would be applicable in a military situation where aerial reconnaissance is required and only unprepared terrain is available for landing. A study by Wylie [4] indicates the complexity of deployment of the canopy and the drop in altitude before control of the system is regained in order to be steered to the desired location. His report indicates that a successful flare manoeuvre had been executed by a control system during landing, in which the vertical and horizontal velocities were reduced to 1.5m/s and 5m/s respectively.

A South African defence company, Denel Dynamics, successfully demonstrated a parafoil retrieval system for a client in order to recover their Seeker UAV. This UAV is shown with parafoil deployed in Figure 1.3. Various algorithms modelling the dynamic behaviour of a parafoil with a suspended air vehicle or payload have been established in order to improve the accuracy of the navigation and control system used in such applications. Examples are the work done by Redelinghuys [15], Slegers et al [16] and Müller et al [17].

Figure 1.3: Denel's Seeker UAV Suspended Beneath a Parafoi (Image kindly provided by Denel Dynamics)

1.5.3 Recreational Paragliding

The sport of paragliding found popularity in the French and Swiss Alps around 1980 where paraglider pilots launched off steep slopes much like hang gliders had been doing for years [7]. Paragliding took off as a sport and the public interest encouraged development and optimisation of the paraglider system which led to increased performance. It became apparent that foot launched parafoils experienced much lower stresses in the canopy during launch, compared to the opening stresses (opening shock) experienced by jump chutes during free fall. This led to manufacturers producing wings from non-porous material with smaller inlets on the leading edge as the canopies were inflated before launch and instant opening was no longer of great concern [7].

Sport paragliding has attracted tens of thousands of enthusiasts who can be seen soaring above mountain slopes on every continent excluding Antarctica [7]. Paragliding World Championships are held every year in which more than 30 countries compete.

1.6 PARAGLIDER LAUNCH TECHNIQUES

1.6.1 THE FORWARD (ALPINE OR SNATCH) LAUNCH

The technique of launching a paraglider by running down a slope is believed to have been refined by French parachutists Jean-Claude Betemps, Andre Bohn and Gerard Bosson at Mieussy, France in 1978. This Snatch launch technique requires the paraglider to be laid out on the ground with the trailing edge of the wing into the wind. The pilot stands with his back to the canopy, facing the wind. The rear risers are draped over the pilot's forearms with the front risers in his hands. Running strongly and smoothly, the pilot makes his way down the slope while leaning forward with his head down. The lines on the leading edge of the parafoil tension first, as the canopy fills with air. The air pressure generated by the forward movement forces air down the open leading edge of the parafoil and causes the canopy to inflate to form its aerofoil shape. The canopy then floats upward towards a position above the pilot and begins to supports his weight. This technique is termed the Forward, Alpine or Snatch launch and is suitable for low wind strengths ranging from zero to 13 km/h [7].

1.6.2 THE REVERSE LAUNCH

The reverse launch is a slight modification to the forward launch which is used in higher wind strengths. The pilot faces the parafoil with his back to the wind and pulls the leading edge towards him to inflate the parafoil. The pilot walks backwards as the higher wind strength leads to a slower ground speed required to pressurise the canopy. Facing the canopy the pilot is better able to resist being pulled over by the parafoil as well as control the parafoil in the early stages of launch. Once the canopy is fully inflated and overhead the pilot turns around to face forward, completing the launch.

1.6.3 THE TOWED LAUNCH

A third paraglider launching technique is the towed launch. This method is used in flat countryside where the pilot is winched forward with his paraglider laid out on the

ground behind him. Once the canopy fills with air it pulls the pilot upwards where he then releases the tow line. This launch technique along with the two previously mentioned techniques are shown in Figure 1.4.

Figure 1.4: The Forward Launch [18], Reverse Launch [19] and Towed Launch [20]

All of the above mentioned launch techniques require careful control by the pilot to ensure that the canopy inflates uniformly and does not collapse. This makes these techniques not ideally suited to unmanned parafoil launch in which smooth gliding flight, immediately subsequent to launch, would need to be achieved consistently and without direct control from a technician.

1.7 Parafoil Testing Techniques

Due to the high sensitivity displayed by ram-air inflated parafoils to atmospheric disturbances, in-flight performance measurements obtained from costly tracking instruments are often inaccurate and can be difficult to obtain. Costs associated with free flight testing include the requirement of an air-vehicle to deploy the test canopy where visual range can become problematic.

Tethered testing of parafoils in a wind tunnel has been performed in order to determine aerodynamic characteristics of the canopy. In 1969, a NASA technical report detailed the performance, stability and control characteristics of various parafoils tethered in a wind

tunnel [21]. The parafoils tested were grouped in a constant-wing-area series and a constant–wing chord series in which both accommodated varying aspect ratio's from 1.0 to 3.0 with 13.66 m^2 being the largest canopy planform area. It is reported by the authors that the parafoils were effectively flown in the Langley full-scale tunnel in the 30 by 60 foot open throat section of the tunnel. It was also noted that the models were, "somewhat unsteady in the tethered flight condition". As a result, the test technique involved controlling the parafoil with its control lines to a wings level state where after the control lines were released and the lift and drag measured by means of a strain gauge balance. This indicated that direct human control was necessary to stabilise the canopy so that data could be obtained.

The accuracy of testing parafoils in a wind tunnel is somewhat limited by scale effects which include Reynolds number where glide performance measurements from subscale models is often of questionable accuracy, as outlined by Brown [22].

Brown [22] details a method for determining lift and drag performance of parafoils making use of a vehicle to pull the ram-air inflated canopy through the air. This technique indicates that in order to launch the parafoil, the canopy should be laid on the ground with its bottom surface facing upwards and its trailing edge closest to the vehicle, similarly to the forward paraglider launch mentioned previously. The vehicle then accelerates quickly while the parafoil inflates and flies overhead. The test apparatus included a protractor device to measure tether angle, a load cell to measure the tether load and a bubble level airspeed indicator all encompassed in the field of view of a video camera. These measurements determined the lift-to-drag ratio and the lift coefficient for the test parafoils ranging in size from 18 to 800 square feet.

Brown mentions that the parafoil must be "actively controlled" in order to keep it above the vehicle. This is performed by a technician who stands in front of the test fixture, controlling the parafoil with the steering lines. Further undesirable effects noted by

Brown include the occasional surging motion of the canopy which occurred even in optimal atmospheric conditions. This effect was the worst when testing high performance parafoils (aspect ratio of 3.66 which achieved an L/D ratio greater than 6) for which suitable data could not be obtained. This hints at a limitation for this testing method. Brown concludes that this method for testing parafoils is useful and economical. Limitations include the need for favourable weather conditions [22]. This towing method was used in NASA's X-38 Space Station Crew Return Vehicle project to assess a subscale 750 ft^2 (69.7 m^2) model parafoil flown behind a vehicle [23] as shown in Figure 1.5.

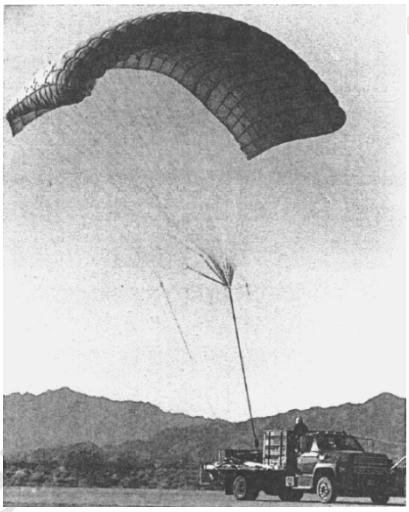

Figure 1.5: Tow Testing 750 ft^2 Parafoil [23]

Further parafoil tests conducted in the X-38 program involved drop testing of pallets from a C-130 aircraft in order to develop the required parachute systems and culminated in successfully retrieving a 6 804 kg prototype crew return vehicle with a 5500 ft^2 (510 m^2) parafoil, dropped from NASA's B-52 aircraft. According to the report, 26 drop test were executed in total and during the development process multiple failures and complications occurred in the deployment of the highly complex system. This project with a budget of $2 billion (started in 1995) serves as an example of the cost

associated with large scale free flight testing and development of autonomously guided parafoil systems.

1.8 Model Parafoil Launch Project

As an undergraduate student the author designed, constructed and tested a model parafoil launch device. This project involved the deployment of a 1.2 m^2 model parafoil with 1.2 kg payload where the flight trajectory was to be assessed for various launch velocities. A catapult concept using a water filled counterweight was implemented to launch the canopy as shown in Figure 1.6.

Figure 1.6: Launch of Model Parafoil

The rotating catapult arm was well suited to the inflation and release requirements of the parafoil/payload system and provided a consistent launch platform from which the flight trajectory could be assessed indoors. The results indicated that launching the parafoil/payload system at a speed close to its glide velocity ensured that the system settled into a stable glide state quickly, providing a consistent trajectory. Figure 1.7 shows a flight trajectory in which the parafoil reaches trimmed glide soon after release.

Figure 1.7: Trimmed Flight Trajectory

Tests were performed where the arm length was halved to 2 m which provided unsatisfactory results. This indicated a possible minimum arm length to parafoil suspension line length ratio of 2:1 for this particular concept, assuming the glide velocity could be achieved at release.

1.9 Project Aim and Scope

With regard to the discussion of parafoil applications, launch and testing techniques, the primary aim of this project is to develop an unmanned parafoil launch system to serve as a platform from which flight dynamic testing can be performed for medium sized canopies. Ideally the launch system should ensure consistent inflation of the specified canopy and release it in the deployed state so as to achieve a trimmed glide soon after launch, maximizing the useful flight trajectory in controlled atmospheric conditions. Subsequent launches should be highly repeatable in order to ensure accuracy, should a statistical approach be used to analyse various trimmed flight configurations of the parafoil and payload system.

The scope of this project includes the mechanical design, optimisation, construction and implementation of a parafoil launch system. A detailed analysis of the resulting flight

path falls outside the scope of this report although flight path images and basic glide slope measurements are displayed in order to indicate successful deployment of the system.

1.10 Plan of Development

Having outlined relevant information regarding the launch of parafoils, this report continues by listing the main specifications for the launch system. Thereafter the final solution is explained, followed by the approach and methodology which led to the chosen concept. Testing and results are then presented followed by conclusions and recommendations for future work in launching unmanned parafoils.

CHAPTER 2

SPECIFICATIONS

2.1 INTRODUCTION

This chapter outlines the design specifications for the launch system. Table 2.1 lists the specifications where after an explanation is provided for each entry. These specifications were determined by Professor Redelinghuys and the author to define the requirements of the launch system. These have been divided into two groups, namely performance and general specifications

2.2 LIST OF SPECIFICATIONS

Table 2.1: List of Specifications

D/W	No.	Requirement	Desired	Tested to	Location
1. Performance Specifications					
D	1	Largest Parafoil to be Launched	6 m^2	6 m^2	2.3.1
W	2	Heaviest Payload to be Launched	80 kg	20 kg	2.3.2
W	3	Maximum Payload Release Velocity	15 m/s	11,6 m/s	2.3.3
D	4	Release Velocity Adjustable	Yes	Yes	2.3.4
W	5	Accommodate Various Payloads	Yes	Yes	2.3.5
D	6	Launch Characteristics Repeatable	Yes	Yes	2.3.6
W	7	Launches in Quick Succession	8 min	5 min	2.3.7
2. General Specifications					
D	8	Transportable by Utility Vehicle	Yes	Yes	2.3.8
D	9	Operate Independent of Grid Power or Other External Power Source	Yes	Yes	2.3.9
W	10	Operated by One Person	Yes	Yes	2.3.10
D	11	Operator Clear of Device at Launch	Yes	Yes	2.3.11
D	12	Cost Within or Below Budget	R30 000	R23 537.29	2.3.12
D	13	Final Report Submission	30/8/10	18/8/10	2.3.13
D = Demand W = Wish					

2.3 EXPLANATION OF SPECIFICATIONS

2.3.1 Largest Parafoil to be Launched

The planform area of the largest canopy to be launched is 6 m^2. This canopy is a scale model of the parafoil tested by Ware & Hassel[21] which has an aspect ratio of 2,5.

2.3.2 Heaviest Payload to be Launched

It is specified that the launch system be able to accelerate an 80 kg payload to the velocity mentioned in 2.3.3. This provides excess capability for possible future use of the device as the maximum payload mass to be launched for this dissertation was 20 kg.

2.3.3 Maximum Payload Release Velocity

This is the maximum velocity at which the payload is to be released. This correlates to the glide velocity of the parafoil/payload system for common wing loading conditions.

2.3.4 Release Velocity Adjustable

The velocity at which the payload is released is to be adjustable to accommodate various wing loading conditions of the parafoil/payload system and ensure versatility.

2.3.5 Accommodate Various Payloads

A generic interface between the payload and accelerating system is to be designed to allow for a variety of payloads to be launched.

2.3.6 Launch Characteristics Repeatable

It is required that the launch velocity and acceleration profile be repeatable for subsequent launches to enable a statistical analysis of the resulting trajectory to be performed.

2.3.7 Launches in Quick Succession

To ensure that multiple flight tests can be performed in one session, the time required to reload the system between launches is to be less than 8 minutes.

2.3.8 Transportable by Utility Vehicle

It is required that the launch system be able to be transported on a utility vehicle to avoid additional costs of hiring larger vehicles. This specification also ensures that the size of the launch system is manageable and within the scope of a partial dissertation masters project.

2.3.9 Operate Independent of Grid Power or Other External Power Source

Ensuring the system operates without power supplied by the national power grid enables the device to be operated in remote locations. This flexibility caters for any launch site without limitations of power cables.

2.3.10 Operated by One Person

The launch system should preferably be operated by one person to avoid accidental triggering of the device by additional personnel while the operator is loading the parafoil or payload.

2.3.11 Operator Clear of Device at Launch

The device is to be designed so that the operator can stand a safe distance away while he triggers the system. A safe distance is defined by the range of all moving parts of the launch system including toppling of the device in any direction during launch.

2.3.12 Cost Within or Below Budget

The budget for the assembly and operation of the launch system is limited to R30 000. This budget cannot be exceeded. This budget covers the hardware used to construct the system which excludes the cost of the parafoil and travel expenses.

2.3.13 Final Report Submission

The final report detailing the design, construction and testing of the device is due for submission on the 30 August 2010.

CHAPTER 3

THE PARAFOIL LAUNCH SYSTEM

3.1 INTRODUCTION

The launch system has been designed to deploy the parafoil/payload system as close to a steady glide state as possible to minimise the altitude drop required by the parafoil to stabilise and reach its trimmed condition. Sensitivity to atmospheric disturbances and the irregular inflation characteristics of parafoils precludes launching non-rigid, unmanned systems in a repeatable fashion. Assessment of multiple concepts led to the final design of the launch device which was to be simple to operate and transport, yet meet the performance specifications outlined for a useful flight testing apparatus to be used beyond this dissertation.

This chapter provides an overview of the complete launch system, outlining the major components and explaining the method of operation. The design process involving conceptual design, concept testing, detailed design and construction that led to assembly of the final launch system is detailed in the following chapters.

3.2 System Overview

A modular approach was taken in development of the final design to ensure that separate subsystems could be tested independently before they were integrated to form the launch device. The launch system consists of two major subsystems, namely the parafoil inflation subsystem and payload acceleration subsystem, which deploy the parafoil and attached payload simultaneously. These subsystems are shown in Figure 3.1 in the relaxed or unloaded state. The parafoil inflation subsystem consists of a steel frame (shown in Figure 3.1) which supports the arm in its rotation from the horizontal to vertical, flinging the parafoil outwards as it inflates. The cross beam mounted on the end of the arm, referred to as the hangar, supports the suspension lines and acts as a pivot around which the open parafoil rotates in the initial stages of launch.

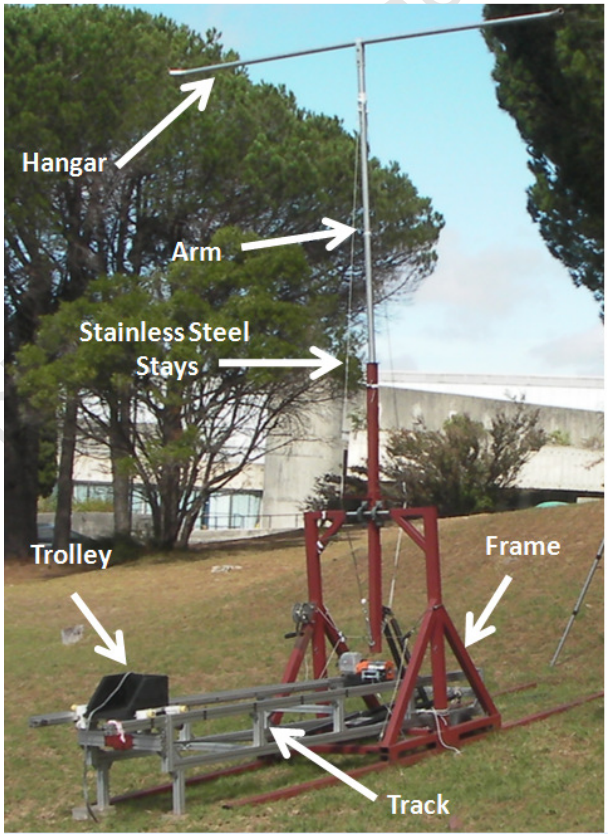

Figure 3.1: Main Components of the Parafoil Launch System

The payload acceleration subsystem consists of an aluminium track and rolling trolley in which the payload is placed. Design considerations included accommodation for various payload masses to be launched which resulted in an adjustable design to meet the different requirements. The two major subsystems are explained in the following sections.

3.2.1 Parafoil Inflation Subsystem

The rotating motion of a catapult arm proved to be a technique well suited to inflating ram-air canopies. Through extensive scaled testing this technique was refined and modified to inflate larger canopies with the intention of minimizing the size of the structure required to ensure successful inflation. Addition of the hangar on the end of the arm allowed the payload to be placed near the fulcrum, which significantly reduced the required arm length by supporting the spread of suspension lines emanating from the confluence point and throwing only the canopy. This minimized the rotational inertia, although an additional system was required to accelerate the payload. The position of the canopy mid way through the inflation process is shown in the ProE rendered image, Figure 3.2.

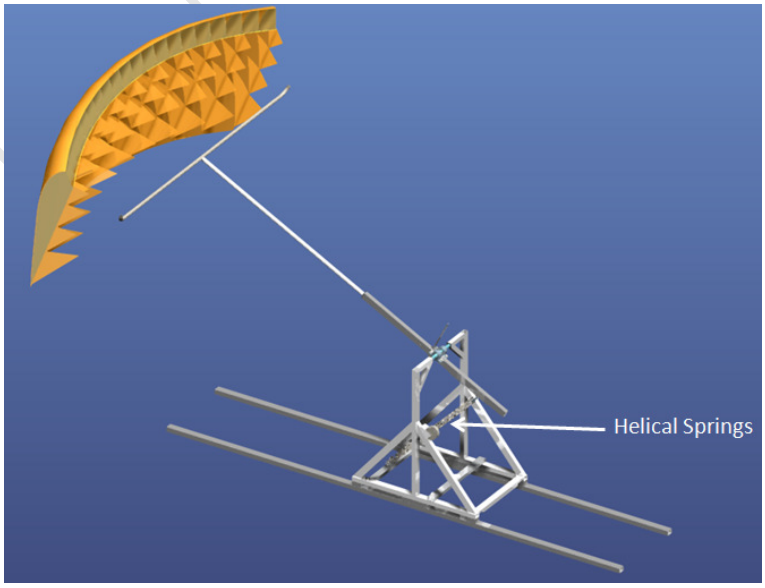

Figure 3.2: Parafoil Inflation Subsystem

Stabilising steel legs protrude forward and backward from the catapult frame which prevents the device from toppling during initial inflation and deceleration of the arm at the vertical once the canopy has been released. These legs were bolted into place for testing and detached for ease of transport. The stainless steel stays that limit the aluminium arm from flexing under the load applied by the canopy are visible in Figure 3.1.

Two large springs, normally used for garage doors, energised the catapult arm, Figure 3.2, Figure 3.5 and Figure 5.1. This arm was loaded to the horizontal position by means of a hand operated trailer winch which connected via a cable directed around pulleys (Figure 3.3) to ensure that the operator was clear of the vertical plane in which the tension springs act. A quick release snap shackle located on the end of the loading cable was used to trigger the device manually by the operator with a 5 m line.

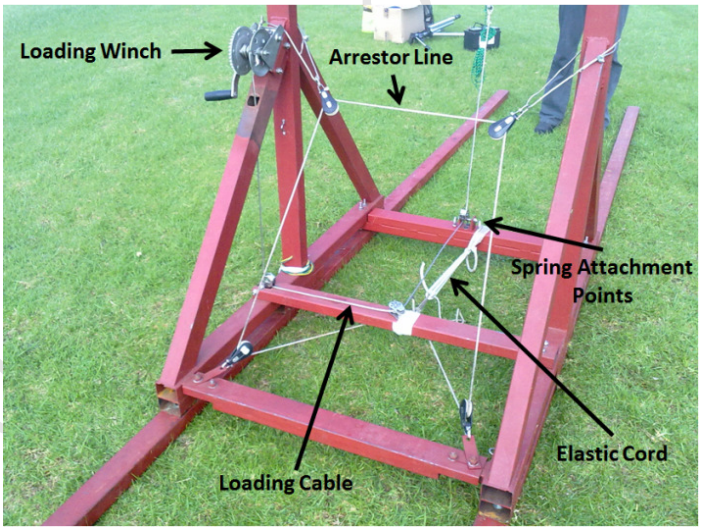

Figure 3.3: Loading and Decelerating Components

The arrestor line stationed across the path of the rotating arm (Figure 3.3) passes through pulleys where it then connects to an energy absorbing elastic cord to form the deceleration system, limiting the arm from overshooting and interfering with the deployed parafoil.

3.2.2 PAYLOAD ACCELERATION SUBSYSTEM

This spring loaded system was designed to accommodate a range of payloads of varying mass up to 80 kg to ensure additional capability for future launches. With this in mind a modular design was developed to accommodate additional springs placed in parallel for added energy, should it be required.

The structure was assembled using a useful range of products from Bosch Rexroth which allowed their extruded aluminium sections to be bolted to one another using brackets and T-nuts to form a strong, yet removable joint between beams. Two parallel sets of two springs in series provided more than enough energy to accelerate a 20 kg payload where doubling this number of springs would just meet the 80 kg payload velocity requirement. The smooth, precision manufactured Bosch Rexroth beams permitted the payload bearing trolley to run directly on the beam surface without requiring additional tracks on which to roll. The trolley is linked to the springs via a Dynex rope passing around a pulley which reduces the overall length of the system. Figure 3.4 shows this subsystem in the relaxed or unloaded state. The battery operated electric winch (with remote) is used to load the springs by pulling the trolley backwards. Adjustment of the loading distance modifies the release velocity for a given payload mass.

Figure 3.4: Payload Acceleration Subsystem

The pulley configuration decelerates the trolley and reduces overshoot by stretching the springs a second time as the trolley passes the neutral point above the pulley. High pretension in the springs adds to this stopping effect and promotes detachment of the payload. The system is triggered by pulling a line attached to the quick release snap shackle located between the loading cable and the trolley.

Situated on the four corners of the trolley are high density polyethylene (HDPE) cars which each mount three polyurethane wheels with ball bearings, locating the trolley both vertically and horizontally as it rolls down the track. Slots machined in the upper surface of the cars allow for adjustment of the horizontal locating wheels to ensure a tight tolerance with the track can be maintained. On top of the steel trolley with attached cars is placed a carbon fibre-foam laminate box which holds the payload. This box includes a steel hook which prevents the payload from lifting out prematurely as the canopy inflates and generates lift.

3.3 METHOD OF OPERATION

At the test site the payload acceleration subsystem is placed inside the frame of the parafoil inflation subsystem and secured in position. The catapult arm is then loaded to the horizontal position with the hand winch, where after the suspension lines from the open canopy are passed over the hangar. Placing the loose payload in the trolley box and attaching the winch cable to the trolley, the payload acceleration subsystem is then loaded to the desired position with the electric winch. The suspension lines are clipped onto the payload and the track's trigger line is clipped onto the arrestor line, making sure it is taught. With the complete system loaded the operator holds the parafoil inflation trigger line extending 5 m from the rig, checking the test site is clear. Figure 3.5 shows the launch device in the loaded state with the parafoil spread out on the hangar.

Figure 3.5: Loaded Launch Device

On triggering the parafoil inflation subsystem the rotating arm inflates the canopy and accelerates it until the arm reaches vertical. Once the arrestor line is engaged the payload acceleration system is triggered automatically, launching the payload down the track. The parafoil/payload system takes flight and descends in a glide slope ideally dictated by the parafoil rigging angle. This device launches the parafoil/payload either

horizontally or at a downward angle, implying that the device must be situated on top of a steep hill of cliff to ensure the longest flight possible.

CHAPTER 4

CONCEPTUAL DESIGN

4.1 CONCEPT IDENTIFICATION

Published parafoil inflation and test techniques provided a starting point from which to begin for launching unmanned parafoils. After manually flying the 6.07 m^2 parafoil like a kite, the suitability of Brown's towed launch method [22] was the first option to be considered for unmanned launch. This conceptual testing took place in a car park with the parafoil secured to the roof of a vehicle which towed it into a slight breeze. Multiple runs were completed of which one is shown in Figure 4.1 where the canopy was not controlled by deflecting the trailing edge flaps, as its suitability for autonomous launch was to be investigated.

Figure 4.1: Tow Test Behind Vehicle

The outcome of the tow testing indicated that the parafoil inflated somewhat consistently but was considerably unstable about the roll axis and rolled over as shown in Figure 4.1. This testing provided insight into the inflation process and development of further concepts began.

The concept of inflating a parafoil with a rotating motion was first identified in the author's previous work. The successful implementation of this method sparked various other concepts to materialise. These concepts were modelled and compared to one another in order to identify the most suitable design that would best meet the specifications. The concepts considered are now explained where after the angular velocity and displacement characteristics of each concept are compared and discussed.

4.1.1 COUNTERWEIGHT CONCEPT

Trebuchet devices are able to hurl projectiles very efficiently with the use of a counterweight and a sling in which the projectile is placed. Their suitability to inflate parafoils in a stable manner was somewhat questionable, resulting in the sling being omitted and the payload placed at the end of the arm in order to constrain the inflating parafoil for this concept. Figure 4.2 shows the Counterweight Concept configuration.

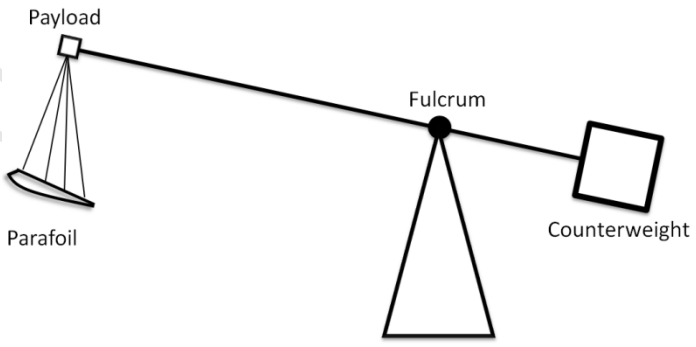

Figure 4.2: The Counterweight Concept

This Counterweight Concept was modelled in order to determine the required counterweight mass to accelerate the payload to the specified release velocity. Initially a model based on conservation of energy was outlined where after a force analysis led to the definition of the angular velocity profile for the concept. Details of the model are presented in Appendix A. This included an approximation for the drag of the parafoil.

4.1.2 Pneumatic Link Concept

Pneumatics was identified as a possible energising source as regulation of the operating pressure or exhaust port flow rate allows for adjustment of actuator speed which would have been useful in the proposed system. A mechanism was developed which consists of a rotating arm, driven by a link connected to a pneumatic piston as shown in Figure 4.3. The parafoil, suspended beneath the payload attached to the end of the arm is flung outward and inflated as the arm rotates.

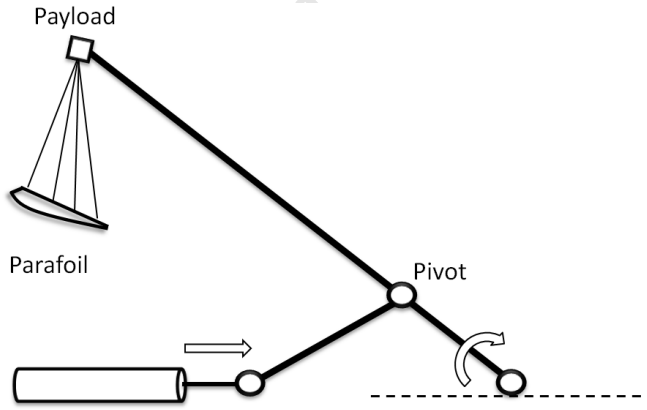

Figure 4.3: Pneumatic Link Concept

This concept was modelled assuming that the velocity of the piston was constant in order to determine the angular velocity of the arm and asses its suitability to deploy the parafoil/payload system. The development and optimisation of the model is detailed in Appendix A.

4.1.3 PNEUMATIC SLIDER CONCEPT

This sliding concept was developed to minimise the radial forces on the driving pneumatic actuator and to manipulate the limited stroke length to provide a longer range over which the force can be applied. Once again pneumatics was intended as the energising source due to its advantages in terms of controllability and automation. This concept consisted of a beam that is rotated by means of a slider coupled to an actuator via a cable passing over pulleys as shown in Figure 4.4.

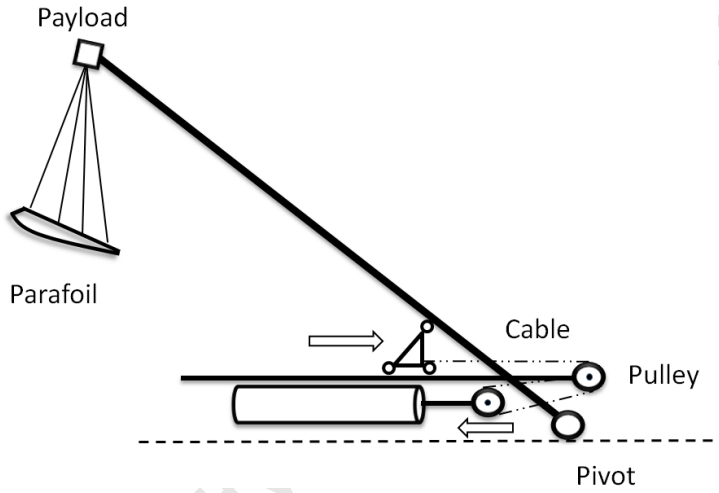

Figure 4.4: Pneumatic Slider Concept

As the piston is retracted, the slider moves along the track while transmitting a force to rotate the arm and release the parafoil. The slider would move at double the speed of the actuator due to the purchase system. A detailed analysis of the mechanism and its characteristics can be found in Appendix A. This concept does not include a method to decelerate the arm as this would have been investigated had the concept been selected.

4.1.4 SPRING CONCEPT

In an effort to reduce the mass and complexity of the launch system, a concept energised by means of springs was developed which would allow for more manageable transportation. Springs, capable of being connected in series or parallel, provide flexibility in terms of adding or removing energy for launching various size parafoils. This concept consists of a spring attached to the arm as well as to the catapult base structure as indicated in Figure 4.5.

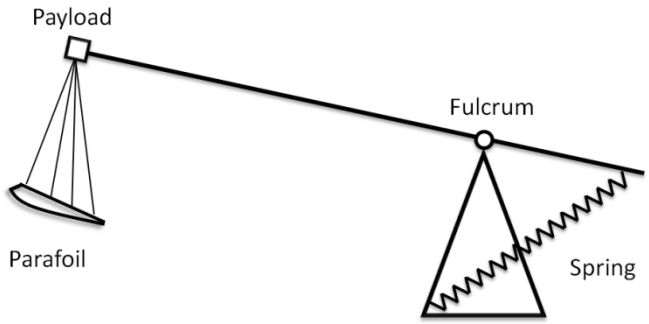

Figure 4.5: Spring Concept

The arm would be winched down from the vertical rest position to load the catapult as shown. Once released the spring contracts and flings the parafoil/payload system into the air. An analysis of this concept is outlined in Appendix A.

A performance comparison of the above mentioned concepts is detailed on the following page.

4.2 Comparison of Concepts

Each concept modelled was optimised to best meet the specifications of the launch system. The four concepts with their unique characteristics are now compared to one another where after their advantages and disadvantages are discussed.

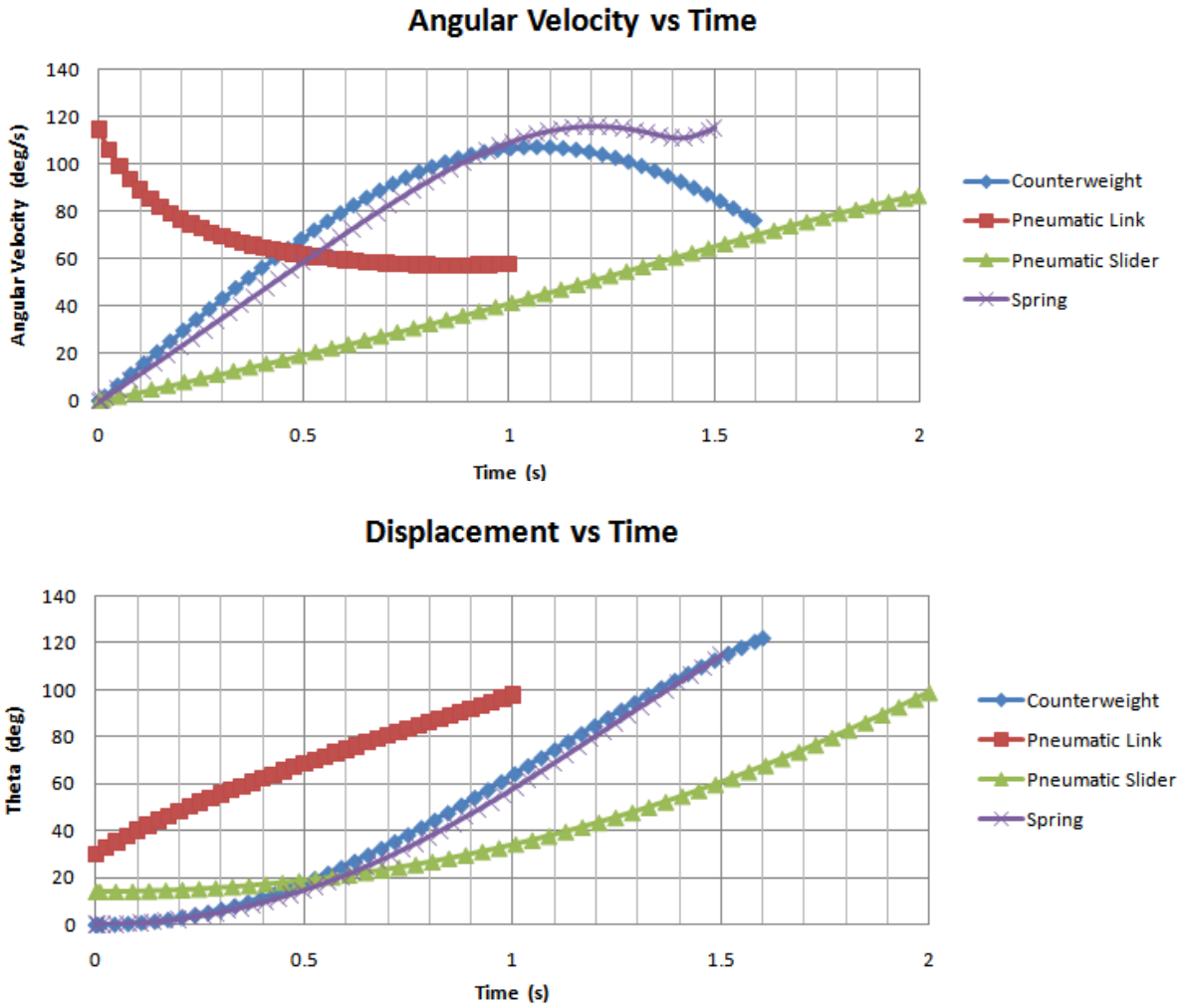

Figure 4.6: Concept Comparison Graphs

Figure 4.6 shows the angular velocity and displacement versus time plots for the concepts considered. Ideally, when the arm reaches vertical (theta = 1.57 rad) the payload would be released in the case of each concept. When each plot on the

displacement versus time graph crosses the $\frac{\pi}{2}$ radian value on the vertical axis, the corresponding time value was noted and projected to the angular velocity graph to find the velocity of the arm at release.

4.2.1 Counterweight Concept Discussion

Although the angular velocity profile was ideal in that the velocity is relatively constant at release, an excessively large counterweight of 2 400 kg with a 10 m arm would be required to achieve this. Advantages of this concept included simplistic design, reduced overshoot if the counterweight was hinged and knowledge that this concept had worked on a smaller scale. Some of the disadvantages include the requirement of specialised equipment to move the counterweight mass, awkward on-site assembly and an extremely large test facility.

4.2.2 Pneumatic Link Concept Discussion

This concept provided a satisfactory angular velocity profile with no acceleration at the vertical position but a lower release velocity when compared to the other concepts. Due to the layout of the concept, an excessively large initial force would be required to accelerate the 10 m arm with the force profile not well suited to pneumatic actuation. The radial reaction forces exerted by the link onto the piston would require careful consideration as commercially available pneumatic actuators cannot support the calculated radial load. Furthermore the custom machining of cylinder end caps and the size of reservoir required, resulted in exceptional size and complexity for an autonomous launch.

4.2.3 Pneumatic Slider Concept Discussion

This concept provided a steady increase in velocity, almost reaching the specified speed but continued to accelerate as the arm passed vertical. This was undesirable as a constant release velocity was preferred to ensure the parafoil/payload system was deployed in a more stable state. The use of cable and pulleys does allow for suitable

manipulation of the input force but would require a rigid arm on which the slider applies the force. This increased mass and resulting inertia adding to the energy losses in the pulleys and wheels would be detrimental to the efficiency. Deceleration of the arm would need to be considered which increases complexity in an already complex concept.

4.2.4 Spring Concept Discussion

The spring concept provided the most flexibility in terms of modifying the acceleration profile. The velocity profile closely follows that of the counterweight concept which has been found to be suitable for launching parafoils on a smaller scale. The spring concept achieves this velocity profile without the disadvantages of transporting and assembling a heavy counterweight. This concept was considered to be easier to implement and operate then the other concepts. Operation independent of an external power source was possible and reconfiguring spring layout allowed for adjustment of launch characteristics for various canopy and payload sizes.

4.3 Further Concept Development

With the most suitable concept and energising source identified, further development began in order to assess whether any improvement or increase in efficiency was possible. The major hurdle involved reducing the overall size of the proposed structure to make transport, construction, assembly and testing more affordable and manageable while still achieving a suitable launch.

An innovative modification to the concept involved moving the payload down the arm toward the fulcrum to reduce the rotational inertia of the system. This would decrease the required arm length at the cost of reducing the payloads linear velocity at release. A Cross bar or ‘hangar’ would be placed at the end of the arm over which the parafoil suspension lines would lie with the canopy hanging off the end. Theoretically this

method could reduce the overall size of the launch system quite substantially, but the actual implementation and launch capability remained questionable.

To assess the practicality of this method, it was decided to modify the existing counterweight catapult previously used for model parafoil launch, to test the proposed modification.

4.3.1 Preparation for Concept Testing

To accommodate adjustment of the payload position along the arm, an aluminium mounting was designed that could clamp onto the arm in any desired position. The payload was then secured to this mounting via an automatic release device that would detach the payload. The release device made use of a spring loaded pin that was released by an electro-magnet linked to an infra-red switching system which could be triggered at varied inclinations of the arm. Details of the automatic release device and associated systems can be found in Appendix A. A cross-section of the release device in the half open position is shown in Figure 4.7.

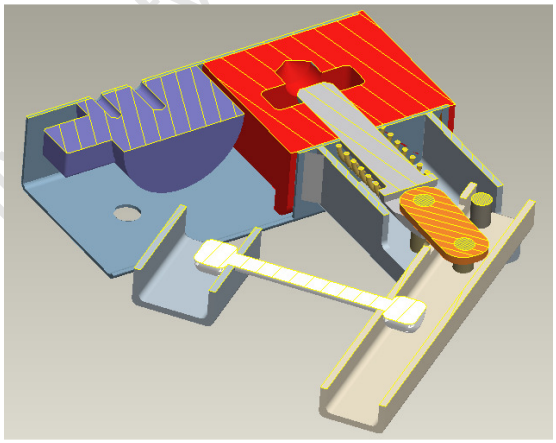

Figure 4.7: Cross-Section of Release Device

The model parafoil (1.2 m^2) was connected to a 1.2 kg payload fitted with white boards on either side to ensure it was visible during testing. This payload then fitted into the

release device pictured above. An appropriate spring was purchased and fitted to the catapult in the position identified by the theoretical model.

4.3.2 Concept Testing and Results

Testing took place on a gradual slope on the University of Cape Town's Upper Campus. Multiple tests were completed where the payload was moved further down the arm toward the fulcrum in each test. In all tests the parafoil inflated well and the payload detached perfectly. The resulting flight trajectories were not ideal in that the initial glide slope was on average 38° which is well below the benchmark glide slope obtained from previous testing of 22°, providing a more suitable range. This was the case for all the tests except Test 3 which provided an outstanding glide slope of 12.7° and a stable flight as shown in Figure 4.8.

Figure 4.8: Test 3 - Shallow Glide Slope

Figure 4.9: Typical Glide Slope for Test Series

This shallow glide slope is compared to the typical deep glide slope shown in Figure 4.9 where the payload positions along the arm are similar.

An obvious trend relating the glide slope to payload position could not be determined from the results of the testing. However, analysing the video footage of each test led to a remarkable discovery in the case of Test 3 which identified the reason for its outstanding trajectory. Directly after release, the payload was struck by the rotating arm which provided additional force to accelerate the payload. This suggested that the payload velocity is critical for a shallow glide slope and its velocity should be comparable to that of the parafoil for a successful launch and flight trajectory.

This finding led to the development of the final concept which reduced the overall size and weight of the launch device to manageable levels.

4.4 SUBSYSTEM CONCEPT

Noting the results of the conceptual tests with the model parafoil, it was decided to treat the parafoil and payload acceleration requirements independently. This resulted in a concept consisting of two separate subsystems, one that would inflate the parafoil and one to accelerate the payload. In this way, the rotational inertia of the arm is considerably reduced and the payload mass is removed from the rotational mechanism. The efficiency of the inflation subsystem is hence drastically improved as the total rotational inertia is greatly reduced. The layout of this concept is outlined in Figure 4.10.

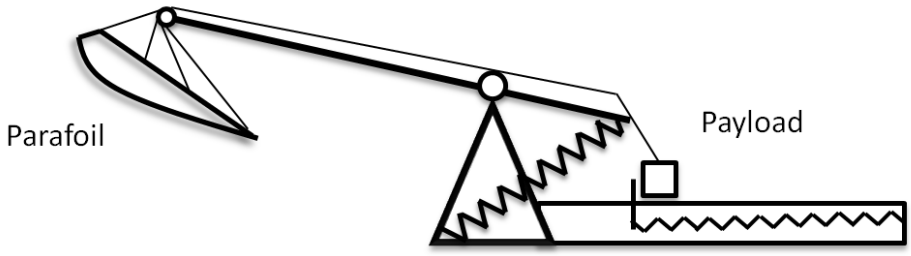

Figure 4.10: Subsystem Concept

The parafoil hangs just over the end of the arm supported by the hangar. Its suspension lines would extend to the payload placed on the linear acceleration subsystem. During launch the canopy is inflated and flung into the air as the payload is accelerated down the track and released.

Although this concept is relatively complex in that the timing of the two systems would be critical, the reduction in size and modular construction ensured manageable assembly and transportation of the system. Springs provided an energy source that could operate without an external power source with the flexibility of accommodating various payload velocities. Disadvantages included keeping the suspension lines clear from snagging the rig during launch as well as the integration of the two subsystems.

CHAPTER 5

PARAFOIL INFLATION SUBSYSTEM

5.1 INTRODUCTION

Once the chosen concept was selected, detailed design began on the first subsystem. Assessment of the existing catapult frame, constructed by the author at undergraduate level, displayed adequate strength with which to support the increased loading of the larger canopy. Apart from cost saving potential, the time and resources required to modify the existing frame, compared to constructing a new structure, was the logical decision in the busy university workshop environment. The resulting design incorporated this original frame where the added modifications are detailed below. Thereafter the assembled subsystem tests are presented.

5.2 STRUCTURE MODIFICATION

To inflate and accelerate the 6 m^2 parafoil to release velocity, additional energy was to be added to the model launch rig to accommodate the drag of the larger canopy. The spring model outlined in Appendix A was adjusted to simulate parafoil inflation without a payload mass. Optimisation of the mathematical model indicated that two 1.5 kJ springs (of the type used in garage doors) placed in parallel would be sufficient to overcome the drag and accelerate the canopy. The attachment points on either end of

the springs, providing the most suitable angular velocity profile for parafoil inflation were identified and the maximum force exerted by the spring combination was found to be 6,2 kN.

With this maximum force outlined, a stress analysis was performed on the load bearing components to ensure adequate safety factors were maintained. Strengthening of the main shaft and addition of a stronger cross beam support were identified as key area's requiring an upgrade. The modifications are outlined below.

5.2.1 CROSSBEAM SUPPORT

A stronger cross beam was designed to support the force exerted by the springs which would act in the middle of the unsupported span. Bending calculations were applied to determine the required flexural rigidity of the beam and defined a suitable steel section. See Appendix B for details.

5.2.2 SHAFT

The hollow shaft supporting the arm via y-bearings was replaced with a solid steel shaft (grade M303) to provide a safety factor of 2. The formula used can be found in Appendix B. Although this safety factor was slightly lower than planned, it meant that the existing bearings and bushes could be used, saving both cost and machining time while still ensuring adequate safety.

5.2.3 HANGAR

An aluminium crossbar or 'hangar' was designed to attach onto the end of the arm for the spread of parafoil lines to pass over as they extend down to the payload. See Figure 5.1. This hangar served as a pivot around which the parafoil rotates as it inflates and moves toward a co-linear position with the arm.

5.2.4 Frame Stability

The stability of the structure needed to be increased to prevent the frame from toppling forward during the initial inflation of the canopy as the spring force caused the rear side of the frame to lift off the ground. With the completion of a force analysis involving the centre of gravity of the frame, it was decided to attach removable steel tubing legs to increase the inertia and stabilise the frame during launch as shown in Figure 5.1

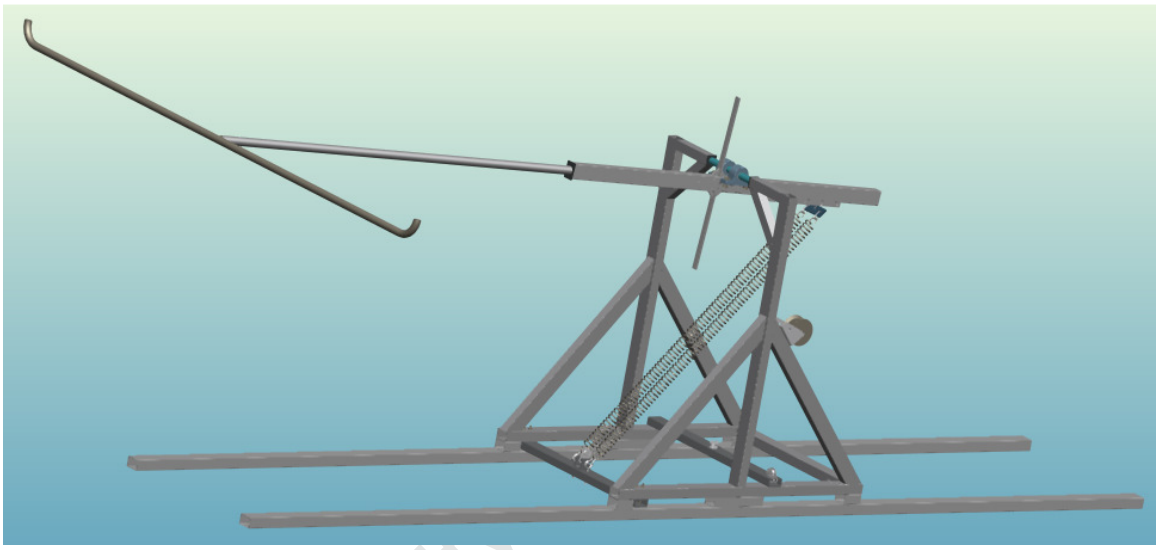

Figure 5.1: Parafoil Inflation Subsystem with Removable Legs

Various other stabilising options such as weights placed on the frame or stakes driven into the ground were considered. Although the legs were somewhat tedious to bolt into place while the frame lay on its side, it allowed the direction and placement of the rig to be easily adjusted between tests without damaging the ground. The legs accommodate for any launch surface and were no more difficult to transport than the arm itself.

5.3 LOADING SYSTEM

The force required to load the catapult arm to the horizontal position was calculated to be 2860 N. This indicated the need for a loading system that would give the operator sufficient mechanical advantage to repeatedly load the device for multiple tests. Several configurations of loading systems were considered before a final layout was selected which placed a hand operated trailer winch (453 kg line pull) in a position that provided easy and safe operation. Pulleys redirected the loading cable as shown in Figure 5.2 through the frame and onto the winch drum.

Figure 5.2: Loading System

The loading cable was attached to a strop on the arm via a snap shackle used to trigger the release of the arm. The quick release snap shackle, rated for a working load of 1 280 kg, was released by pulling the trigger line (line coiled up in Figure 5.2) which extended to 5 m to ensure the operator was safely clear of the rig during launch.

5.4 Arm Deceleration System

To prevent the arm with the added inertia of the hangar from overshooting the vertical position and interfering with the parafoil/payload system after release, a deceleration system was needed to arrest the rotating arm. Assessment of various concepts was undertaken where after the most suitable concept was implemented. This consisted of an arrestor line mounted across the path of the swinging arm which was directed by means of pulleys to the bottom of the frame to an elastic cord which absorbed the energy. Figure 5.3 shows the orientation of the arrestor line deceleration system which is engaged when the arm reaches the vertical.

Figure 5.3: Arrestor Line Deceleration System

5.5 Parafoil Inflation Testing

Once all the systems had been assembled the arm was secured in place and supported with a stay forward and aft for flexural rigidity in the vertical plane. The parafoil was placed over the hangar and the suspension lines fastened to the arm in order to test the subsystem‘s ability to inflate the parafoil without releasing a payload. Multiple tests were performed where the loading angle was increased for each test until full load was obtained. The results of these subsystem tests were encouraging as the parafoil inflated

well in each test (see Appendix B for an image) and the deceleration system prevented the arm from any excessive overshoot.

Analysing the video footage of the tests by stepping through the frames enabled the inclination of the arm to be measured for each time step. This provided data which could be plotted and compared to the theoretical model to assess its accuracy. The results of two tests are plotted in Figure 5.4 along with the predicted performance of the theoretical model. The initial approximation modelling the parafoil drag as a "flat plate" was assumed to be the worst case scenario, however plotting test data with the model's data (Figure 5.4) indicates that this approximation was closely matched to the actual drag performance of the canopy during launch.

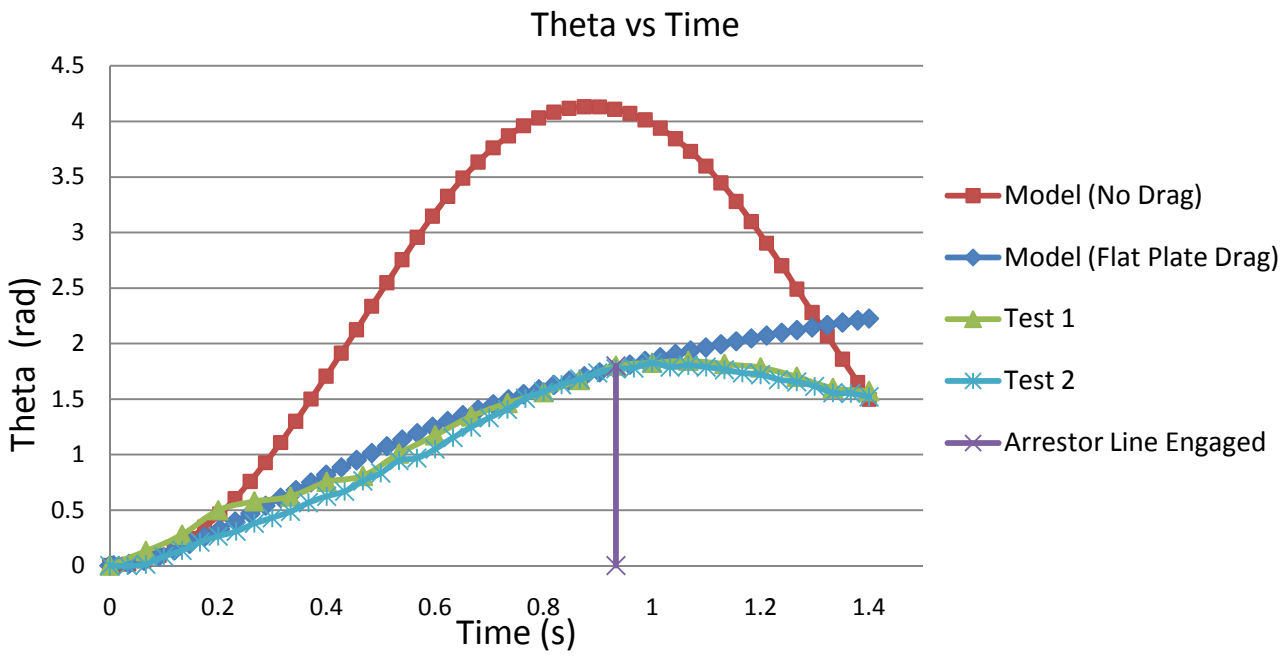

Figure 5.4: Actual Performance vs Theoretical Model Prediction

The vertical line in Figure 5.4 indicates the time at which the arrester line is engaged where after the actual test results show the arm decelerating. The theoretical model does not take the arrestor line into account and thus the predicted and test results were

expected to diverge from that point onwards. The accuracy of the measured data points are estimated to be within 2° (0.035 rad) on either side as slight blurring of the arm in the respective video frames was present.

Figure 5.4 shows the exceptional velocity (the gradient) predicted by the model for the case where parafoil drag is not included in the launch simulation. This case was tested where the parafoil was excluded, producing a “no load” test of the subsystem. This test was a failure as the aft support stay snapped when the arrestor line was engaged and resulted in the aluminium arm bending at the point where it exits the bush inserted into steel tube section of the arm. The support stays were replaced with higher gauge steel cable and the parafoil inflation subsystem was determined to be fully capable of inflating the 6 m^2 parafoil in a repeatable fashion as required for launch.

CHAPTER 6

PAYLOAD ACCELERATION SUBSYSTEM

6.1 INTRODUCTION

Successful implementation of the inflation subsystem led to the design phase of the payload acceleration subsystem with which it would interface. Accelerating the payload required four times the energy used for parafoil inflation, indicating the need to assess multiple sources to ensure adequate, yet safe operation.

This chapter details the process in which the payload acceleration subsystem was modelled, designed, constructed and tested in order to be integrated with the first subsystem to form the complete launch device.

6.2 ENERGISING SOURCE

The specifications indicated that a payload of up to 80 kg be released at 15 m/s. Pneumatics, electric motors, rockets, petrol engines, hydraulics and springs were considered as energising sources to meet this energy requirement for payload acceleration. Each source was assessed in terms of mass, cost, power requirement,

repeatability and complexity to implement, in order to identify the most practical solution. Pneumatics was regarded as a likely candidate where additional detail can be found in Appendix C. Springs were eventually chosen over pneumatics as they offered lower cost, ease of transportation and significantly reduced complexity with regard to control of the system.

6.3 SPRING MODEL

A model was created which simulated the spring loaded system in order to determine the force necessary to release the payload at the defined velocity. A combination of garage door springs was used for their high spring constant and modular capability in adding or removing energy from the system. Each spring could comfortably provide 1.5 kJ of energy without permanent deformation. Eight such springs were arranged in four parallel sets of two springs in series to ensure adequate energy was supplied. It was decided to link the end of the springs to a rope which passes around a pulley before attaching to the trolley holding the payload mass, in order to optimise the length of the subsystem. This configuration also decelerated the trolley once it had passed over the pulley by extending the springs once again and promoting detachment of the payload while reducing trolley overshoot. The orientation is shown in Figure 6.1 in the loaded state.

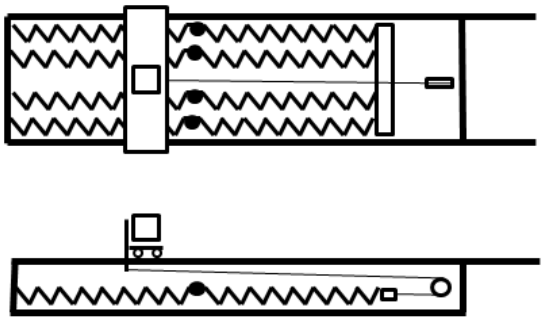

Figure 6.1: Payload Acceleration Concept – Top and Front Views

Identifying the effective spring constant (see Appendix C) and the extension of the springs, the applied force was determined which enabled the acceleration profile of the payload to be defined. Numerically integrating the acceleration for an 80 kg payload provided plots for the velocity and displacement with respect to time as shown in Figure 6.2. This was checked analytically as shown in Appendix C. Losses are not included which can be noticed by the trolley's oscillating movement after payload release, Figure 6.2.

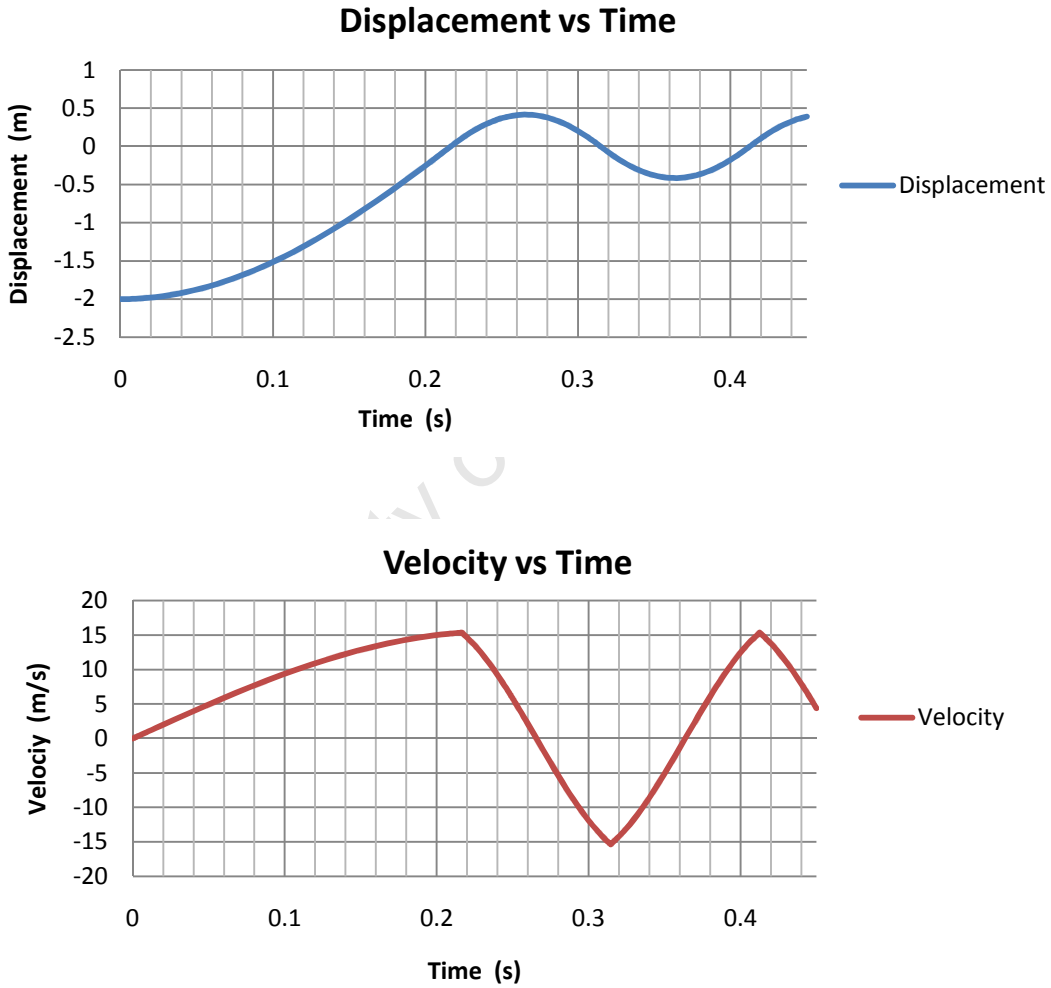

Figure 6.2: Spring Model Results

It is assumed that the payload detaches precisely at the point where the trolley passes the pulley and begins to decelerate. The loading force for this configuration was 8856 N. Adjusting the configuration for a 40 kg payload involved removing four springs which

provided sufficient energy to release the payload at the required velocity in a similar manner.

This concept offered flexibility with regard to release velocity and payload mass while operating without externally provided power, assuming the system could be loaded either by hand winch or battery operated electric winch.

6.4 TRACK DESIGN

In an effort to minimise mass and ensure transportability, aluminium was defined as the material of choice which in addition provided good resistance to corrosion. Bosch Rexroth components supplied by Tectra Automation, offered a convenient solution for the track as mentioned in Chapter 3. This range of components, designed for the manufacturing industry to allow for quick assembly and easy reconfiguration, was ideally suited to the developmental nature of this project.

With the spring force defined, the loading on the track could be determined and an appropriate design developed. The track would experience both radial loads from the payload as well as high compression loads from the springs when fully loaded as explained in Appendix C. The cross beam supporting the pulley (Figure 6.3) was specified with a suitable strength safety factor. The pulley was mounted on steel plates through which the beam passed, as discussed in Appendix C.

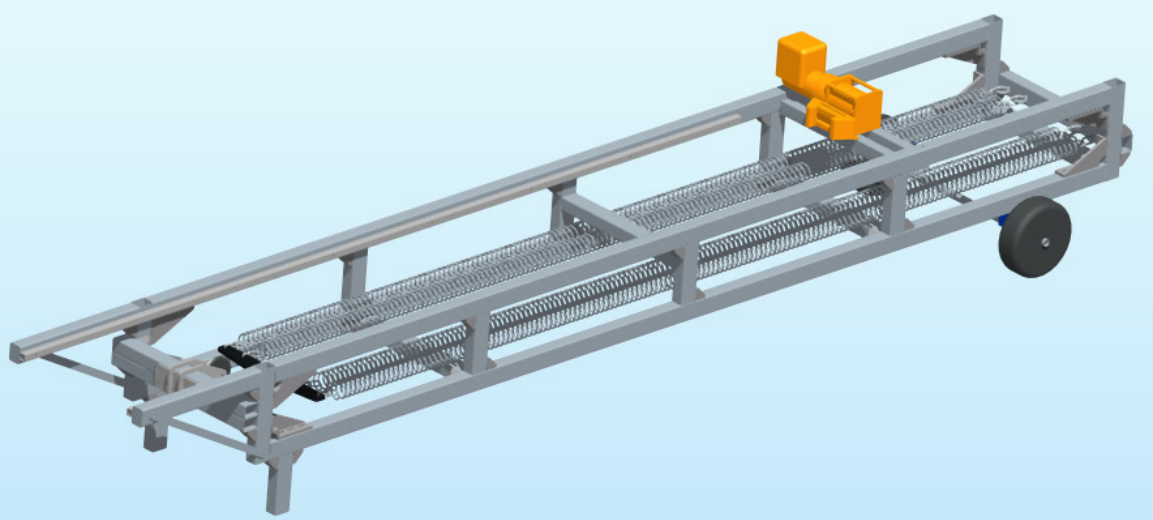

Figure 6.3: Track Design

The remote operated loading winch shown in Figure 6.3 was mounted onto two square steel tubes welded to an 8 mm steel plate. This American manufactured WARN battery operated electric winch was rated for a working load of 1678 kg enabling it to easily load the springs in less than 15 seconds. The winch mounting experiences both shear and torsion for which design calculations can be found in Appendix C. Power for the winch was supplied by a 12 Volt, 80 Ah deep cycle battery which was easily transportable.

6.5 Trolley Design

Multiple configurations of rollers and guides were considered for the design of the trolley which supports the payload along the track. Low friction, accurate positioning, low mass and rigidity were primary requirements for the design. The chosen concept used polyurethane wheels with skateboard ball bearings that ran on the upper surface of the 60 x 45 aluminium extrusion. The wheels were mounted on steel shafts which were pressed into an HDPE mounting block, details of which can be found in Appendix C. The mounting blocks or “cars” were bolted to a steel frame providing rigidity and alignment as well as supporting the box which houses the payload, Figure 6.4.

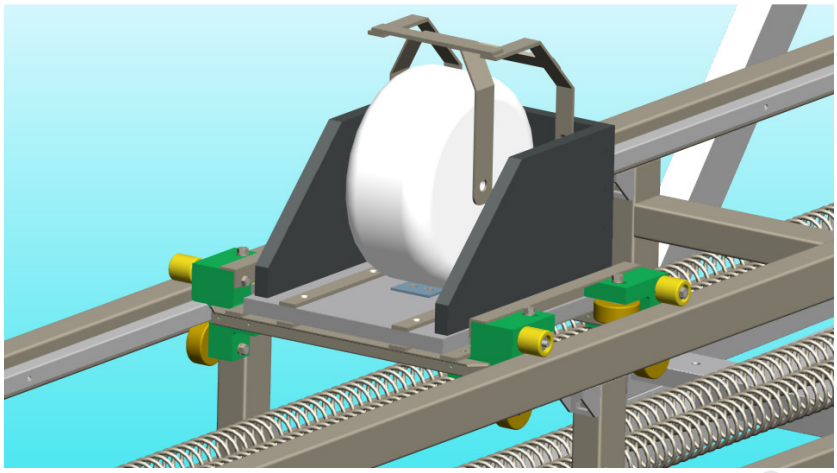

Figure 6.4: The Trolley

The box was constructed from a carbon fibre and high density foam sandwich composite which reduced the mass without compromising strength. The payload consisted of three disk shaped weights that were wrapped in foam to prevent damage on impact. A steel handle bolted to the axle passing through the weights was used as an attachment point for the parafoil. The springs attach to a Dynex rope which passes though the pulley on the frame and attaches to the bottom of the trolley. This trolley is then pulled back to its loaded position by the winch cable which connects via a quick release snap shackle. An image detailing the attachment points for both the rope and snap shackle can be found in Appendix C.

6.6 Subsystem Testing

Once assembly was completed, the payload acceleration subsystem was tested with a 40 kg payload to ensure suitable operation. The loading distance was incremented for each release until full load was obtained. The device performed as predicted where the overshoot was minimal and blocks placed behind the track's pneumatic wheels were necessary to support the reaction force. Figure 6.5 shows a test where the trolley is loaded to its maximum position and the resulting trajectory of the payload is displayed.

Figure 6.5: Payload Acceleration Subsystem Test

The white payload can be seen bouncing off the ground in the above image constructed from frames at constant time intervals. Calculating the release velocity from the video frames indicated that the 40 kg payload was released at 9 m/s at full load. Converting this energy for the case where a 20 kg payload is used resulted in a calculated release velocity of 12.7 m/s. This analysis suggested that approximately 20% of the spring energy is lost to friction between the rope and pulley as well as the rolling resistance of polyurethane wheels on the track.

With the two independent subsystems performing as intended in multiple tests, they were combined to form the complete launch device, ready for flight testing.

CHAPTER 7

TESTING AND RESULTS

7.1 INTRODUCTION

This chapter details the multiple flight tests conducted with the full launch system to assess its capability in launching unmanned parafoils and to determine whether useful data could be extracted from the corresponding flight paths. Explanations of notable tests and results are presented accompanied by trajectory images that portray the dynamics of the parafoil/payload system in flight. The outdoor flight testing was limited to windless days to ensure atmospheric disturbances were kept to a minimum. This played a major role in determining suitable test locations and test schedules.

This chapter begins with a brief explanation of the parafoil rigging angle which defines the trim of the parafoil during stable flight. Thereafter the testing process is detailed and results presented.

7.2 PARAFOIL TRIM

The rigging angle of a parafoil, measured from the quarter chord position on the lower surface of the canopy to the confluence point, dictates the angle of attack (α) and thus glide angle at which the parafoil trims in stable flight. Trim settings with estimated

corresponding α values of 2°, 4°, 6° and 8° were measured and marked on the suspension lines according to a trim model developed by a colleague, Ph.D. student S. Rhodes. Details of the trim settings are displayed in Appendix D. This trim model was the best approximation available for the provisional "proof of concept" testing completed for this project. Deflection of the parafoil's trailing edge flaps was not considered and the control lines were set loose for all tests conducted.

7.3 Initial Flight Test Results

For the initial tests of the launch system the parafoil was trimmed for a low angle of attack value of 2° as outlined in Appendix D. This setting was used so as to provide a shallow glide slope along which the parafoil would trim to maximise the time of flight above the gradually sloping hill on which the assembled launch system was situated. Loading the system with a 21 kg payload clipped to the parafoil suspension lines, the parafoil/payload system was launched from the maximum load condition down the track. The parafoil inflated and the payload detached as expected, resulting in the flight trajectory shown in Figure 7.1 where intervals between frames are fixed 0.33 seconds apart. A description of the method used to generate trajectory images such as Figure 7.1 can be found in Appendix D.

Figure 7.1: Initial Launch System Test

Analysis of this test showed that as the payload was released, the suspension lines were not completely taught but tensioned soon afterwards as the payload mass was supported by the canopy. The canopy flew smoothly until striking the ground as shown in the last frame in Figure 7.1. Analysis of the video footage indicated that the payload was released at 11.6 m/s which was possibly too fast when compared to the predicted glide speed of 7.5 m/s as outlined in Appendix D. Plotting the payload trajectory at fixed intervals of 0.067 seconds for this test showed the payload oscillating slightly, then descending more steeply before it struck the ground, Figure 7.2.

Figure 7.2: Payload Trajectory in Initial Test

This indicates that the parafoil had not reached its stable glide state in which the payload descends at a fixed angle, and thus a longer flight would be necessary to identify this glide slope. The oscillation of the payload hints that the flight modes from which the dynamic motion of the parafoil/payload system is comprised, may possibly be extracted should the flight path be long enough for a full period of oscillation to be identified.

Seven launches were conducted in this test series with similar results, with the exception of a few tests in which the payload lifted out of the trolley prematurely, resulting in the parafoil/payload system falling short of the expected range. This problem was solved by adding the steel hook to the trolley which constrained the payload from lifting out prematurely. Further modifications included the addition of a spreader bar between the payload and the suspension lines of the parafoil. This divided the port and starboard suspension lines which connect at two separate confluence points. Figure D.3, showing the layout of the payload spreader bar and parafoil can be found in Appendix D. Separating the lines allowed the rotating arm to swing through between the two confluence points and prevented the lines from snagging during launch. According to Müller et al [24], an increase in the separation distance of the

confluence points increases the stability of the payload oscillating around the vertical axis. Separation of the confluence points is a common practise found on most manned and unmanned parafoil systems.

7.4 SECOND TEST SERIES

With the launch capability successfully demonstrated in the initial test series, further tests were conducted in order to obtain flight data from the video footage of the flight path. Objectives included achieving a longer flight path from which the glide slope for various rigging angle settings could be measured as well as variation of the release velocity to find the optimum launch velocity.

The second test series took place on a windless day which turned out to be exceptionally rare in Cape Town. The parafoil was rigged for alpha angles of 2°, 4° and 6° for which a noticeable difference could not be determined as the corresponding flights were once again relatively short and the parafoil/payload system did not settle into a fixed (measurable) glide slope. Appendix D contains a trajectory image showing this lack of steadiness in the flight path. Nine tests were completed during which the launch system operated flawlessly, indicating that the minor technical issues mentioned before had been resolved.

Variation of the release velocity provided good results. Although the image quality is poor, Test 5 shown in Figure 7.3 clearly indicates how the 4° rigged canopy approaches stall after launch when the payload is accelerated to 11.6 m/s. The excess kinetic energy of the payload causes it to move well in front of the canopy which then stalls slightly, before dropping at a steeper glide angle.

Figure 7.3: Launch Above Optimum Velocity

This exchange of potential and kinetic energy along a sinusoidal flight path can be characterised by the phugoid dynamic stability mode as outlined by Cook[25]. Detail can be found in Appendix D. Figure 7.4 shows the trajectory of the payload for the same test where consecutive payload images are 0.27 seconds apart.

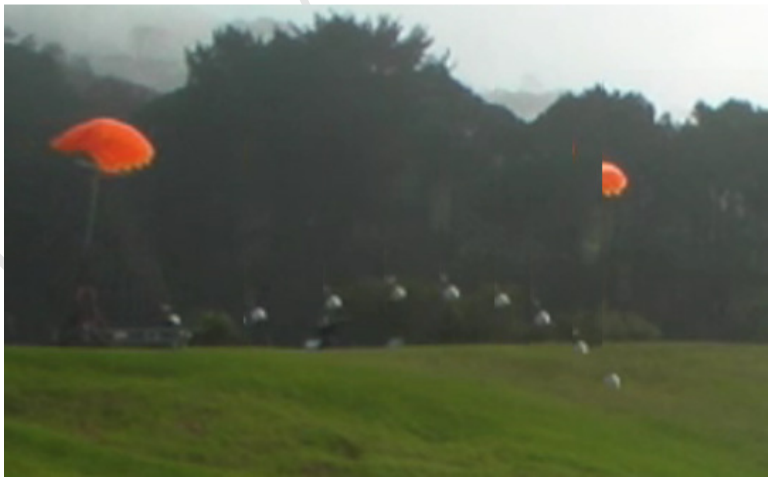

Figure 7.4: Payload Trajectory Test 5

Classical approximations indicated that this lightly damped, low frequency oscillation is directly proportional to the velocity of the body [26] as shown in Appendix D. For the above mentioned test the period of oscillation was approximated from Figure 7.4 which

was found to be 4.2 seconds, somewhat matching the predicted phugoid period of 3.6 seconds for a flight velocity of 8 m/s. This analysis is not accurate and ideally a complete oscillatory period would be required to characterise the motion. Had consecutive amplitudes of the oscillation been measurable, the damping factor ζ could have been determined providing a useful result.

The payload release velocity was then reduced incrementally where the optimum was determined to be approximately 8.4 m/s in windless conditions. Release velocities below 7.7 m/s were tricky to compare as the resulting trajectories were very short due to the low gradient of the grass slope.

Variation of the track's inclination indicated that an inclination below the horizontal improved range when compared to horizontal launch. The downward velocity component ensured the suspension lines remained taught during launch and the payload velocity vector was better aligned with the expected glide slope. Short flight times remained a limiting factor for accurate flight path analysis and dynamic mode identification. Further testing was then conducted at a steeper launch site in an attempt to obtain a longer flight path.

7.5 Cross Wind Test Series

Poor judgement of the weather forecast resulted in a brief test series which took place in an eight to twelve knot cross wind. Wind gusts during the inflation process caused the windward wingtip to curl underneath the canopy and prevented adequate inflation, resulting in the canopy collapsing, Figure D.6.

The other 3 tests in the series were successful. The canopy turned into the wind in each case. Figure D.7 showing this flight path can be found in Appendix D.

7.6 FINAL TEST SERIES

The dry dock facility at Simon's Town naval base was identified as a suitable launch site for testing the launch system. The dry dock is deep with close to vertical sides and its interior is somewhat protected from wind. Once permission and access for vehicles carrying test equipment had been granted for the naval base, a test date was set based on a five day weather forecast.

Unfortunately weather conditions were not ideal on the test day as a moderate South-Easterly breeze was blowing down the length of the dry dock. Testing began none the less. The parafoil/payload system was launched into the wind initially. Results were unsatisfactory as the canopy stalled and turned unpredictably in the gusts before dropping steeply to the floor of the dry dock.

A move to a more protected end of the dry dock allowed for launch in the direction of the prevailing wind. A number of launches were executed in between gusts. The launch device was placed on a trolley to clear an obstacle (bollard used to secure ships in the dry dock) as shown in Figure 7.5. The track was inclined at an angle of 6,3° below the horizontal. Two assistants were required to hold the parafoil prior to launch to prevent the wind from moving the canopy.

Figure 7.5: Launch device in loaded state

Five tests were conducted from this launch position on the south side of the dry dock. Two parafoil trim angles were tested at two different velocities. Unfortunately the number of flight tests was limited due to time constraints. The first test in this position, Test 4, provided a good flight with the launch velocity set to 8.4 m/s where the parafoil angle of attack was rigged for 6°. Test 5 was a repeat of test 4 with the release velocity increased to 11.6 m/s. Both flights settled into a steady glide slope with the slower release velocity resulting in the parafoil settling into glide sooner. Launch at the higher velocity (Test 5) is shown in Figure 7.6 which depicts the motion of the parafoil/payload system.

Figure 7.6: Launch at 11,6 m/s With α Set to 6° (Test 5)

The 13.5 m deep dry dock was relatively narrow which limited the location of the video camera to capture the flight paths for the various tests. The camera perspective shown in Figure 7.6 provided adequate coverage of the launches and corresponding flights although contact of the payload with the bottom of the dry dock could not be captured due to the limited field of view. This camera angle was not directly perpendicular to the flight path but was fixed for all tests completed, allowing for glide angles to be

compared. Figure 7.7 shows a plot of the payload for Test 5 where the glide slope is measured with respect to the horizontal of the video frame. This apparent glide slope was found to be approximately 44° for both Test 4 and 5 where the angle of attack was constant at 6°.

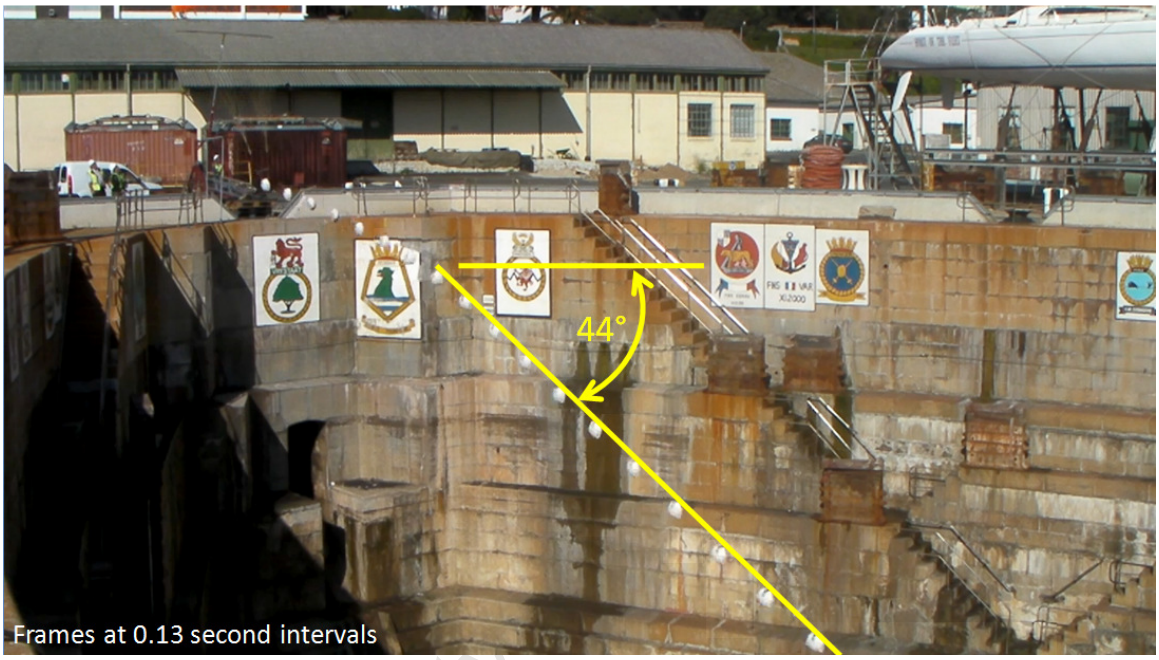

Figure 7.7: Apparent Glide Slope Measurement Test 5

It is important to note that the stated glide angle of 44° in Figure 7.7 is not the exact glide slope angle as would be seen by a camera perpendicular to the flight. However, as the camera was positioned in the same position for all flights, glide path angles could be compared to some degree.

Tests 6 and 7 were conducted with release velocity settings of 8,4 m/s and 11,6 m/s, respectively, and the parafoil was trimmed for an angle of attack of 2°. Analysis of the Test 6 flight video showed that the parafoil did not inflate perfectly due to a wind disturbance and the canopy did not trim to a stable glide. Test 7 resulted in a good stable flight as shown in Figure 7.8. The payload can be seen to be yellow due to the

application of yellow duct tape used to reattach the foam padding which was damaged on touchdown in the previous test.

Figure 7.8: Launch at 11,6 m/s With α Set to 2° (Test 7)

Plotting the payload trajectory only, indicated that the parafoil/payload system settled into a stable apparent glide slope of 40°, Figure 7.9.

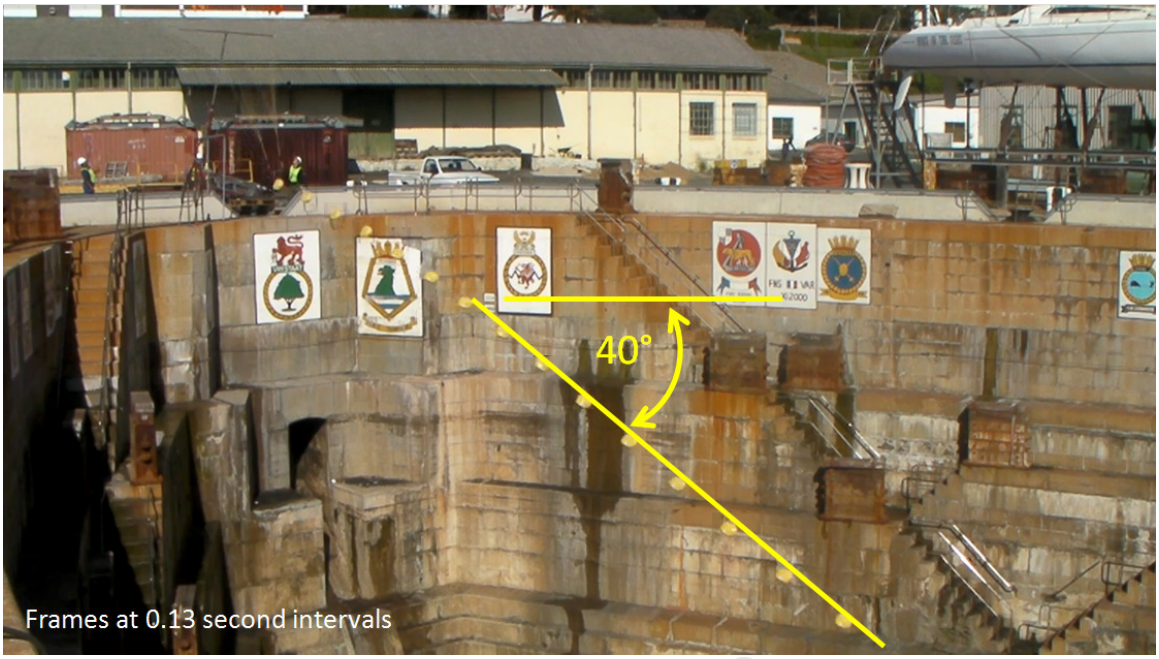

Figure 7.9: Glide Slope Measurement Test 7

Test 8 was conducted with a lighter payload (10 kg) where the trim angle remained fixed at 2°. The track was loaded to the 8.4 m/s setting used in previous tests although the actual release velocity would be closer to 12 m/s due to the payload mass being halved. This test was a failure as the canopy did not inflate consistently (most likely due to wind disturbance) during launch and the payload accelerated beneath a partially filled parafoil. After release the suspension lines finally tensioned uniformly and the canopy inflated, only to fly into the side wall of the dry dock, indicating the consequences of irregular inflation.

CHAPTER 8

CONCLUSIONS AND RECOMMENDATIONS

8.1 INTRODUCTION

This chapter concludes this design, construction and test project. The performance of the launch system is measured against the specifications and the practicality of the device outlined. Recommendations are listed to guide further research involving launch and flight trajectory analysis of unmanned parafoil systems.

8.2 DESIGN AND IMPLEMENTATION

The parafoil launch system worked well and successfully demonstrated capabilities that may be useful for future unmanned parafoil flight-analysis projects. The design proved to be effective and efficiently deployed the canopy and payload using relatively low cost springs as the energising source. The modular design incorporating the parafoil inflation and payload acceleration subsystems ensured the launch system could be disassembled to a manageable size for transportation to the various test sites by the department's utility vehicle in a single trip. Assembly of the device at the test site required at least two people and loading the device on and off the utility vehicle required four. Once assembled the system could be loaded for

launch by a single operator and triggered from a safe distance in accordance with the specifications.

The launch system was tested with a 21 kg payload and four springs which successfully deployed the 6 m^2 parafoil with a suitable wing loading condition as shown in the previous chapter. The payload acceleration subsystem was designed to launch 80 kg using eight springs. Although not tested for such large payloads, this ensures increased capacity for future projects with suitably sized parafoils.

8.3 PERFORMANCE

The parafoil launch system performed as expected with the two major subsystems integrating well to deploy the parafoil/payload system in a repeatable manner. The payload release velocity was easily adjusted with the electric winch and provided adequate range for the test series conducted.

The parafoil's susceptibility to wind disturbances was noted when launching into, and across the prevailing wind direction with the canopy turning into the wind while in flight. Wind effects were also noted during launch where cross winds tended to disturb the parafoil's wingtip and led to irregular inflation.

A downward inclination of the track was identified to increase range when compared to horizontal launch as the payload's velocity vector was closer to the trimmed glide slope, resulting in the trim condition occurring earlier.

The limited number of tests performed at the dry dock indicated that parafoil trim angles dictated the glide slope during stable flight where α angles of 6° and 2° resulted in glide slopes of 44° and 40° respectively (as measured from the camera's perspective). This indicates that the launch system is a suitable test platform from which future parafoil trim studies could be conducted.

8.4 TESTING RECOMMENDATIONS

To improve the number of tests and quality of results, it is recommended that a dedicated launch site with minimal atmospheric disturbances be identified where access can be granted for a few days to allow for a full battery of tests to be completed. A large aircraft hangar may be ideal should elevation of the launch device be possible.

Mounting accelerometers and gyroscopes onto the payload and canopy could provide a more detailed analysis of the dynamic behaviour of the system in flight. The trajectory images constructed displayed the general trend in test flights but failed to provide accurate dynamic data of the system. Camera angles were also a limiting factor. Availability of improved data may aid in the identification of the dynamic flight modes of the parafoil/payload system. Further recommendations include launching higher performance canopies where higher lift to drag ratios may reduce the height requirement of the launch site yet still provide suitable flight duration. Increasing canopy aspect ratio and cascading the suspension lines may improve the lift to drag ratio and result in a shallower glide.

8.5 DESIGN RECOMMENDATIONS

Recommendations regarding the design of the launch system include automating the trigger of the payload acceleration subsystem and adding protective screens around the springs in the track. These modifications would improve safety and reduce the time required for the operator to be in close proximity to the loaded launch device.

Furthermore, the weight of the steel frame of the parafoil inflation subsystem could be reduced and the method of attaching the stabilising legs could be improved.

REFERENCES

[1] A. Max, Men of The Red Beret. London, UK: Century Hutchinson Ltd, 1990.

[2] C.A. Knapp and W. R. Barton, "Controlled Recovery of Payloads at Large Glide Distances, Using the Para-Foil," Journal of Aircraft, vol. 5, no. 2, p. 112, 1967.

[3] Dutch Space - An EADS Astrium company. http://www.dutchspace.nl/pages/business/content.asp?LangType=1033&id=187, [Accessed: Mar. 12, 2009].

[4] T. Wyllie, "Parachute Recovery for UAV Systems," Aircraft Engineering and Aerospace Technology, vol. 73, no. 6, pp. 542-551, 2001.

[5] R.A Machin, "Design and Testing X-38 Spacecraft Primary Parafoil," in AIAA Modeling and Simulation Technologies Conference, Denver, 2000, pp. 14-17.

[6] J. S. Lingard, "Ram-air Parachute Design," in 13th AIAA Aerodynamic Decelerator Systems Technology Conference, Clearwater Beach, 1995, pp. 1-51.

[7] I. Currer and R. Cruickshank, Touching Cloudbase. North Yorkshire: Leading Edge Press, 1992.

[8] J. E. Murray et al., "Further Development and Flight Test of an Autonomous Precision Landing System Using a Parafoil," Dryden Flight Research Center, California, NASA Technical Memorandum 4599, 1994.

[9] H. Altmann and J. Windl, "ParaLander: A Medium-Weight Demonstrator for Autonomous, Range-Optimized Aerial Cargo Delivery," AIAA Aerodynamic Decelerator Systems Technology Conference, 2005, pp. 1-10.

[10] J. Potvin, G. Peek, and B. Brocato, "Modeling the Inflation of Ram-Air Parachutes Reefed with Sliders," Journal of Aircraft, vol. 38, no. 5, pp. 1-10, October 2001.

[11] L.R. Jamison, "A Method for Calculating Parachute Opening Forces for General Deployment Conditions," Journal of Spacecraft, vol. 4, no. 4, pp. 498-502, 1966.

[12] A. G. Sim, E. J. Murray, D.C. Neufeld, and R.D. Reed, "The Development and Flight Test of a Deployable Precision Landing System for Spacecraft Recovery," NASA Dryden Flight Research Facility, California, NASA Technical Memorandum 4525, 1993.

[13] T. Bennet and R. Fox Jr., "DESIGN, DEVELOPMENT & FLIGHT TESTING OF THE NASA X-38 7,500 FT2 PARAFOIL RECOVERY SYSTEM," in 17th AIAA Aerodynamic Decelerator Systems Technology Conference and Seminar, California, 2003, p. 1.

[14] NASA Website. http://www.dfrc.nasa.gov/Gallery/Photo/X-38/Medium/EC01-0339-77.jpg, [Accessed: Mar. 12, 2009].

[15] C. Redelinghuys, "A Flight Simulation Algorithm for a Parafoil Suspending an Air Vehicle,"

Journal of Guidance, Control, and Dynamics, vol. 30, no. 3, pp. 791-803, May-June 2007.

[16] N. Slegers and M. Costello, "Model Predictive Control of a Parafoil and Payload System," Journal of Guidance, Control and Dynamics, vol. 28, no. 4, pp. 816-821, August 2005.

[17] S. Müller, O. Wagner, and G. Sachs, "A High-Fidelity Nonlinear Multibody Simulation Model for Parafoil System," in 17th AIAA Aerodynamic Decelerator Systems Technology Conference, Monterey, California, 2003, pp. 1-10.

[18] M. Dalmasso, Chamonix-Mont-Blanc Website. http://world.chamonix.com/img/bigsportsparapente.jpg, [Accessed: Apr. 20, 2010].

[19] Google Image Result "Paraglider Reverse launch", [Accessed: Sept. 15, 2008].

[20] Google Image Result, "Paragliding Towed Launch". http://en.wikipedia.org/wiki/Paragliding, [Accessed: Apr. 20, 2010].

[21] G.M. Ware and J.L. Hassel Jr., "Wind-Tunnel Investigation of Ram-Air-Inflated All-Flexible Wings of Aspect Ratio 1.0 to 3.0," Langley Research Center, Hampton,Va, NASA Technical Memorandum 1969.

[22] G.J. Brown, "Tethered Parafoil Test Technique," Vertigo Inc., Lake Elsinore, California, AIAA 89-0903 1989.

[23] R.A. Machin, C.S. Iacomini, C.J. Cerimele, and J.M. Stein, "Flight Testing the Parachute System for the Space Station Crew Return Vehicle," Journal of Aircraft, vol. 38, no. 5, pp.

786-799, September-October 2001.

[24] S. Müller, O. Wagner, and G. Sachs, "Dynamic Problems of Parafoil Landing Systems for Reentry Vehicles," Institute of Flight Mechanics and Flight Control, Technische Universität München, Neufahrn, Germany.

[25] M.V Cook, Flight Dynamic Principles, Second Edition. Burlington, MA, USA: Elsevier Ltd, 2007, ch. 6, p. 146.

[26] H. Ashley, Engineering Analysis of Flight Vehicles, D. Bershader, Ed. Reading, Massachusetts, USA: Addison-Wesley, 1974, ch. 7, p. 238.

[27] J.E. Shigley, C.R. Mischke, and R.G. Budynas, Mechanical Engineering Design, Seventh Edition. New York, USA: McGraw-Hill, 2004, ch. 18, p. 941.

[28] J. E. Shigley, C.R. Mischke, and R.G. Budynas, Mechanical Engineering Design, Seventh Edition. New York, USA: McGraw-Hill, 2004, ch. 5, p. 218.

[29] R.J. Roark, Formulas for Stress and Strain Fourth Edition. Tokyo, Japan: McGraw-Hill, 1965, ch. 9, p. 196.

[30] C.S. Iacomini, "Investigation of Large Scale Parafoil Rigging Angles - Analytical and Drop Test Results," in 15th AIAA Aerodynamic Decelerator System Conference, Toulouse, France, 1999.

APPENDIX A

SUPPORTING THEORY AND CALCULATIONS

CONTENTS

The development of a mechanism to launch an unmanned parafoil and payload system is challenging as consistent inflation can be difficult to obtain with ram-air inflated canopies. The specifications define a device capable of transferring a substantial amount of energy to the parafoil/payload system. Analysis of possible concepts was required to ensure the design was practical and within the scope of a partial dissertation.

A.1 MECHANISM MODELLING

The rotating arm technique identified in the author's previous testing of model parafoils has been retained as it was ideally suited to unmanned parafoil inflation, providing consistent inflation when compared to alternative techniques.

The following mechanisms incorporate the rotating arm technique in modified forms to allow launching the large parafoil systems outlined in the specifications. Some of the concepts considered are now detailed where after the most suitable one is selected.

A.1.1 COUNTERWEIGHT CONCEPT

This concept consist of a counterweight mass attached to one end of a rotating arm with the payload and attached parafoil placed on the opposite side as shown in Figure A.1.

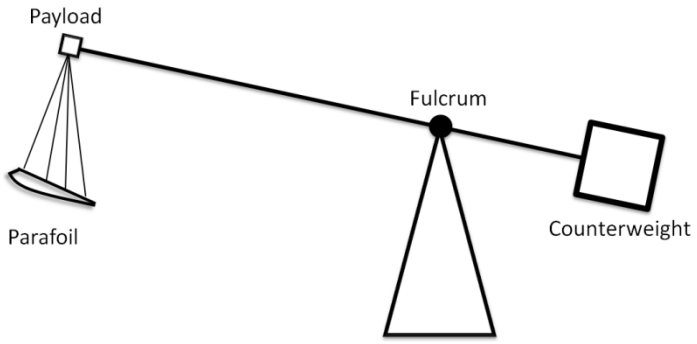

Figure A.1: Counterweight Concept

This system was modelled using the conservation of energy principle. Friction was assumed to be negligible and the systems energy in the initial state was set equal to that in the final state. The arm was approximated as a uniform thin rod with regard to its rotational inertia and the payload and counterweight were both treated as point masses. These assumptions were deemed to be sufficient for this first approximation in assessing the suitability of this concept. The initial gravitational potential energy in the system was equated to the energy in the final state as shown below. The subscripts refer to the counter weight mass, beam mass and payload mass.

$$E_{Initial} = E_{Final}$$

$$M_{cw}gh_{cw_i} + M_b gh_{b_i} = M_b gh_{b_f} + M_p gh_{p_f} + \frac{1}{2}M_{cw}(\omega R_{cw})^2 + \frac{1}{2}M_p\left(\omega R_p\right)^2 + \frac{1}{2}I_b\omega^2 \quad \text{(A.1)}$$

The initial gravitational potential energy of the payload is neglected as it is assumed that the payload rests on the ground in the initial state.

The known rotational inertia of a thin road was used in conjunction with the parallel axis theorem to calculate the rotational inertia of the beam about the fulcrum. The length ratio from counterweight to fulcrum and payload to fulcrum is 1:4.

$$I_b = \frac{13}{75}M_b L^2$$

Solving for ω from eq. (A.1) gives:

$$\omega = \sqrt{\frac{g\left[M_{cw}h_{cw_i} + M_b\left(h_{b_i} - h_{b_f}\right) - M_p h_{p_f}\right]}{\frac{1}{2}\left[M_{cw}{R_{cw}}^2 + M_p{R_p}^2 + I_b\right]}}$$

This equation was used to create plots which characterise the system. The angular velocity was converted to linear velocity by multiplying by the radius from fulcrum to payload to provide the results shown in Figure A.2

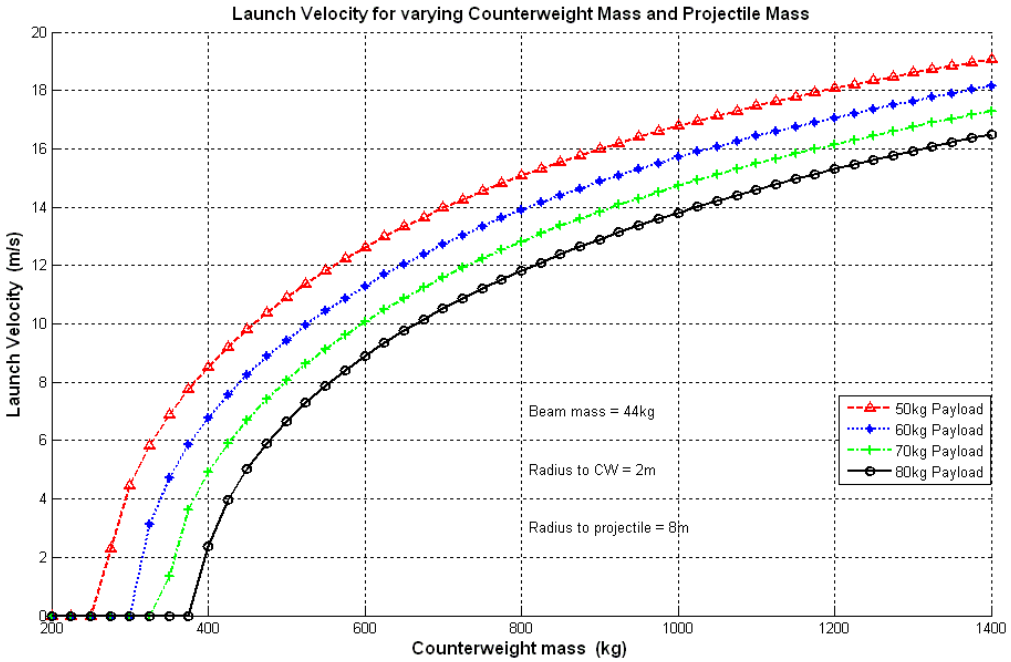

Figure A.2: Energy Required for Counterweight Concept

A counterweight mass weighing approximately 1200 kg would be required to accelerate a payload of 80 kg to the specified 15 m/s as indicated by Figure A.2. This was calculated using a beam mass of 44 kg and beam length of 10 m. This arm length was determined from the basic ratio tested on the scale launcher in which the distance from fulcrum to payload was double that of the parafoil line length. Figure A.2 also indicates that there is a maximum release velocity for this configuration. This maximum possible release velocity was determined by taking the limit of the energy equation as the counterweight mass tends towards infinity. This resulted in a theoretical maximum release velocity of 28 m/s. This energy model does not include the additional drag exerted by the parafoil as it inflates.

With the required counterweight mass defined, approximations for the aerodynamic forces were introduced and a kinetic model based on Newton's second law for moments was developed. It was intended to obtain a continuous solution for the motion as a function of time, and not only the final state. The drag force exerted by the parafoil was

approximated as a flat plate drag condition with a drag coefficient (C_D) of 2 to account for the "worst case" scenario.

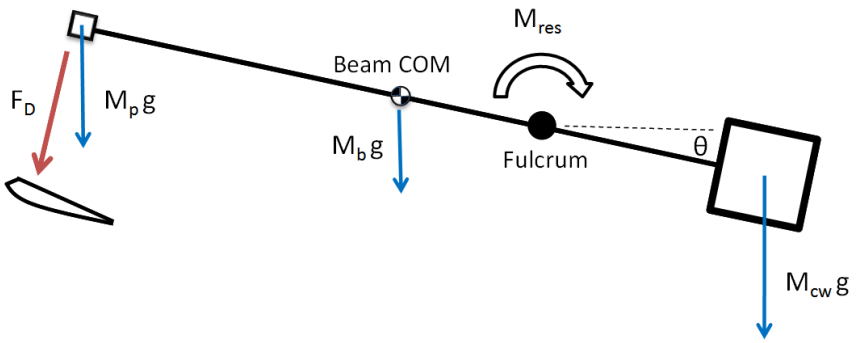

Figure A.3: Forces Creating Moments on Rotating Arm

The moment due to parafoil drag was added to the gravitational moments to allow calculation of angular acceleration from:

$$M_{res} = I_0\ddot{\theta}$$

$$\ddot{\theta} = \frac{-M_p g(R_p cos\theta) - M_b g\left(\frac{3}{10}Lcos\theta\right) - M_{cw} g(R_{cw} cos\theta) - \frac{1}{2}\rho(\dot{\theta}R_p)^2 C_D A_p R_p}{I_0} \quad \text{(A.2)}$$

$$\text{Where } I_0 = I_b + I_p + I_{cw} = \frac{13}{75}M_b L^2 + M_p {R_p}^2 + M_{cw} {R_{cw}}^2$$

This second-order differential equation was solved in *MATLAB* using *ode45* solver which is based on an explicit Runge-Kutta scheme. The equation was represented as a block diagram in *SIMULINK* which can be found in Appendix E. This model outlined the performance characteristics of this concept by plotting displacement and angular velocity versus time for various input parameters. An example is displayed in Figure A.4.

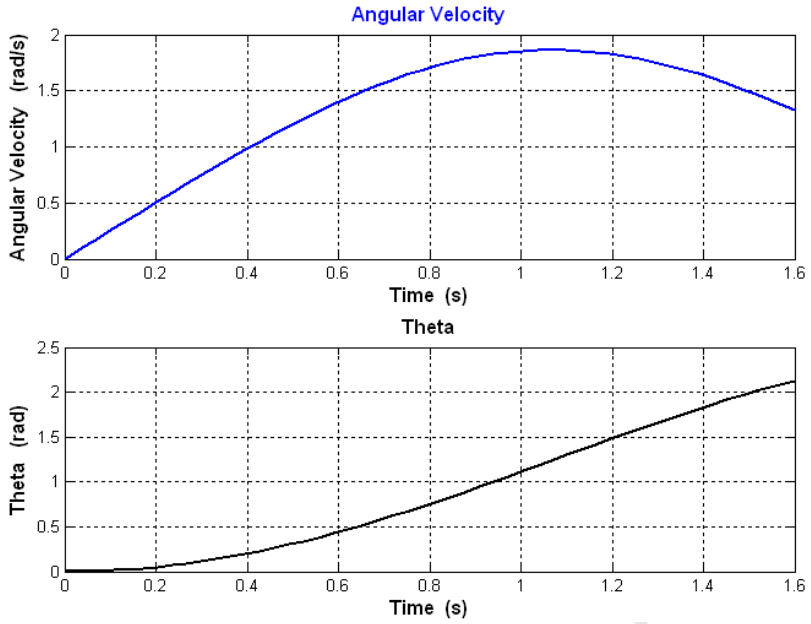

Figure A.4: Angular Velocity and Displacement vs Time for Counterweight Concept

This model provided insight into the acceleration profile that the parafoil and payload would be subject to, where a gradual initial acceleration and constant velocity at release are desired. The payload would ideally detach just before the arm reaches vertical. The model does not account for payload detachment. The inclusion of "flat plate" parafoil drag ensured that the system would be slightly over designed and accommodate for any frictional losses. This inclusion of the drag raised the required counterweight mass to 2 400 kg.

The Counterweight concept provided a suitable acceleration profile for inflating the parafoil and enabled the specified release velocity to be achieved. This concept would require a release mechanism to ensure the payload is detached at the correct time as the arm rotates. Disadvantages include an excessively large counterweight and heavy arm to support this weight as well as the 80 kg payload at the opposite end.

A.1.2 PNEUMATIC LINK CONCEPT

Pneumatics was identified as a possible energising source that can be regulated to drive an actuator at various speeds by adjusting the operating pressure or exhaust port flow rate. A mechanism was developed that consists of a rotating arm which is driven by a linkage connected to a pneumatic piston as shown in Figure A.5.

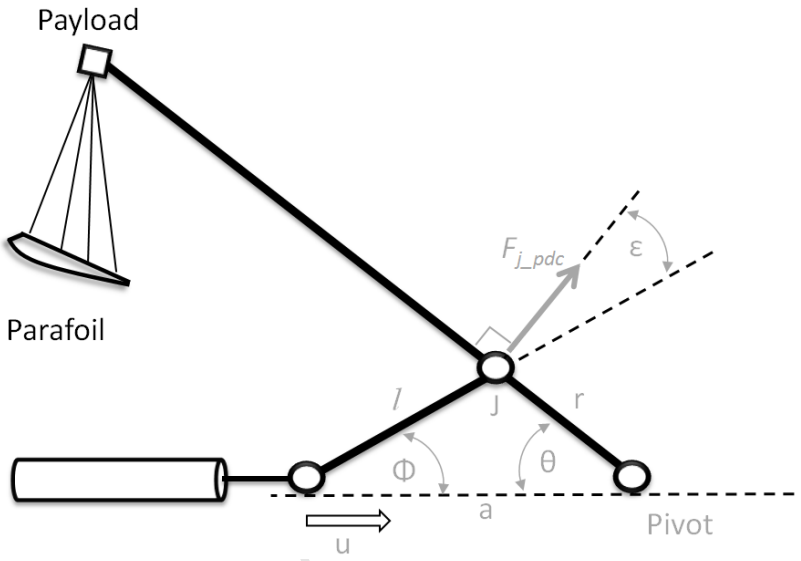

Figure A.5: Pneumatic Link Concept

A mathematical model was developed to simulate the concept and determine the force requirements to launch the parafoil/payload system at the required velocity. It was assumed that the piston velocity 'u' was constant. The various angles of geometry are related by:

$$\varphi = \sin^{-1}\left(\frac{r}{l}\sin\theta\right)$$

$$\varepsilon = \frac{\pi}{2} - (\varphi + \theta)$$

We also have:

$$\dot{a} = -u$$

$$a = l\left(\frac{\cos\varepsilon}{\sin\theta}\right)$$

Writing the cosine rule for angle θ identified an equation which was implicitly differentiated to determine a relationship defining the angular velocity of the arm.

$$\cos\theta = \left(\frac{a^2 + r^2 - l^2}{2ar}\right)$$

$$\therefore -\sin\theta\,\dot{\theta} = \frac{\dot{a}}{2r}\left[1 - \left(\frac{r^2 - l^2}{a^2}\right)\right]$$

Substituting from above and rearranging provides an equation for the angular velocity.

$$\dot{\theta} = \frac{u}{2r\sin\theta}\left[1 - \left(\frac{r^2 - l^2}{a^2}\right)\right]$$

Differentiating this equation once again, resulted in the equation for the angular acceleration of the arm as shown.

$$\ddot{\theta} = \frac{d}{dt}\left[\frac{u}{2r\sin\theta}\left(1 - \frac{r^2 - l^2}{a^2}\right)\right]$$

$$= -\frac{u}{2r(\sin\theta)^2}\cos\theta\,\dot{\theta}\left(1 - \frac{[r^2 - l^2]}{a^2}\right) + \frac{u}{2r\sin\theta}\left(2\,\frac{[r^2 - l^2]}{a^3}\,\dot{a}\right)$$

$$\therefore \ddot{\theta} = -\frac{u}{2r\sin\theta}\left[\frac{1}{\tan\theta}\dot{\theta}\left(1 - \frac{r^2 - l^2}{a^2}\right) + \left(2u\,\frac{r^2 - l^2}{a^3}\right)\right] \qquad \text{(A.3)}$$

The model was optimised by means of changing the lengths of '*r*' and link '*l*' as well as the velocity '*u*' in order to determine the most suitable angular velocity profile and release speed. Figure A.6 graphs the characteristics of this concept for different lengths of link '*l*' where the initial θ value is 30°.

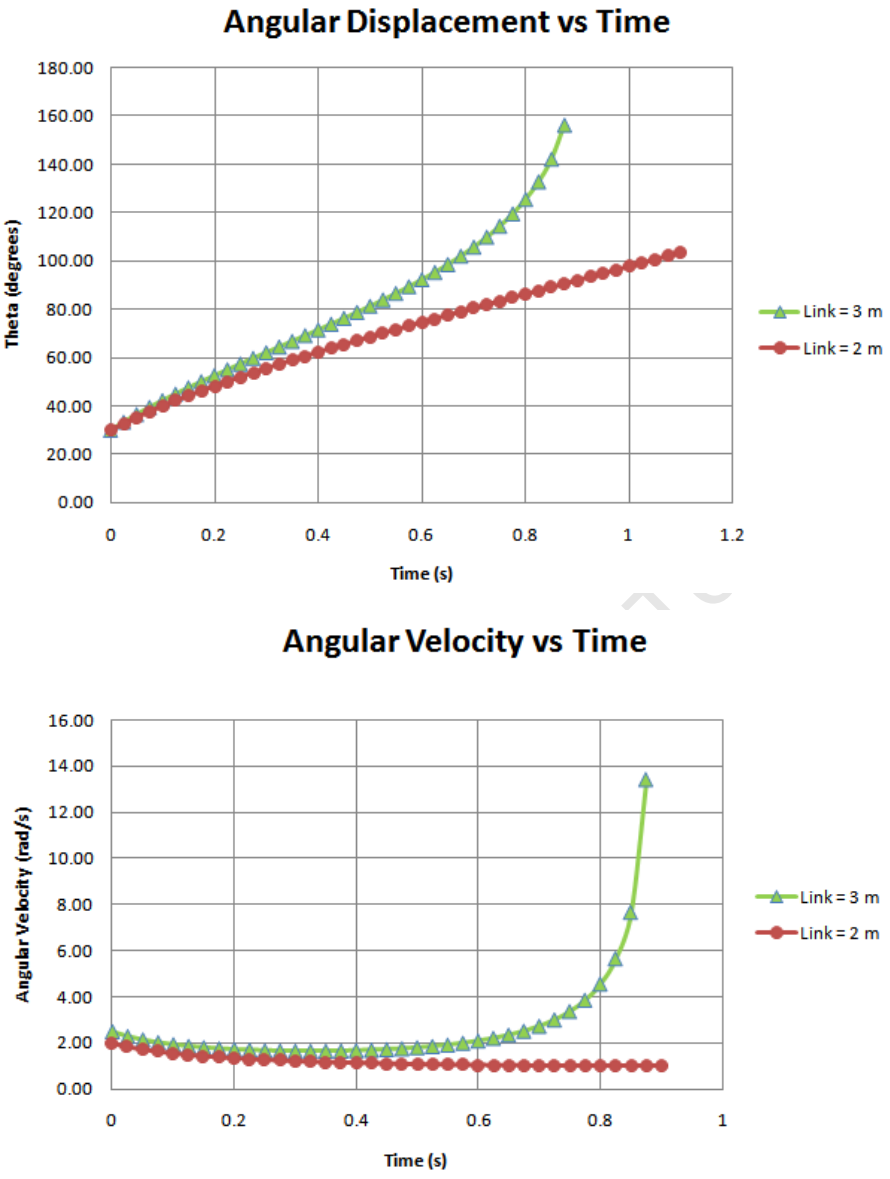

Figure A.6: Characteristics of Pneumatic Link Concept

This conceptual model provided a satisfactory angular velocity profile although the initial velocity would be relatively high as the parafoil is inflating. A link length of 2 m was determined to be the optimum as the release velocity at the vertical was constant with a piston velocity of 4 m/s. A force analysis was completed to specify a pneumatic piston and assess viability of the concept. Applying Euler's Law to this concept and re-

arranging provided an equation for the perpendicular force requirement on the beam at point 'J' which included the parafoil flat plate drag as follows.

$$F_{j\_pdc} = \frac{L}{r}\left[L\left(\frac{M_b}{3} + M_p\right)\ddot{\theta} + g\cos\theta\left(\frac{M_b}{2} + M_p\right) + \frac{1}{2}\rho\left(\dot{\theta}L\right)^2 C_D A_p\right] \qquad \text{(A.4)}$$

A plot of the perpendicular force Fj_pdc required to accelerate the beam to the angular velocity profile in Figure A.6 (link = 2 m) is shown in Figure A.7. It can be seen that an initial force of approximately 12 kN in magnitude is required.

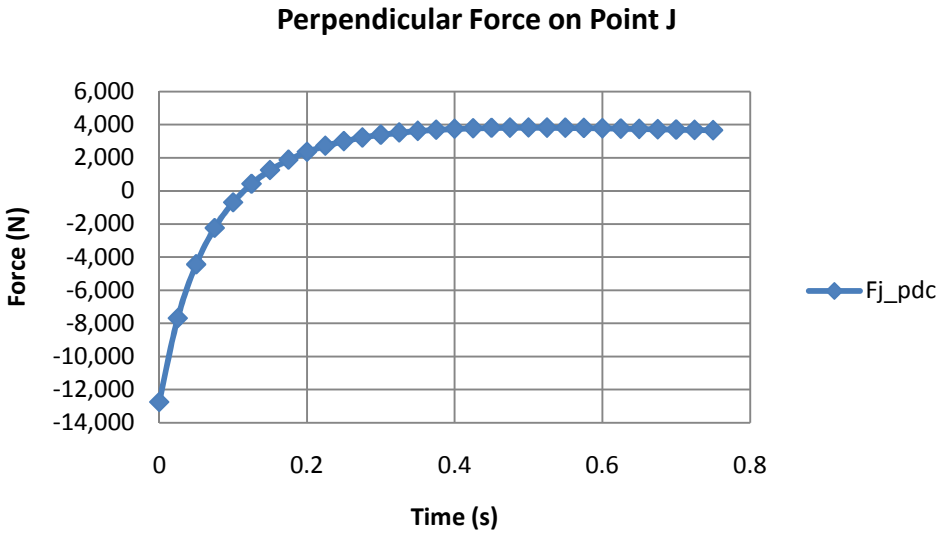

Figure A.7: Perpendicular Force Requirement

Although there are minor inaccuracies in the model such as the instantaneous angular velocity at the initial point, this does not negate the fact that an initial force with a large magnitude will be required. Considering the force applied from the link onto the arm at pivot 'J' (of which the perpendicular force is a component) amplifies this initial force requirement substantially at small θ values. After meeting with a local pneumatic system supplier FESTO, it was suggested that this force profile would not be ideally suited to a pneumatic drive. Additional difficulties included the sheer size of the

actuator and accumulator required as well as the cost of custom machining additional ports in the end cap and the automated control system. Further complications include supporting the large reaction force on the piston as the maximum radial load that a pneumatic piston with an outer diameter of 125 mm (largest standard cylinder bore diameter) can accommodate is 1000 N at 5% stroke length. The largest stroke length commercially available is 2000 mm.

This concept would require an automated release device to be designed to detach the payload at the desired angle. The scale and cost of implementing this concept resulted in this being an unsuitable option and thus further concepts were investigated.

A.1.3 Pneumatic Slider Concept

To address the problem of radial forces on a pneumatic actuator, a sliding concept was introduced which could utilise the advantages that pneumatic actuators offer in terms of controllability and automation. This concept consisted of a beam that is rotated by means of a pneumatically energised slider that moves along a linear track as shown in Figure A.8.

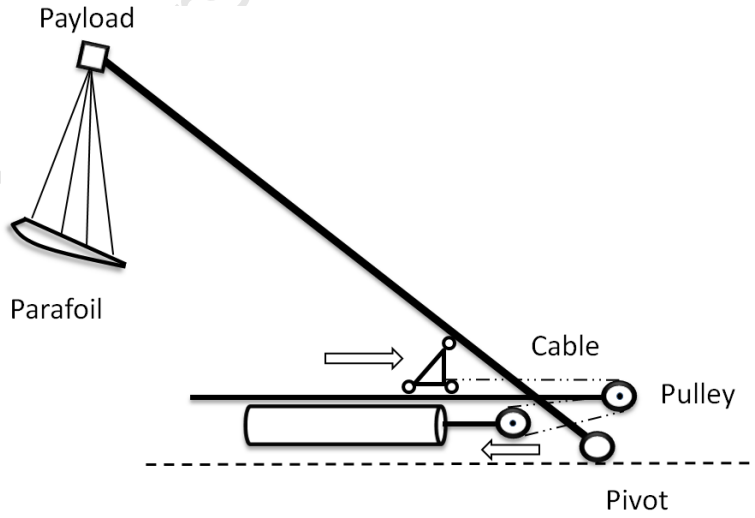

Figure A.8: Pneumatic Slider Concept

The pneumatic actuator retracts the piston and accelerates the slider via a purchase system consisting of a pulley fixed to the piston and one secured to the fixed track. This allows the slider's range to be double that of the piston stroke (limited to 2000m) with the slider's velocity double that of the piston's velocity. The slider would roll on two parallel tracks in the horizontal plane and slide along the beam via a roller that transmits the load to rotate the beam. The parafoil is suspended below the payload which is attached to the end of the arm as in the previous concepts. A model was developed to allow optimisation of the angular velocity profile and the force requirement in order to assess the viability of the concept. It was assumed there was no friction between the rolling components and that the actuator supplied a constant force along its stroke. The parafoil drag (approximated as a flat plate) was taken into account in the force analysis as shown below in Figure A.9.

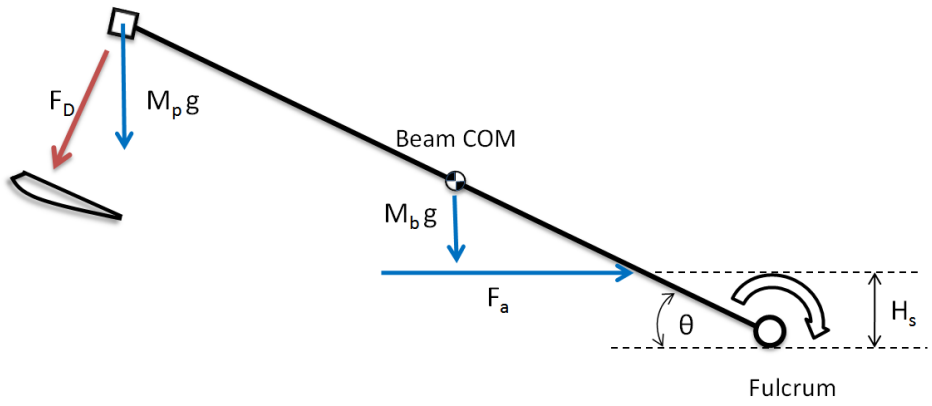

Figure A.9: Forces Creating a Moment on the Arm - Pneumatic Slider Concept

An equation for the angular acceleration of the arm was determined from the forces identified in Figure A.9 where the height of the slider above the horizontal datum is denoted as H_s.

$$\ddot{\theta} = \frac{-F_a H_s + L\left[g\cos\theta\left(\frac{M_b}{2} + M_p\right) + \frac{1}{2}\rho\left(\dot{\theta}L\right)^2 C_D A_p\right]}{I_0} \qquad \text{(A.5)}$$

$$\text{Where} \quad I_0 = I_b + I_p = L^2\left(\frac{M_b}{3} + M_p\right)$$

This equation was formed into a block diagram in *SIMULINK* (Figure E.2) which was integrated numerically to provide the plots shown in Figure A.10, characterising this concept for a constant applied force of 14921 N. This force was defined using two 125 mm bore pistons at an operating pressure of 12 bar in which the force on the slider is halved through the purchase system. The length of H_s was 0.24 m and the initial angle θ = 14° in the rest position.

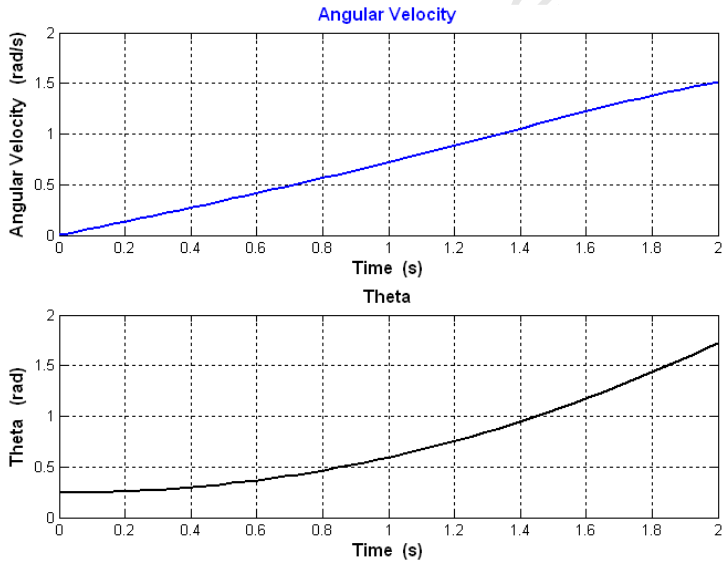

Figure A.10: Characteristics of Pneumatic Slider Concept

It can be seen from Figure A.10 that angular velocity increases almost linearly and reaches approximately 1.5 rad/s when the arm is vertical. This equates to a release velocity of 12 m/s for an 8 m arm which is slightly below the velocity specification of 15 m/s. The angular velocity is still increasing at this point and thus was determined not to be ideal as a more constant release velocity was desired for the payload and parafoil to

settle into a stable glide state. This concept does not account for the deceleration of the arm after it has reached vertical and would require further investigation. Once again the size and expense of a pneumatic system is somewhat problematic.

A.14 SPRING CONCEPT

In an effort to reduce the size and external power requirement of the energising source, a concept using springs was developed. Springs offer flexibility in terms of changing the angle of the spring and or the number of springs in various configurations. Loading the springs manually with a hand winch would allow testing on remote sites without the requirement of an external power source. The structure of the concept is displayed in Figure A.11.

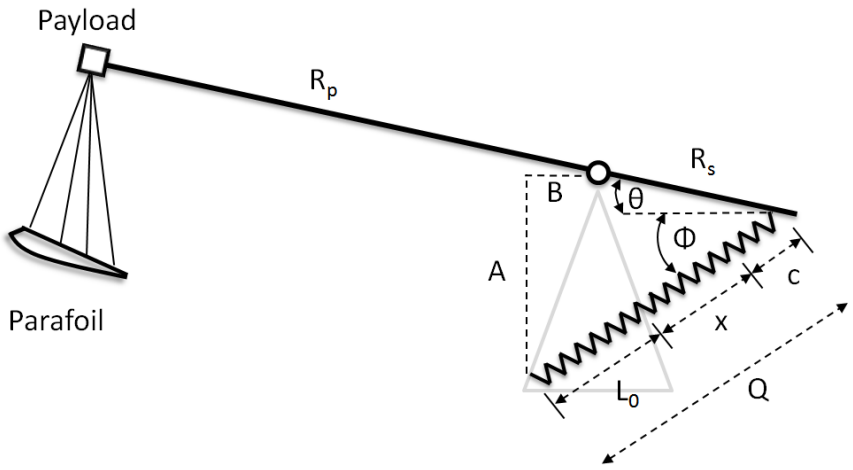

Figure A.11: Spring Concept

A model was created to optimise the placement and stiffness coefficient of the required spring element. It was assumed that the spring operated in its linear range. Summing the moments about the fulcrum in a manner similar to the previous concepts provided the angular acceleration equation. Parafoil "flat plate" drag is included.

$$\mathrm{Q} = \sqrt{(\mathrm{A} - \mathrm{R_s} \sin\theta)^2 + (B + \mathrm{R_s} \cos\theta)^2}$$

$$F_s = kx = k(Q - L_0 - c)$$

$$I_0 = I_b + I_p = \frac{13}{75} M_b L^2 + M_p {R_p}^2$$

$$\ddot{\theta} = \frac{F_s \sin(\theta + \varphi) R_s - \frac{1}{2}\rho \dot{\theta}^2 {R_p}^3 C_D A_p - g \cos\theta \left(M_p R_p + M_b \left[\frac{L}{2} - R_s\right]\right)}{I_0} \qquad \text{(A.6)}$$

Equation (A.6) was represented by a block diagram in *SIMULINK,* (Figure E.3*)* and integrated numerically to enable optimisation of the concept. The spring securing points (lengths A and B, Figure A.11) and spring constant (k) were varied to find optimum launch characteristics. For example, Figure A.12 shows the effect on the angular velocity profile for a change in the vertical position (length A) of the spring attachment point.

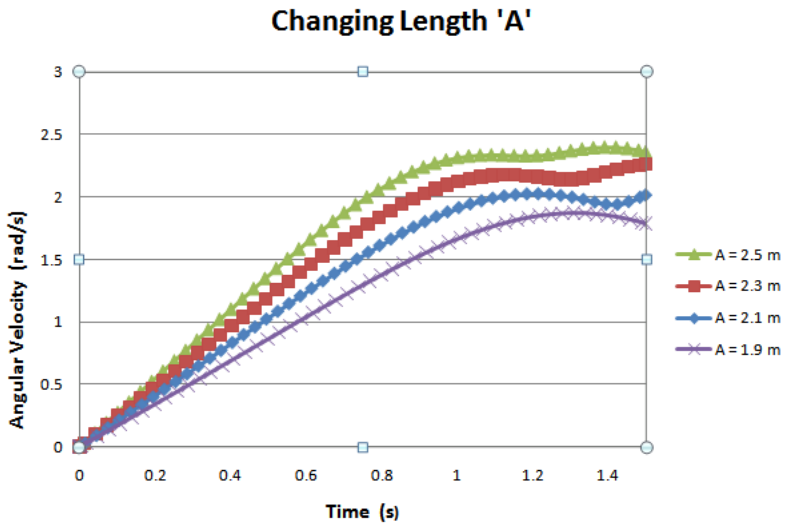

Figure A.12: Effect of Changing Vertical Spring Securing Point

This concept was noted for its flexibility as modifying the input variables could significantly change the velocity profile. Figure A.12 shows how the maximum velocity can be adjusted by small increments of the spring's attachment point.

A.2 Release Device Design

In preparation for conceptual testing, a system to release the payload at any given inclination of the arm was designed. It was required to be triggered electronically so that adjustment of the device's position on the arm could be easily accommodated. It was also required that the payload be released with a high reliability to avoid the parafoil lines from snagging and being damaged by the catapult.

A spring loaded design was developed which was triggered by means of an electromagnet. A 12 volt electromagnet, with a holding force of 35 kg was obtained, as well as a coil spring (18 mm outer diameter) for which the stiffness constant was determined to be 2300 N/m. The device is loaded with the lever locked in place when the steel block contacts the energised electromagnet. The components of the release device are indicated in Figure A.13, which shows the device half open.

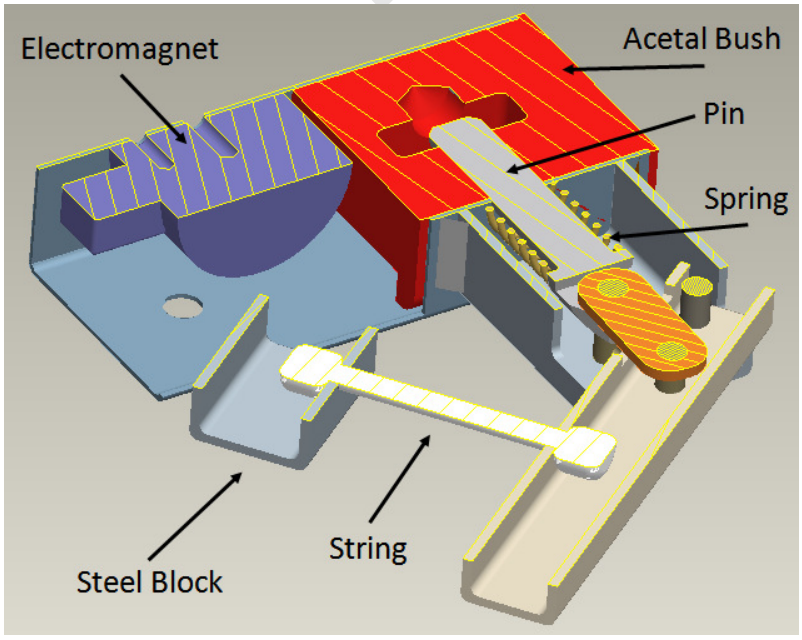

Figure A.13: Cross Section of Release Device

An eye attached to the bottom of the payload was inserted into the device and held in place by the spring loaded pin which passes through it. When the electromagnet is disengaged, the pin is forced outwards with a force of 46 N, releasing the payload. The stainless steel pin was machined to a sliding fit tolerance of H7 g6 within the Acetal bush and was oiled to ensure release under load.

An infra-red switching device was designed to switch off the electromagnet and thus trigger the release of the payload. When an object passed between the infra-red transmitter and the receiver, the voltage across the electromagnet was switched to zero by a relay in the electronic circuit. This autonomous triggering device worked well ensuring that release occurred at the predetermined position. This triggering device was used for the conceptual tests with the model parafoil and was not incorporated in the final design.

APPENDIX B

PARAFOIL INFLATION SUBSYSTEM

CONTENTS

This appendix includes design calculations and a test image relating to the parafoil inflation subsystem. An assembly drawing of this subsystem can be found in Appendix F on page F 3.

B.1 CROSSBEAM SUPPORT CALCULATION

The loading condition on the cross beam includes the force from each spring as well as the force required to load the arm exerted through the loading cable. Figure C.1 shows the loading condition.

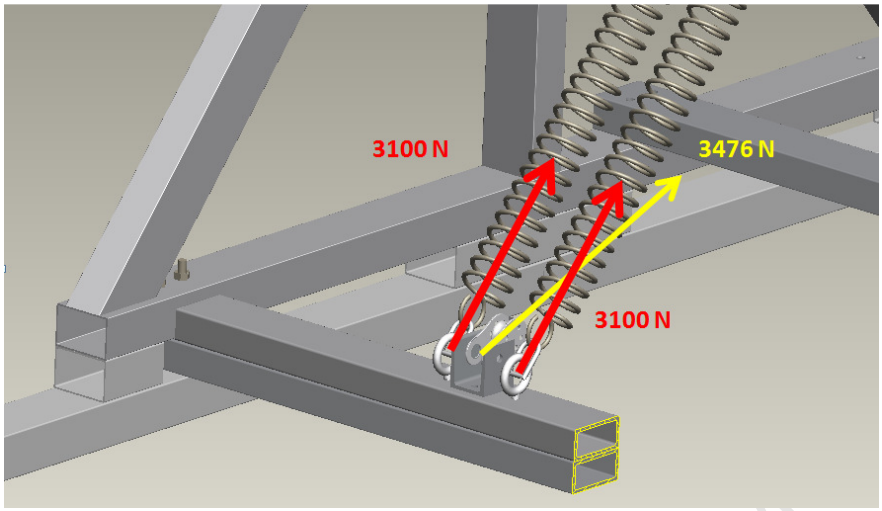

Figure B.1: Cross-section of Crossbeam Showing Loading Condition

Decomposing these forces into their vertical and horizontal components allowed for bending moment diagrams to be determined (Figure B.2) in two perpendicular planes.

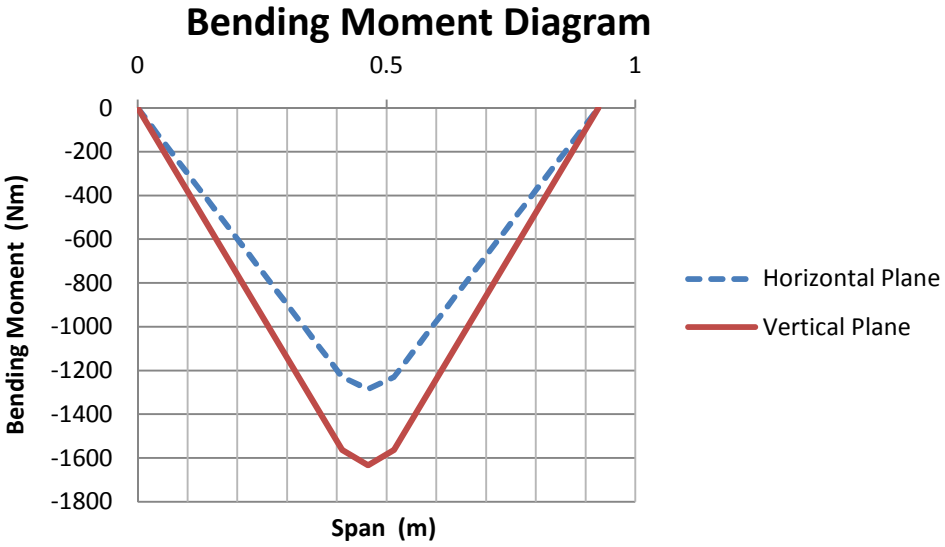

Figure B.2: Bending Moment Diagram for Crossbeam

Bending of the rectangular beam in the two perpendicular planes was assessed where the maximum stress was calculated in each case. These stresses were then added directly as they act in the same cross-sectional plane at the corners of the rectangular

beam to identify the maximum stress. The safety factor was then calculated using the minimum yield stress for the steel supplied as shown.

$$n = \frac{300\ MPa}{80.4\ MPa} = 3.7$$

B.2 SHAFT CALCULATION

To support the increased loading on the main shaft the hollow shaft was replaced with a solid M303 steel shaft which was inserted into the mounting bushes in the frame. The conservative maximum shear stress formula [27] shown below was used to determine the safety factor on the shaft. This was found to be 2 for this case where no torque was applied and the maximum bending moment was 514 Nm.

$$d = \left\{ \frac{32n}{\pi S_y} (M^2 + T^2)^{1/2} \right\}^{1/3}$$

M303 was used for its excellent machinability and anti corrosion properties. The yield strength and ultimate tensile strength for this material was in the range of 240 MPa to 619 MPa respectively. The mounting of the shaft with the arm attached via y-bearings is shown in Figure B.3

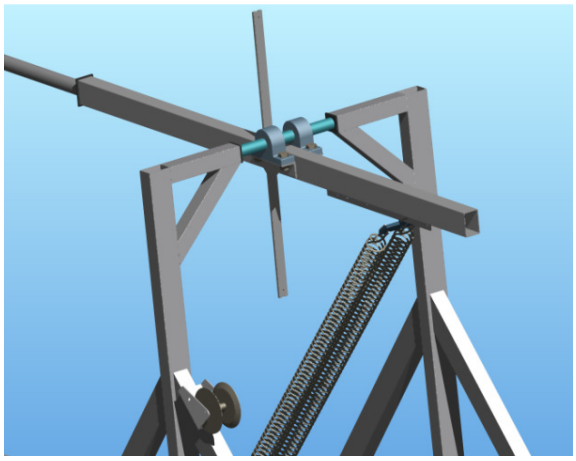

Figure B.3: Shaft Layout

B.3 PARAFOIL INFLATION TESTS

Once all the systems were designed and constructed, testing of the full parafoil inflation subsystem took place. These tests were successful in that the parafoil inflated consistently each time as it was flung into the air. Figure B.4 shows a snap shot where the parafoil can be seen spreading as it approaches its fully inflated state.

Figure B.4.: Parafoil Inflation

In the build up to final testing of this subsystem, a “no load” test was performed where the arm was accelerated without a parafoil in place. This resulted in an extreme velocity being achieved and the aft support stay snapped as the arm contacted the deceleration subsystem and bent slightly. Both support stays were replaced with heavier gauge steel cable to prevent similar failure in future.

APPENDIX C

PAYLOAD ACCELERATION SUBSYSTEM

CONTENTS

This appendix includes design calculations for the Payload Acceleration Subsystem and details the orientation of the car and trolley units. An assembly drawing of this subsystem can be found on page F 4 in Appendix F.

C.1 ASSESSMENT OF ENERGISING SOURCE

Multiple sources were considered to input the energy into the linear launch system. Rockets were ruled out at an early stage due to storage and fire hazard complications. Calculations showed that a 14 hp petrol motor would offer adequate power but this was disregarded due to limitations in velocity adjustment as a gear box and clutch would need to be developed. This gearing requirement was the same for an electric motor with the additional prerequisite of a generator. Pneumatics was identified as a suitable option and was investigated further.

For a track length of 2 m, a 56 m/s^2 acceleration was required resulting in a force of 4.5 kN. Pneumatic equipment supplier FESTO stocked a piston with a bore diameter of 125 mm and stroke length of 2000 mm which could theoretically produce 7 kN at 6 bar. Complications arose as additional ports in the cylinder end caps would need to be machined and the reservoir size for low operating pressures was exceptional for operating at safer low pressures. Furthermore a complex control system was required to direct the valves and monitor the position of the piston to avoid any damage. A quote from FESTO confirmed the high cost where the machining and delivery time of custom end caps were not suited to the time frame of this project.

C.2 SPRING CONCEPT

Garage door springs supplied by a local manufacturer with a spring constant of 1837 N/m were capable of supplying 1.53 kJ while operating in their linear range and avoiding permanent deformation. Placing two springs in series and attaching four such sets in parallel (as shown in Figure C.1) formed a combination that could supply adequate energy to accelerate an 80 kg payload with excess energy to accommodate for inevitable friction and drag losses.

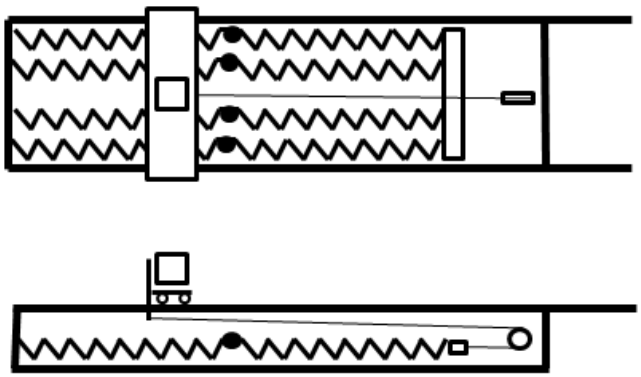

Figure C.1: Spring Configuration – Top and Front Views

A numerical model was created in *SIMULINK* that was used to simulate the acceleration of various payloads and trolley masses. It was assumed that the payload mass detached precisely at the point where the force applied by the spring becomes zero and only the trolley overshoots the zero point. The motion of the trolley is described by equations (C.1) and (C.2). The corresponding *SIMULINK* model can be found in Appendix E, Figure E.4.

For x < 0 $$\left(M_p + M_t\right)\ddot{x} + k_{2x4}(x) - 4F_i = 0 \quad \text{(C.1)}$$

For x > 0 $$(M_t)\ddot{x} + k_{2x4}(x) + 4F_i = 0 \quad \text{(C.2)}$$

The *SIMULINK* model was verified analytically by integrating the equation of motion for undamped free vibration of the trolley. The force exerted on the trolley by two of the springs in series included the pretension which had to be overcome before any deflection took place. This model simulates the initial acceleration up to the point where the trolley reaches zero displacement, Figure C.2, where the payload is expected to reach its maximum velocity.

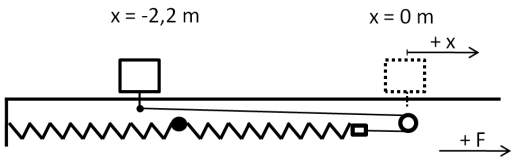

Figure C.2: Direction of Displacement and Force

$$F_{2\ series} = -\left[k_{2\ series}(x) - F_i\right]$$

Now with four parallel sets of two springs in series provided a force of:

$$F_{2x4} = -\left[k_{2x4}(x) - 4F_i\right]$$

Where the equation of motion for the trolley is defined by Newton's second law, as shown in equation (C.1).

This was solved analytically where the pretension force was converted into additional spring deflection to give the equivalent force. This approximation was made as only the first half of the motion is modelled. This simplified Eq. (C.3) to the standard form of Eq. (C.4).

$$\left(M_p + M_t\right)\ddot{x} + k_{2x4}\left(x_{eq}\right) = 0 \qquad \text{(C.4)}$$

Assuming undamped free vibration, the solution was assumed to be of the form shown below:

$$x = C\cos\omega_n t + D\sin\omega_n t$$

The coefficients were determined from the initial conditions where the equivalent maximum displacement (x_{eq}) was -2.41 m and the trolley was released from rest.

$$x_0 = C = -2.41\ m \text{ and } \dot{x_0} = D\omega_n = 0\ m/s$$

$$x = x_0\cos\omega_n t + \frac{\dot{x_0}}{\omega_n}\sin\omega_n t$$

Differentiating the above equation with respect to time provided the maximum velocity the payload mass could theoretically achieve.

$$\frac{dx}{dt} = x_0\left(-\sin\omega_n t\right)\omega_n$$

This indicated the maximum velocity to be 16.3 m/s which correlated well with the SIMULINK model's result.

C.3 Structural Design of Track

C.3.1 Column Loading Analysis

An assessment of the long columns extending the length of the frame which would be subject to compression in the loaded state was carried out to determine the safety factor. The 45 x 60 mm aluminium Bosch Rexroth extrusion was found to be adequate as shown below.

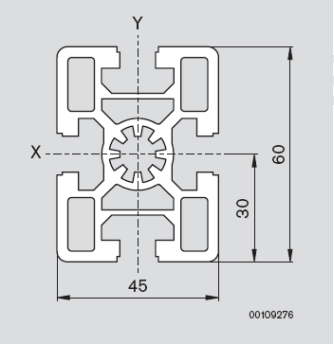

C.3: Cross Section of Bosch Rexroth Aluminium Extrusion

$$I_{45x60_X} = 372 \times 10^{-9}\ m^4 \qquad I_{45x60_Y} = 227 \times 10^{-9}\ m^4$$

$$A_{45x60} = 11 \times 10^{-4}\ m \qquad M = 3\ kg/m$$

$$E = 70\ GPa \qquad S_{y0.2\%} = 195\ MPa$$

The Euler column formula [28] was used to determine the critical compression load each of the four beams could withstand before reaching a state of unstable equilibrium.

$$\frac{P_{cr}}{A} = \frac{\pi^2 E}{\left(\frac{l}{k}\right)^2}$$

Where the radius of gyration: $k = \sqrt{\frac{I}{A}}$

The critical load was determined to be 12.8 kN for each column which led to a safety factor of 2,9.

C.3.2 Bend Loading Analysis

Assuming a "worst case" loading condition for a 3,5 m simply supported beam with a 40 kg point load applied at the centre, the safety factor for the Rexroth extrusion was determined to be 3,5. This was a very conservative value as the beam was supported by three vertical struts which added rigidity.

The pulley that experiences a loading of 17,7 kN is mounted onto two 8 mm laser cut steel plates through which the beam passes. These two plates are welded to another perpendicular plate which is bolted onto the beam to spread the loading, Figure C.4.

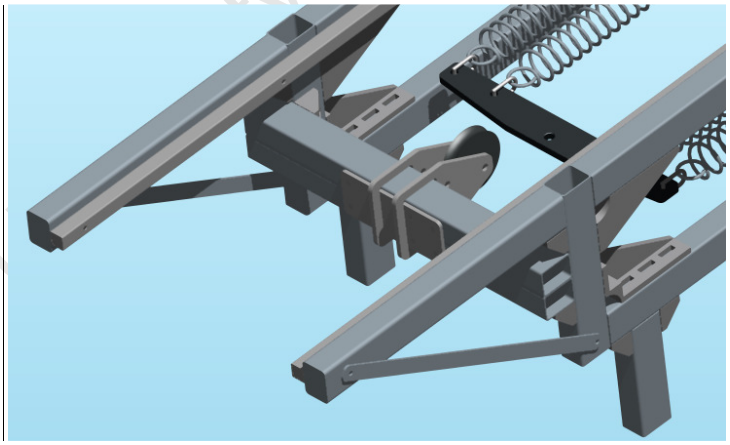

Figure C.4: Pulley Mounting

Assuming that the load on the beam is two point loads, bending criteria were applied which then determined the safety factor to be 2. This analysis was considered

conservative as the load is actually spread across the flat plate bolted to the beam. The normal stress in the laser cut steel plates was determined to be 40 MPa.

C.3.3 WINCH MOUNTING

The design of the winch mounting included two 38 x 38 mm square tubes with a wall thickness of 2,5 mm welded onto a 6 mm thick steel plate bolted to the frame with four M10 bolts. The loading condition applied from the winch on to the mounting configuration is displayed in Figure C.5. Reaction forces at the bolt holes have been omitted.

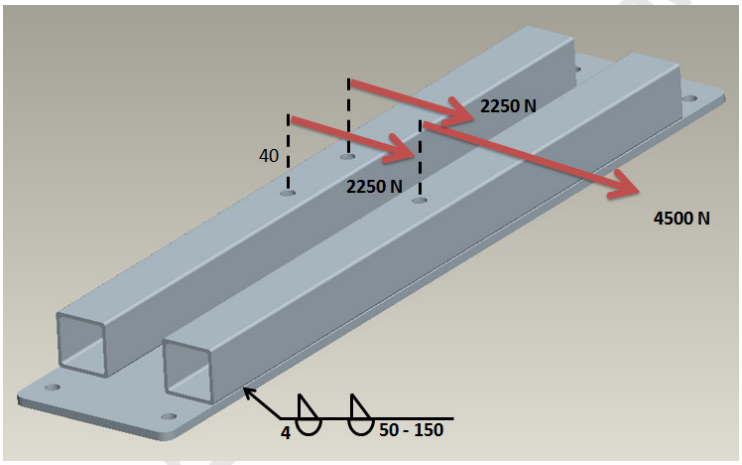

Figure C.5: Forces Applied Onto Winch Mounting

As the mounting experiences both torsion and shear, separate analyses were completed for the components individually to ensure the combined state would be well safe. Firstly a weld calculation was performed for the attachment of the tubing to the plate.

Throat area for welds on either side of the tube: $A = 1.414hb = 1.128 \times 10^{-3}\ m^2$

Primary Shear: $\tau' = 4\ MPa$

Secondary shear where the unit second moment of area is define by $I_u = \frac{bd^2}{2}$ where b is the equivalent length of the welds combined, to give

$$\tau'' = 16.3\ MPa$$

thus the shear magnitude is the Pythagorean combination.

$$\tau = 16.8\ MPa$$

The safety factor is determined using the shear yield strength from distortion energy theory:

$$n = \frac{0.557 S_y}{\tau} = 12$$

With the weld strength more than adequate, the torsional stress of the front rectangular tube was assessed assuming it was fixed at one end with the torque being applied at the centre of the tube length. The equation, as indicated by Roark[29] is an approximation based on mathematical analysis.

Factor K, to be used in the following torsional deflection equation was determined where b is the tube's side length and t the wall thickness

$$K = \frac{2t^2(b-t)^4}{2bt - 2t^2}$$

$$\theta = \frac{TL}{KG}$$

K was substituted into the torsional deflection equation, along with the length of half that of the tube, a torque of 266 Nm and the shear modulus of mild steel. This resulted in a negligible degree of twist.

A stress analysis was performed using Roark's [29] equation for the average stress near mid-length of a side for a hollow rectangle which has been modified below for a hollow square.

$$S = \frac{T}{2t(b-t)^2}$$

This resulted in an average stress of 42.2 MPa which was considered acceptable.

Lastly, the tensile bolt loading was determined to be 7,2 kN to counteract the applied moment. High tensile M10 bolts were used which comfortably accommodated this load as well as the direct shear.

C.4 Trolley Design

The selected design used polyurethane skateboard wheels and bearings as they were well specified to handle the loading and speeds required. Steel shafts were machined to support these wheels which were press fitted into high density polyethylene (HDPE) mounting blocks (Figure C.6) forming one of the four cars which support the trolley. Machine drawings of the car assembly and car part can be found in Appendix F.

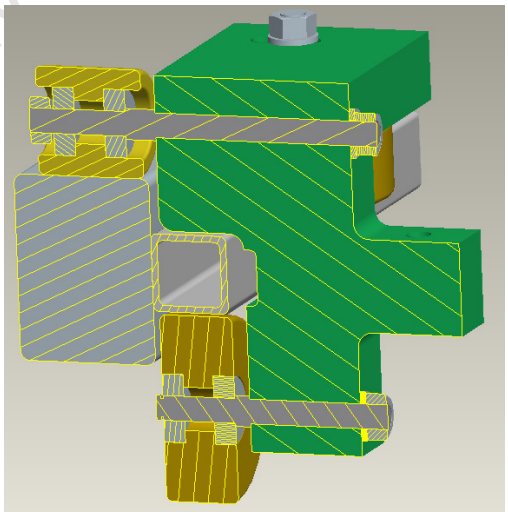

Figure C.6: Cross-section of Car Assembly

This configuration of the wheels constrained the trolley both vertically and horizontally where a slot machined in the HDPE blocks allowed for fine tuning of the horizontal locating wheel on each car. Engineering drawings of the HDPE blocks can be found in Appendix F. The main load bearing wheel (top left in Figure C.6) was secured by two NYLOC nuts on either side of the shouldered shaft where a slot was machined in one end to accommodate a screwdriver for tightening. The remaining two wheels were located by shouldered shafts with circlips and NYLOC nuts on their respective ends. The lower wheel runs on square 25x25 mm aluminium tubing bolted onto the Rexroth extrusion, preventing the car from lifting off the track. These cars were bolted to a steel frame providing alignment as well as support for the payload basket as shown in Figure C.7.

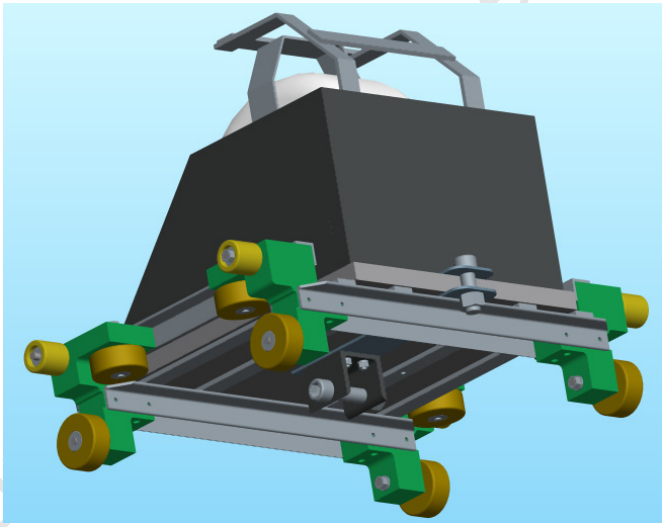

Figure C.7: Trolley Assembly

Beneath the trolley an M16 bolt onto which the Dynex rope is attached can be seen in Figure C.7. The vertical M16 bolt on the rear side of the trolley is the attachment point for the quick release snap shackle which connects to the loading cable. These high tensile M16 bolts were rated with a proof strength of 970 MPa which provided adequate safety factors for the intended application.

An investigation of the moment acting on the HDPE blocks as a result of the loading cable and Dynex rope attachment not being exactly co-planar was performed to ensure yielding of the HDPE (yield strength 30 MPa) did not occur.

APPENDIX D

FLIGHT TESTING AND DATA CAPTURE

CONTENTS

This appendix contains detail regarding parafoil trim settings used in the flight tests, construction techniques used to create trajectory images and information relevant to explaining the test results presented in chapter 7.

D.1 PARAFOIL TRIM

The rigging angle which essentially defines the angle of attack of the free stream velocity relative to the bottom of the canopy is an important parameter that governs how the parafoil performs. A study by Iacomini et al [30] found the range of suitable angles of attack or "alpha corridor" for a large scale, 750 ft^2 parafoil subject to tow testing to be between 5 and 17 degrees. Tethered wind tunnel tests published by Ware and Hassel [21] indicate that their parafoil (of which the one used in this dissertation is a 2/3 scaled replica) could be flown at angles of attack between -10° and +80° for which lift and drag coefficients were obtained. Current parafoil trim research by Ph.D. student S. Rhodes was used to rig the parafoil for the tests mentioned in Chapter 7. This determined the confluence point for angles of attack of +2°, 4°, 6° and 8° to be at the positions shown in Figure D.1 and Table D.1 relative to the forward most point on the chord line. The suspension line lengths (Table D.1) are labelled alphabetically where 'A' is the forward most line on the wing chord.

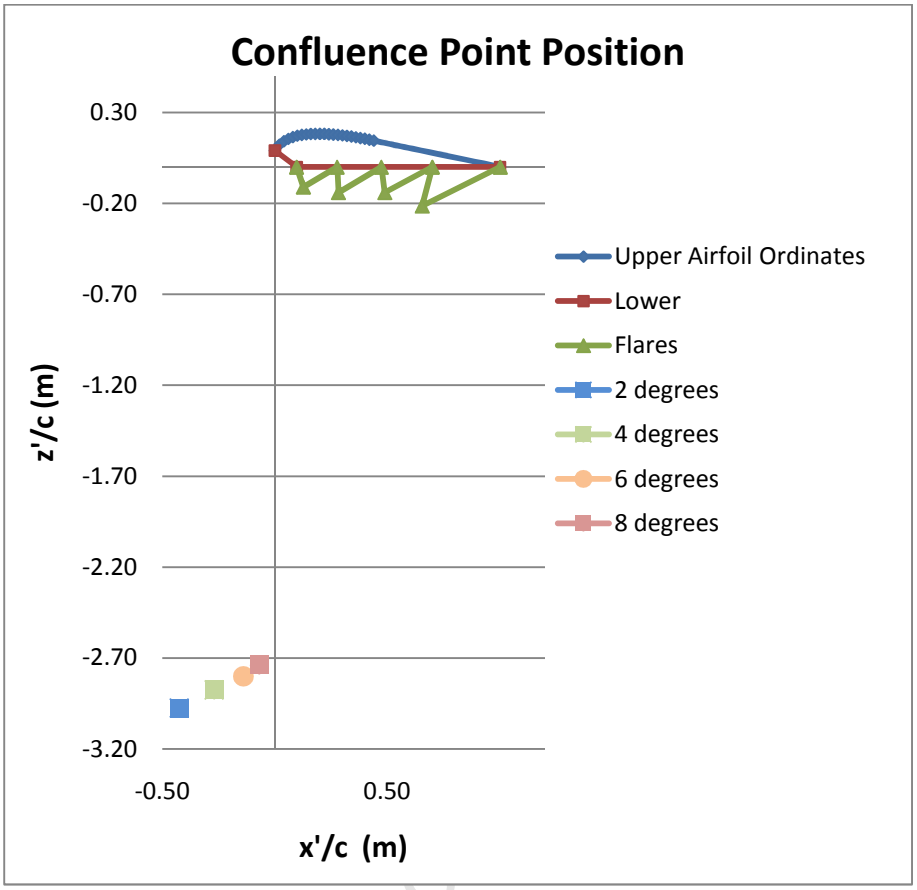

Figure D.1: Plot of Confluence Point Positions

Table D.1: Co-ordinates of Confluence Points and Corresponding Line Lengths

Alpha	**+ 2°**	**+ 4°**	**+ 6°**	**+ 8°**
x'/c (m)	-0.43	-0.27	-0.14	-0.07
z'/c (m)	-2.98	-2.88	-2.80	-2.74
Suspension Line	**Length (m)**	**Length (m)**	**Length (m)**	**Length (m)**
A	4.55	4.36	4.22	4.11
B	4.56	4.35	4.20	4.09
C	4.64	4.43	4.26	4.14
D	4.62	4.39	4.20	4.10

D.2 CONSTRUCTION OF TRAJECTORY IMAGES

Trajectory images were created from the video footage of the flight tests in order to extract data and to compare the effects of changing input parameters. These images accurately depict the flight path followed by the parafoil/payload system and proved useful in the development of the launch system.

The flight test footage was filmed with a digital video camera that captures 30 frames per second. Stepping through the frames allows the initial frame for the flight trajectory to be captured and saved as an image. Stepping forward through a predetermined number of frames provides an image of the parafoil/payload system at a time interval that is calculated using the frame rate and number of frames since the last image. A rectangle encompassing just the parafoil/payload system is selected and saved as a second image. This second image can then be superimposed on the initial frame by identifying distinguishing features in the background and lining up the second image to correspond with the background features. This method was surprisingly accurate as the second image could visually be located with the accuracy of about 2 pixels provided a detailed background was present.

Payload release velocity was calculated from images constructed in a similar manner where the distance between consecutive payload images could be measured and the time interval was known. This made flight analysis and velocity measurement possible without additional sensors such as accelerometers and gyroscopes. Figure D.2 shows the trajectory of the payload for a fully loaded track condition where the parafoil was not connected. This can be compared to Figure 7.2 for the case where the parafoil is attached to view the difference in range.

Figure D.2: Release of Payload Only

D.3 Glide Velocity Approximation

The predicted glide velocity of the parafoil/payload system was determined using the below mentioned formula.

$$V_{glide} = \sqrt{\frac{2g\left(\frac{M_p}{A_p}\right)}{\rho\, C_T}}$$

Substituting values for payload mass of 21.2 kg, canopy area 6.07 m^2, air density 1.225 kg/m^3 and an approximate C_T value of 1 resulted in a glide velocity of 7.5 m/s.

D.4 Confluence Point Spreader Bar

Addition of this aluminium spreader bar (Figure D.3) ensured the parafoil suspension lines were held clear of the rotating catapult arm to prevent snagging.

Figure D.3: Payload, Spreader Bar and Canopy

D.5 TRANSIENT FLIGHTS

In the last test of the second test series the launch system was placed above the steepest grass slope at UCT in an attempt to maximise the flight length and identify a stable glide. The successful launch is shown in trajectory image, Figure D.4.

Figure D.4: Longest Flight – 2nd Test Series

Plotting the payload for this test at shorter intervals indicated that stable glide had not yet been achieved, Figure D.5. The straight yellow line serves as a reference to

emphasise this. The release velocity was 8.4 m/s and the angle of attack setting 6°. The total flight time was 2,5 seconds.

Figure D.5: Transient Flight

D.6 Cross Wind Tests

Eight to twelve knot cross winds were not ideal conditions for parafoil launch. In one of the four tests conducted in this brief test series, the wind caused the windward side of the canopy (port side in this case) to collapse and drop to the ground, Figure D.6.

Figure D.6: Collapse of the Canopy in Cross Wind

The launch device is located on the hill in the top right corner of Figure D.6. The cross wind is blowing from right to left and the port side of the parafoil can be seen curling underneath itself. Successful tests in this test series can be summarised by Figure D.7 in which the canopy gradually turns into the wind.

Figure D.7: Canopy Turns Into Cross Wind

D.7 PHUGOID FLIGHT MODE

The phugoid oscillation and short period pitching oscillation are defined as longitudinal dynamic stability modes that are excited whenever an aircraft is disturbed from its equilibrium state. The more noticeable phugoid mode has a low, undamped natural frequency in the range between 0.1 and 1 rad/s. Further information is available in Cook [25].

Classical approximations of the phugoid flight mode indicate this lightly damped, low frequency oscillation is nearly independent of aircraft size, weight and altitude but directly proportional to the speed [26]. The period of this oscillation indicated by Ashley, is shown below where u_0 is the velocity.

$$T = \sqrt{2}\pi \frac{u_0}{g}$$

APPENDIX E

MATLAB CODE

CONTENTS

This appendix shows the block diagrams generated in *SIMULINK* that were used to model the respective concepts. The various input variables were varied where the simulation results were plotted in *MATLAB* figures in order to understand and optimise each concept's characteristics quickly and efficiently.

E.1 COUNTERWEIGHT CONCEPT MODEL

In order to determine the angular velocity profile of the counterweight concept, a block diagram simulating eq. (A.2) was constructed in *SIMULINK* and solved numerically to identify the systems characteristics. This block diagram is shown in Figure E.1.

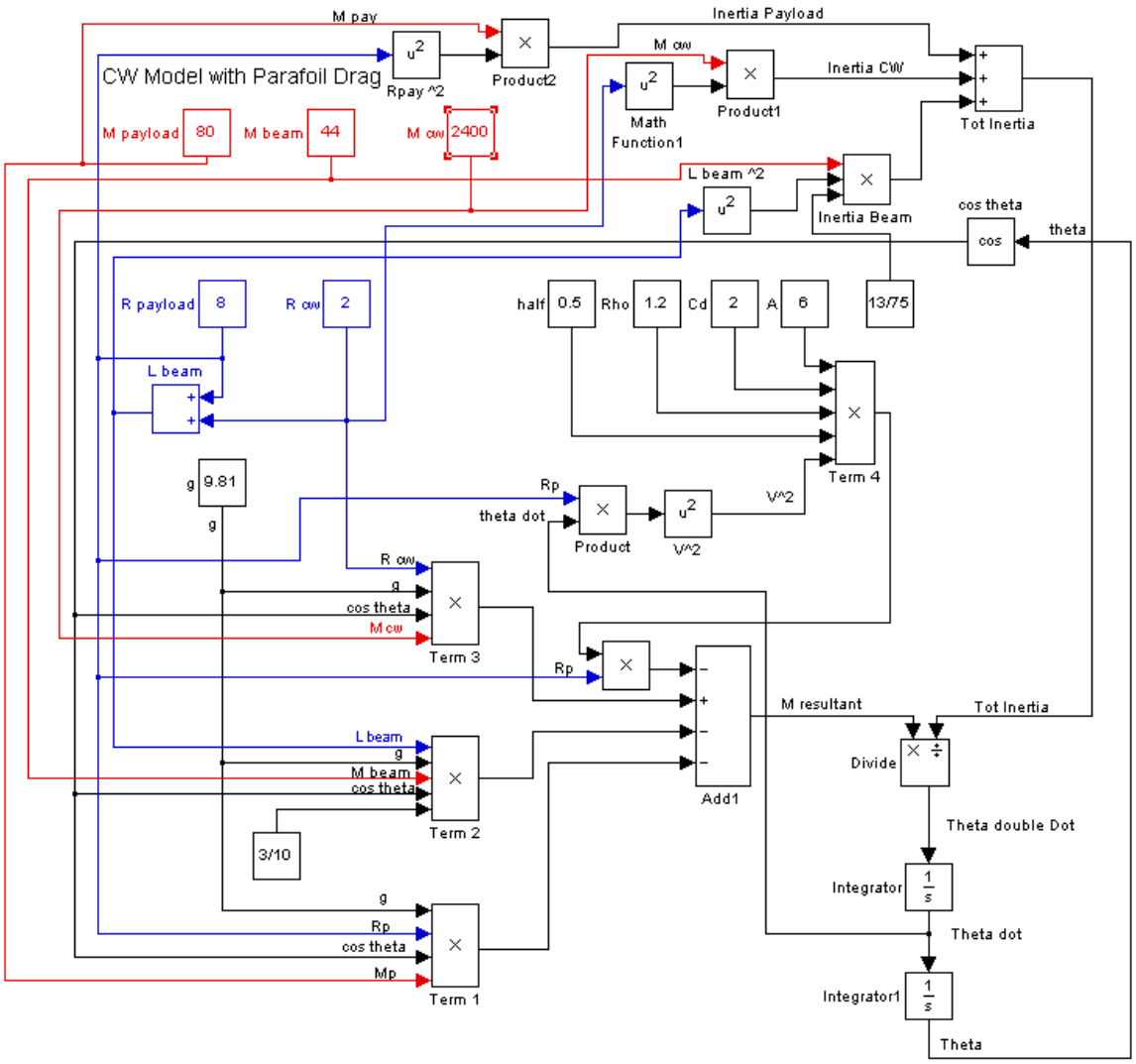

Figure E.1: Block Diagram for Counterweight Concept

E.2 PNEUMATIC SLIDER CONCEPT MODEL

In a similar manner to that shown in the case of the counterweight concept, the angular acceleration for the pneumatic link concept, defined in eq. (A.5), is integrated in the *SIMULINK* block diagram shown below in Figure E.2

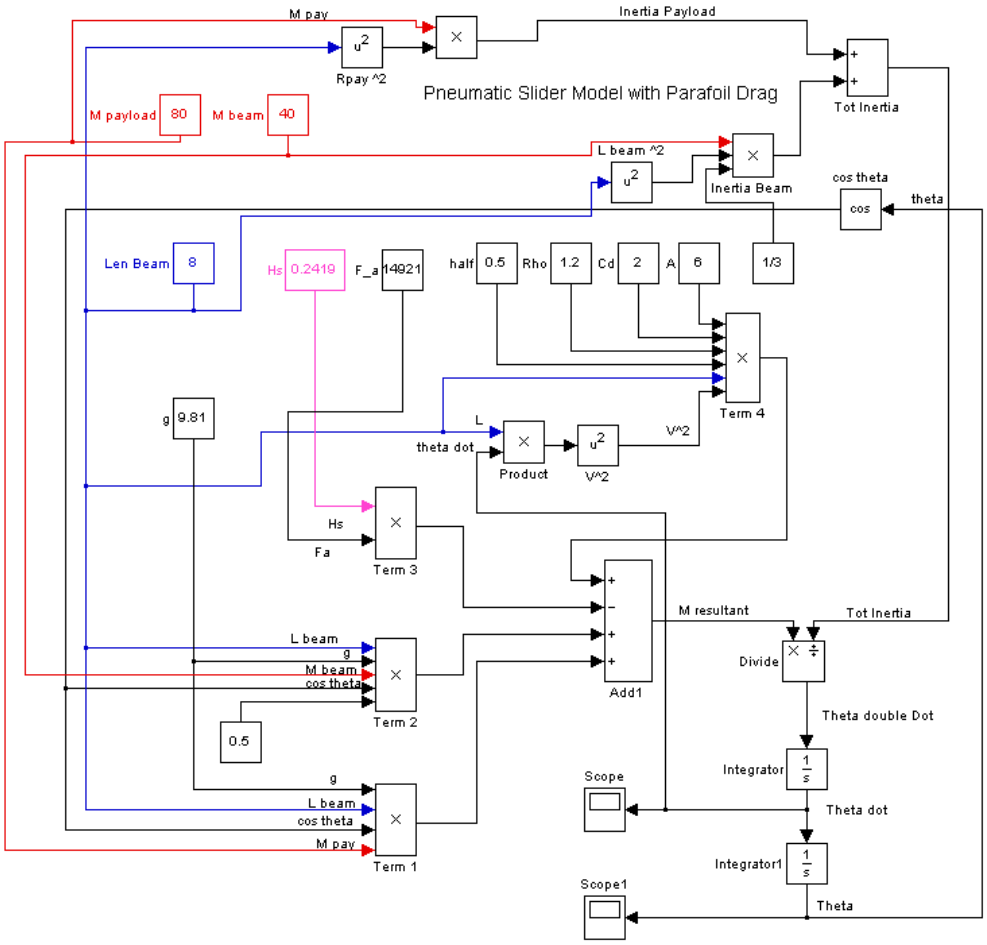

Figure E.2: Block Diagram for Pneumatic Link Concept

E.3 SPRING CONCEPT MODEL

The *SIMULINK* block diagram created to integrate the angular acceleration defined in eq. (A.6) for the spring parafoil inflation concept is shown in Figure E.3.

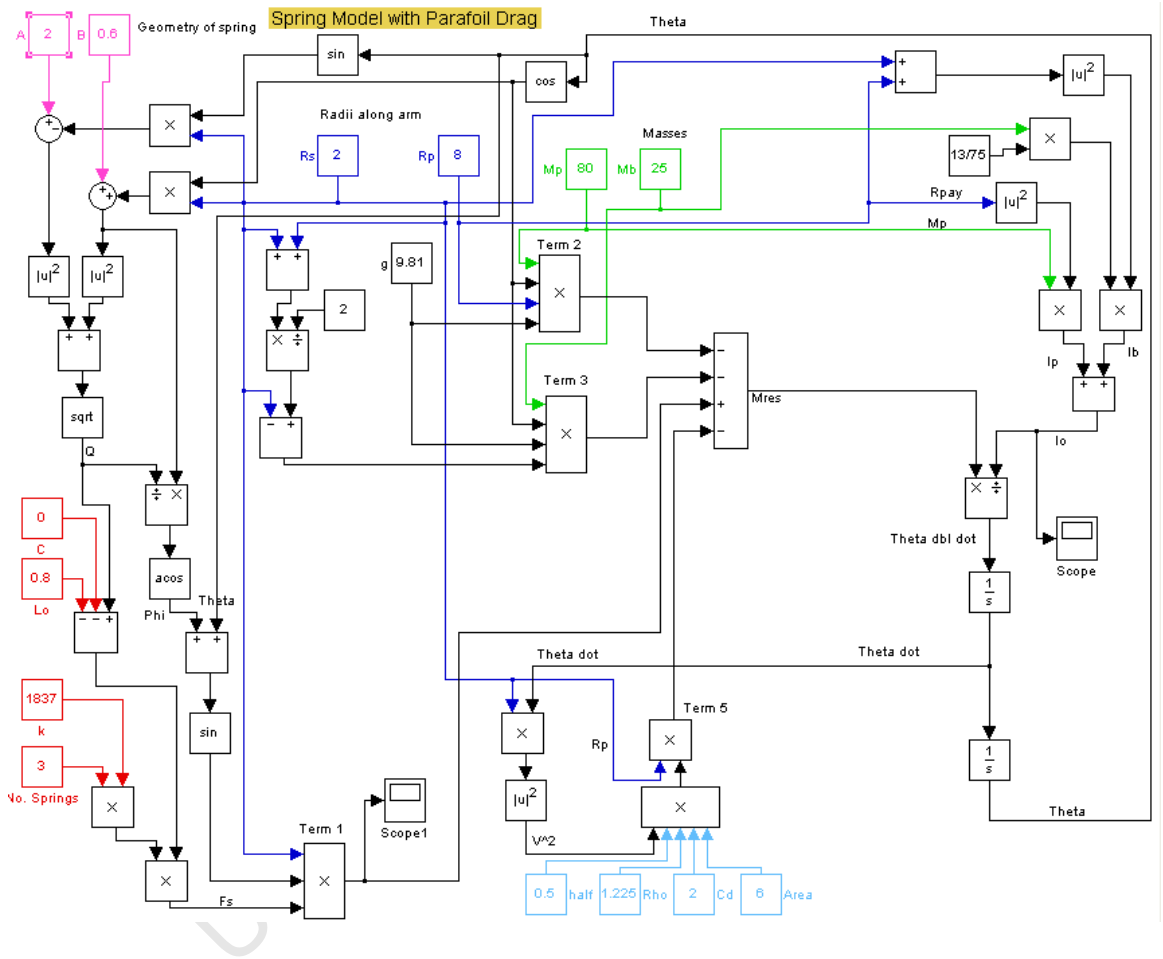

Figure E.3: Block Diagram for Spring Concept

E.4 LINEAR TRACK MODEL

This *SIMULINK block* diagram models the spring loaded linear track as defined by equations (C.1) and (C.2).

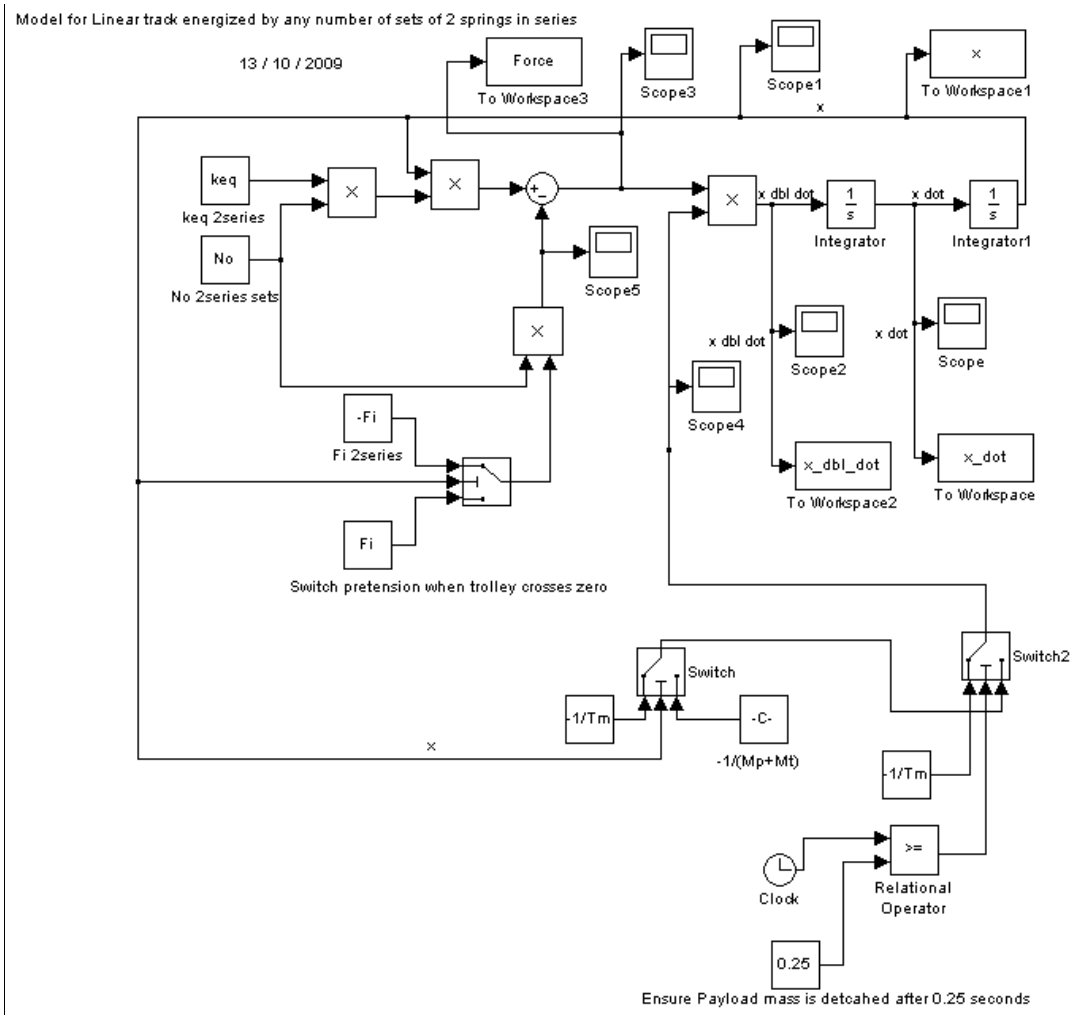

Figure E.4: Block Diagram for Linear Track

APPENDIX F

DRAWINGS

CONTENTS

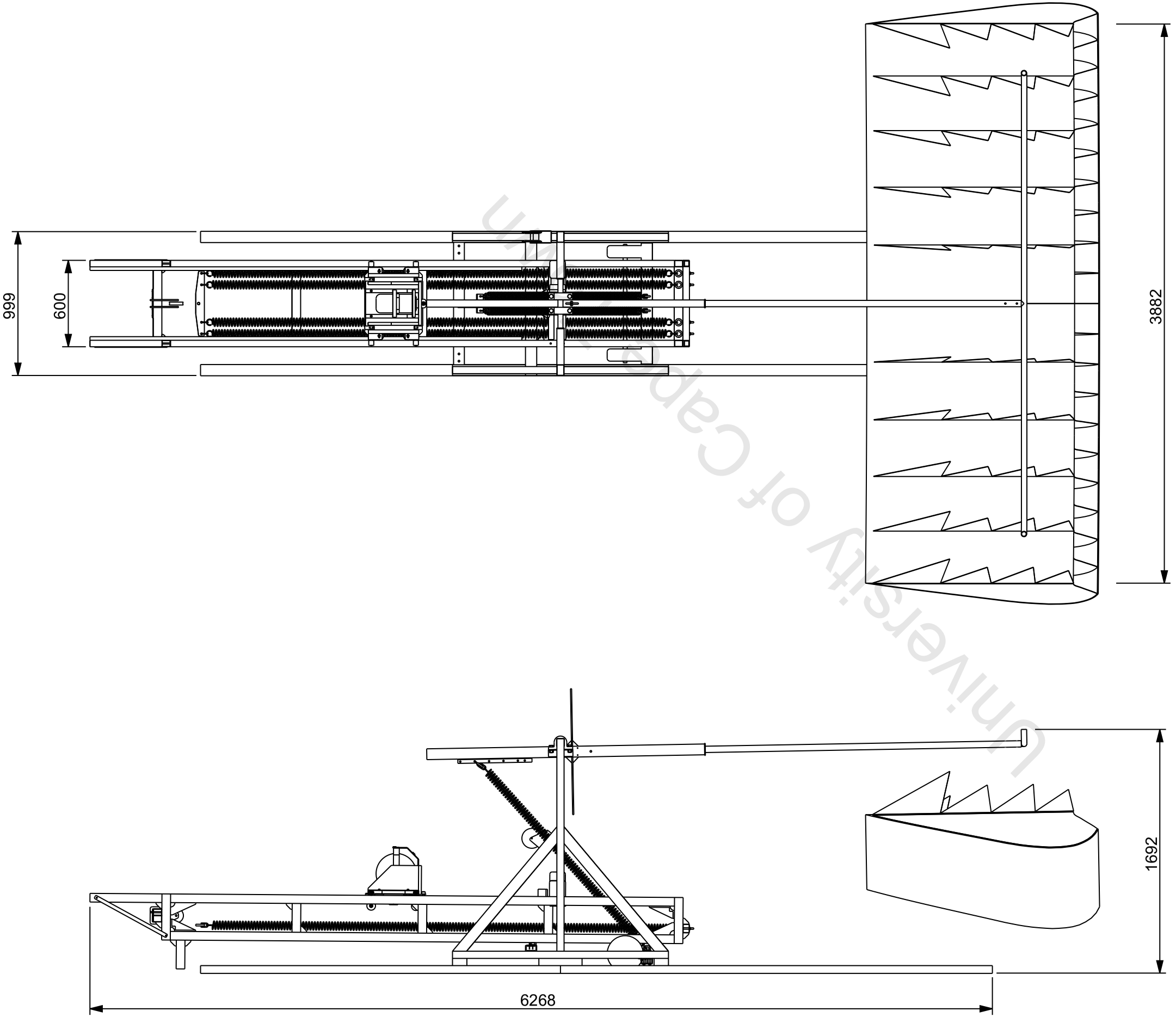

Item	Name	Qty	Material	Remarks
20	WINCH	1		
19	WIDTH2	1	STEEL_LC	
18	WIDTH1_ADD	1	STEEL_LC	
17	WIDTH1	1	STEEL_LC	
16	VERT_PULLEY_MOUNT	1		
15	SPRING_ASSEMBLY	1		
14	REXROTH_TRACK	1		
13	PULLEY	2		
12	PARAFOIL_A	1		
11	MHN110	4		
10	MHB0400	4		
9	LEG_SHORT	2	STEEL_LC	
8	LEG	2	STEEL_LC	
7	EYEBOLT	2	STEEL_LC	
6	EXTENSION_BUSH2	1	NYLON	
5	EXTENSION_BUSH1	1	NYLON	
4	BUSH	2	NYLON	
3	BASE	1		
2	AXLE	1	STEEL_LC	
1	ARM_MOUNTING	1		

University of Cape Town
Department of Mechanical Engineering

Title
Full Launch System

Dimensions in mm Tolerance U.O.S.	Scale	Date	Sheet	of
	0,035	9 July 2010	1	5
	Drawn By		Drawing Number	
0.1	Norton, W		F 2	

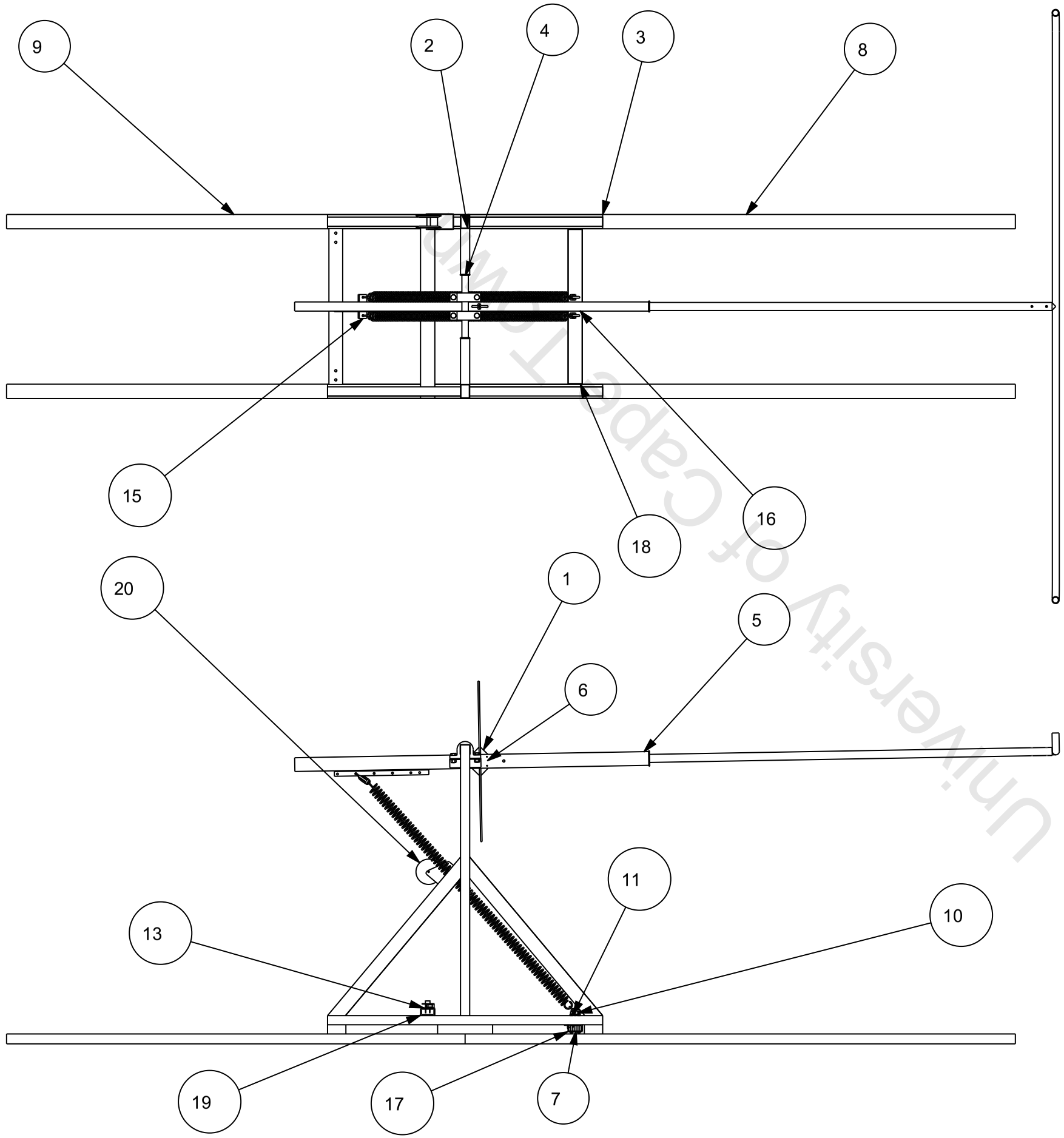

Item	Name	Qty	Material	Remarks
20	WINCH	1		
19	WIDTH2	1	STEEL_LC	
18	WIDTH1_ADD	1	STEEL_LC	
17	WIDTH1	1	STEEL_LC	
16	VERT_PULLEY_MOUNT	1		
15	SPRING_ASSEMBLY	1		
14	REXROTH_TRACK	1		
13	PULLEY	2		
12	PARAFOIL_A	1		
11	MHN110	4		
10	MHB0400	4		
9	LEG_SHORT	2	STEEL_LC	
8	LEG	2	STEEL_LC	
7	EYEBOLT	2	STEEL_LC	
6	EXTENSION_BUSH2	1	NYLON	
5	EXTENSION_BUSH1	1	NYLON	
4	BUSH	2	NYLON	
3	BASE	1		
2	AXLE	1	STEEL_LC	
1	ARM_MOUNTING	1		

University of Cape Town
Department of Mechanical Engineering

Title
Parafoil Inflation Subsystem

Dimensions in mm Tolerance U.O.S.	Scale	Date	Sheet	of
	0,040	9 July 2010	2	5
	Drawn By		Drawing Number	
0.1	Norton, W		F 3	

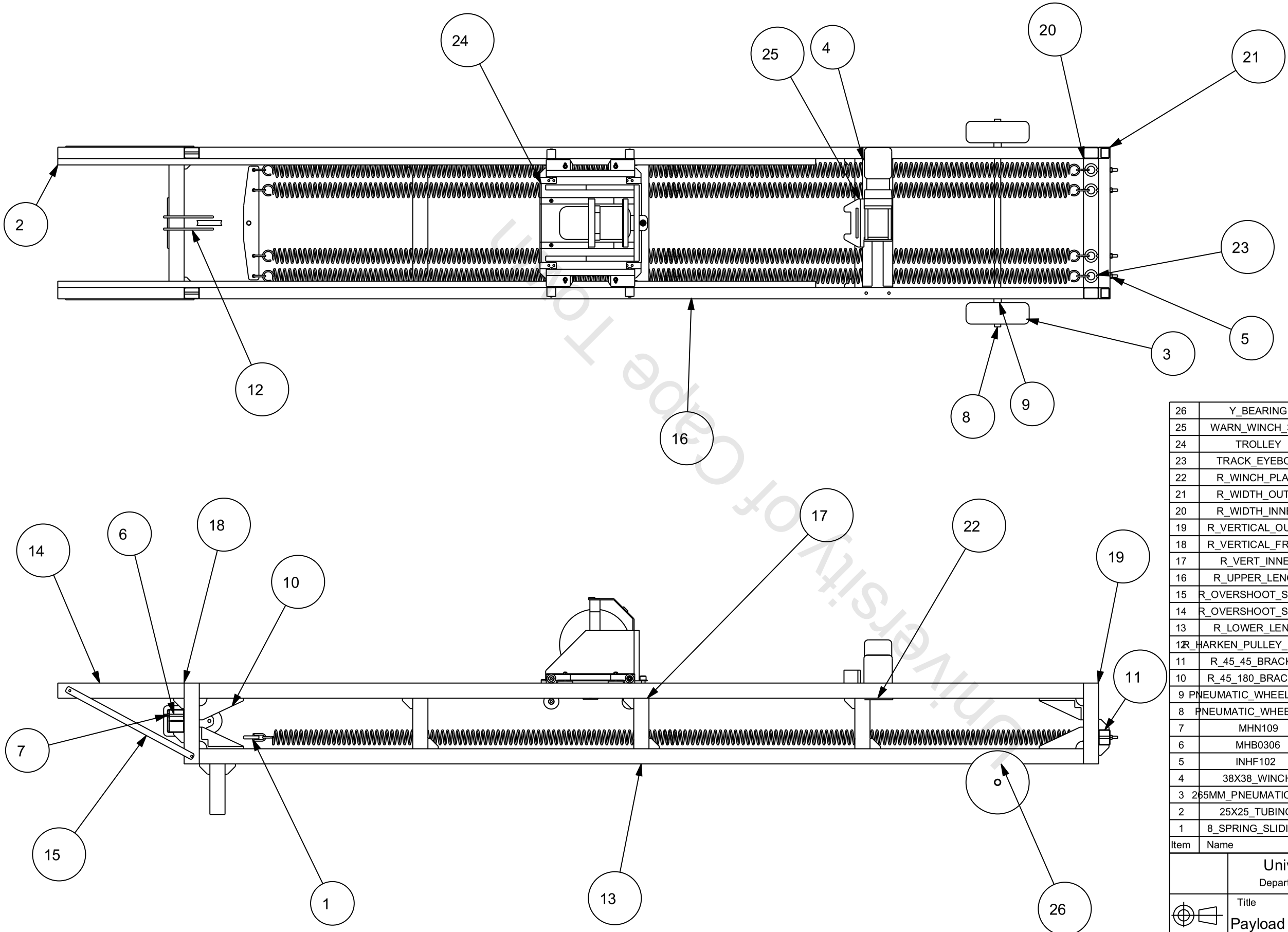

Item	Name	Qty	Material	Remarks
26	Y_BEARING	2	STEEL_LC	
25	WARN_WINCH_3700	1	STEEL_LC	
24	TROLLEY	1		
23	TRACK_EYEBOLT	4	STEEL_LC	
22	R_WINCH_PLATE	1	STEEL_LC	
21	R_WIDTH_OUTER	3	STEEL_LC	
20	R_WIDTH_INNER	4	STEEL_LC	
19	R_VERTICAL_OUTER	2	STEEL_LC	
18	R_VERTICAL_FRONT	2	STEEL_LC	
17	R_VERT_INNER	8	STEEL_LC	
16	R_UPPER_LENGTH	2	STEEL_LC	
15	R_OVERSHOOT_SUPPORT	2	STEEL_LC	
14	R_OVERSHOOT_SECTION	2	STEEL_LC	
13	R_LOWER_LENGTH	2	STEEL_LC	
12	R_HARKEN_PULLEY_MOUNTING	6		
11	R_45_45_BRACKET	34	STEEL_LC	
10	R_45_180_BRACKET	8	STEEL_LC	
9	PNEUMATIC_WHEEL_SPACER	2	STEEL_LC	
8	PNEUMATIC_WHEEL_AXLE	1	STEEL_LC	
7	MHN109	2		
6	MHB0306	2		
5	INHF102	4		
4	38X38_WINCH	2	STEEL_LC	
3	265MM_PNEUMATIC_WHEEL	2	STEEL_LC	
2	25X25_TUBING	2	ALUM_308	
1	8_SPRING_SLIDING	1		

University of Cape Town
Department of Mechanical Engineering

Title
Payload Acceleration Subsystem

Dimensions in mm Tolerance U.O.S.	Scale	Date	Sheet	of
	0,065	9 July 2010	3	5
0.1	Drawn By: Norton, W		Drawing Number: F 4	

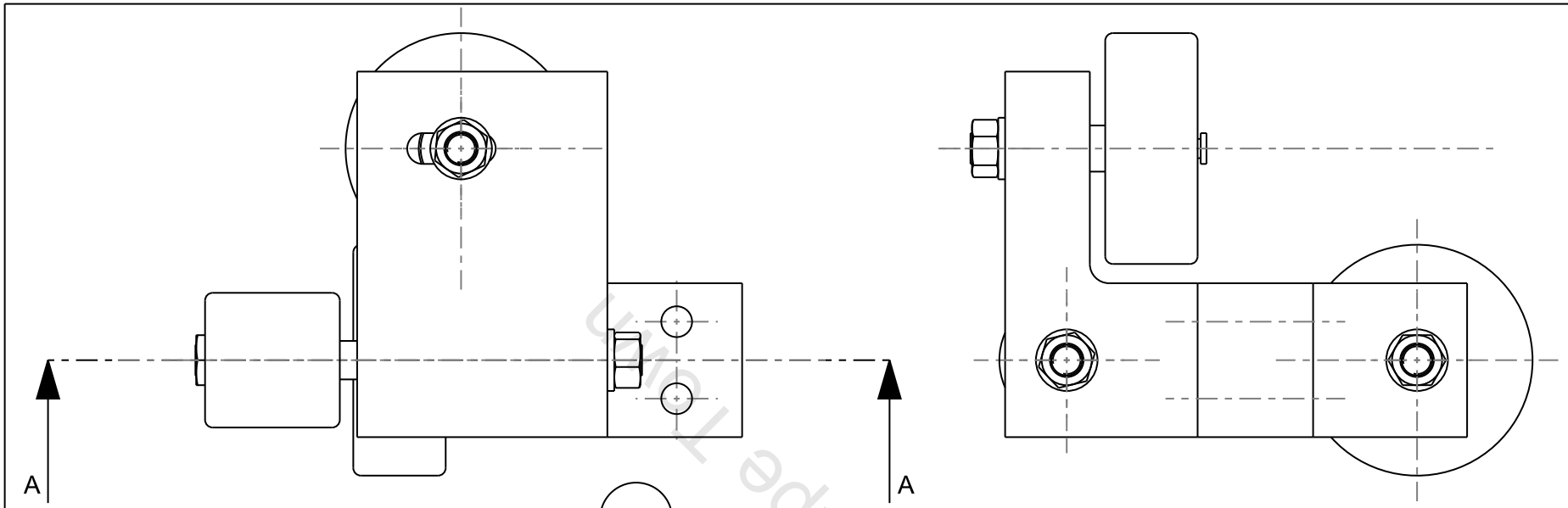

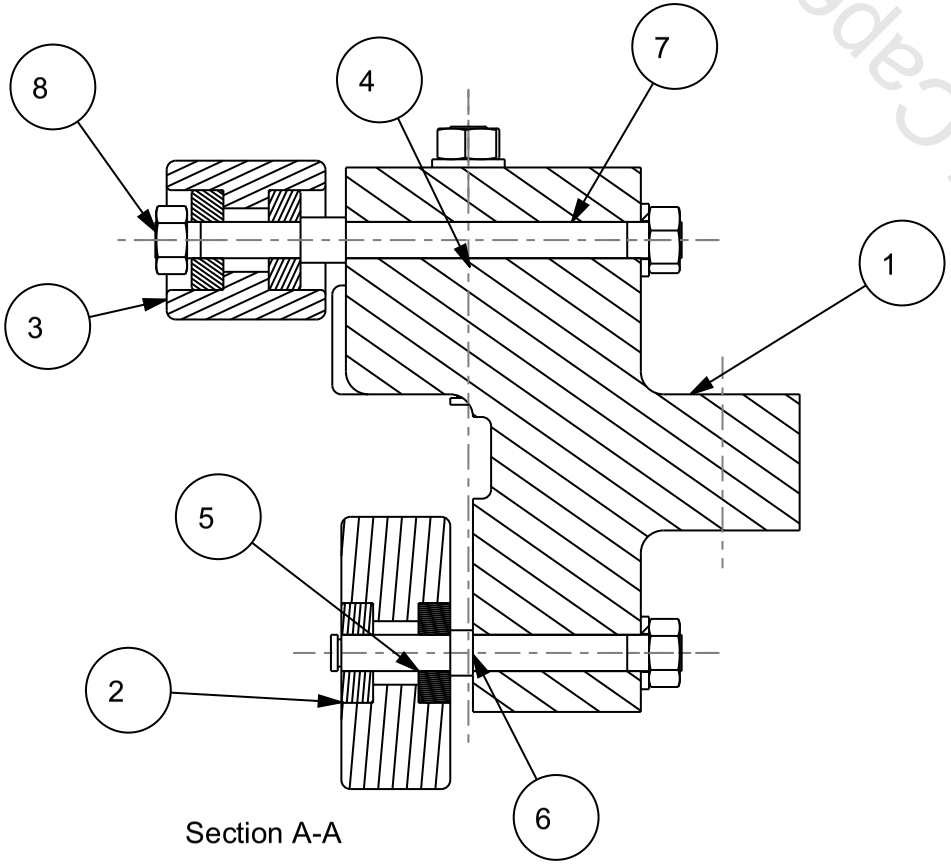

Section A-A

Item	Name	Qty	Material
9	IWPNA09	3	
8	INHF101	4	
7	TOP_SHAFT	1	STEEL_LC
6	BOTTOM_SHAFT	1	STEEL_LC
5	BEARING_608	6	STEEL_LC
4	ALIGNING_SHAFT	1	STEEL_LC
3	SKATEBOARD_WHEEL	1	NYLON
2	ROLLER_BLADE_WHEEL	2	NYLON
1	CAR	1	HDPE_CHEVRON_9708

University of Cape Town
Department of Mechanical Engineering

Title
Car Assembly

Dimensions in mm Tolerance U.O.S.	Scale	Date	Sheet	of
	0,600	10 July 2010	4	5
	Drawn By		Drawing Number	
0.1	Norton, W		F 5	

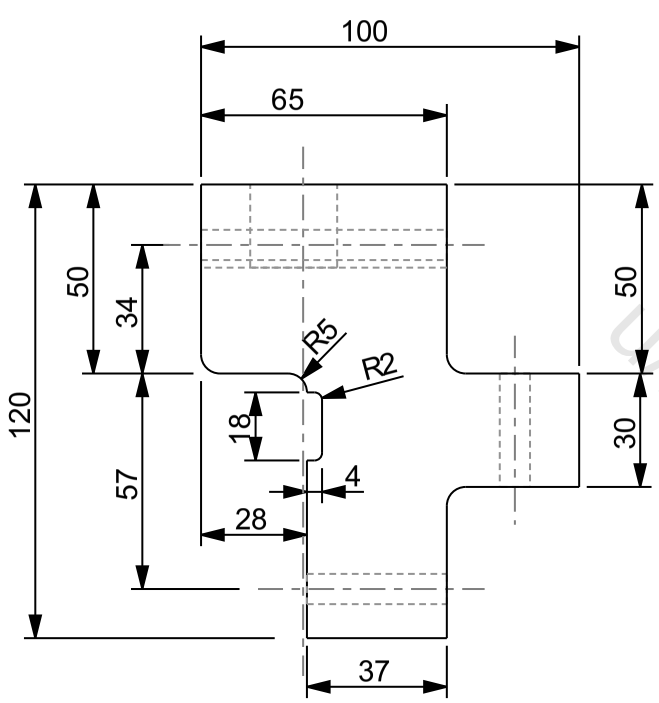

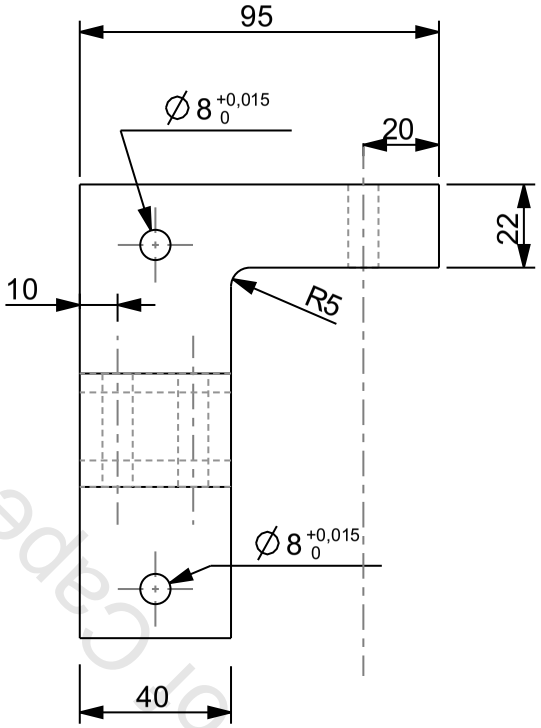

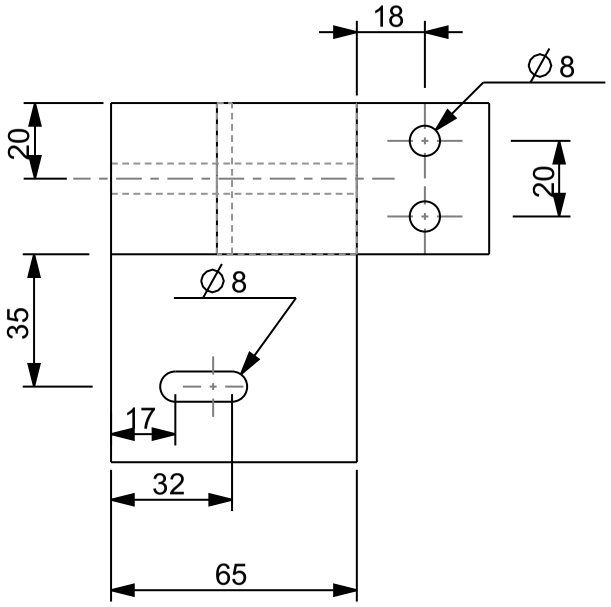

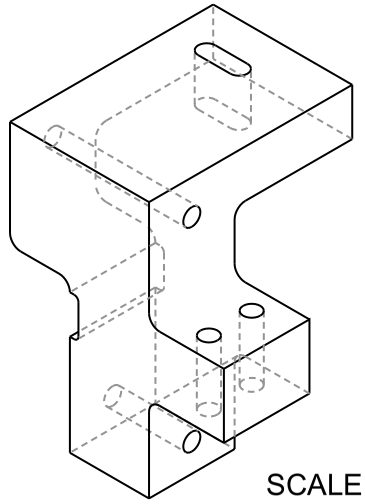

SCALE 0,400

	HDPE	2	Black
Item	Material	Qty	Remarks

University of Cape Town
Department of Mechanical Engineering

Title: CAR

Dimensions in mm Tolerance U.O.S.	Scale	Date	Sheet	of
	0,500	10 July 2010	5	5
	Drawn By		Drawing Number	
0.1	Norton, W		F 6	